Beyond the Classical Performance Limitations Controlling Uncertain MIMO Systems: UAV Applications

2nd Session

Mario Garcia-Sanz

Automatic Control & Computer Science Department
Public University of Navarra
31006 Pamplona, Spain
(Email: mgsanz@unavarra.es)

NATO. RTO-LS-SCI-195, May-June 2008

Report Documentation Page

Form Approved
OMB No. 0704-0188

1. REPORT DATE **MAY 2008**	2. REPORT TYPE	3. DATES COVERED **00-00-2008 to 00-00-2008**

4. TITLE AND SUBTITLE **Beyond the Classical Performance Limitations Controlling Uncertain MIMO Systems: UAV Applications**	5a. CONTRACT NUMBER 5b. GRANT NUMBER 5c. PROGRAM ELEMENT NUMBER
6. AUTHOR(S)	5d. PROJECT NUMBER 5e. TASK NUMBER 5f. WORK UNIT NUMBER
7. PERFORMING ORGANIZATION NAME(S) AND ADDRESS(ES) **Public University of Navarra,Automatic Control & Computer Science Department,31006 Pamplona Spain,**	8. PERFORMING ORGANIZATION REPORT NUMBER
9. SPONSORING/MONITORING AGENCY NAME(S) AND ADDRESS(ES)	10. SPONSOR/MONITOR’S ACRONYM(S) 11. SPONSOR/MONITOR’S REPORT NUMBER(S)

12. DISTRIBUTION/AVAILABILITY STATEMENT
Approved for public release; distribution unlimited

13. SUPPLEMENTARY NOTES
See also ADM002223. Presented at the NATO/RTO Systems Concepts and Integration Panel Lecture Series SCI-195 on Advanced Autonomous Formation Control and Trajectory Management Techniques for Multiple Micro UAV Applications held in Glasgow, United Kingdom on 19-21 May 2008.

14. ABSTRACT

15. SUBJECT TERMS

16. SECURITY CLASSIFICATION OF:			17. LIMITATION OF ABSTRACT	18. NUMBER OF PAGES	19a. NAME OF RESPONSIBLE PERSON
a. REPORT **unclassified**	b. ABSTRACT **unclassified**	c. THIS PAGE **unclassified**	**Same as Report (SAR)**	**86**	

Standard Form 298 (Rev. 8-98)
Prescribed by ANSI Std Z39-18

Outline

1.- QFT Controller Design Technique Fundamentals

2.- Real-world QFT control applications and examples

3.- Non-diagonal MIMO QFT controller design methodologies

4.- Application: Robust QFT control for a MIMO Spacecraft with flexible sunshield

5.- Switching robust control: Beyond the linear limitations.

6.- Example: Switching control for Unmanned Vehicles

4.- Application: *Robust QFT control for a MIMO Spacecraft with flexible sunshield*

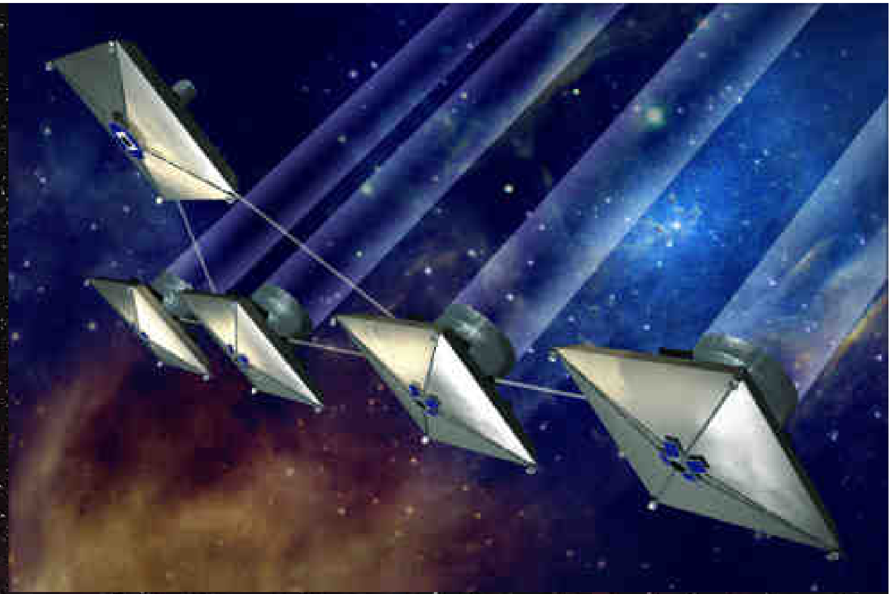

Non-diagonal MIMO QFT Controller Design for a Darwin-type Spacecraft with large flimsy appendages.

ESA-ESTEC, Noordwijk (Holland)

Research Project

4.1.- Introduction

Telescopes:

From Greek's Gnomon,

Tycho's Quadrants,

Kepler's and Galileo's Refractor,

or Newton's Reflector.

To Modern telescopes / Radio-telescopes on Earth: Mauna Kea, Monte Palomar, Cerro Paranal, Arecibo, etc).

Hubble: a telescope in space (1990)

(*Hubble Space Telescope*, **HST**):

- Refractor telescope. Aperture of 2.4 m.
- Magnification power much higher than the one allowed on Earth.
- Orbit: 600 km above Earth's surface.

Discoveries of First Magnitude

4.2.- Control of Darwin-type Spacecraft with Large Flexible Appendages.

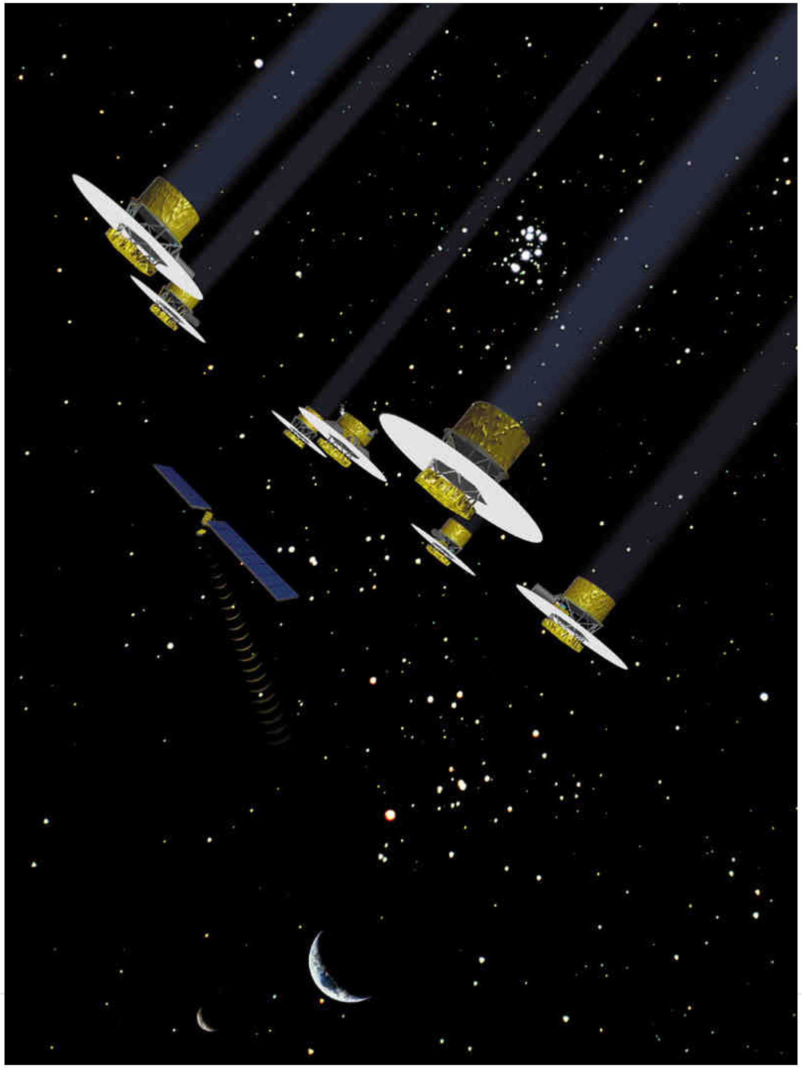

Non-diagonal MIMO QFT Controller Design for a Darwin-type Spacecraft with large flimsy appendages.

ESA-ESTEC, Noordwijk (Holland)

Ref: M. Garcia-Sanz, I. Eguinoa, M. Barreras, S. Bennani

"Non-diagonal MIMO QFT Controller Design for Darwin-type Spacecraft with large flimsy appendages".

Journal of Dynamic Systems, Measurement and Control, **ASME,** USA. Vol. 130, January 2008**.**

OBJECTIVE:

To study exo-planets and life

It is necessary

Infrared analysis

Instruments that work at temperature near zero Kelvin

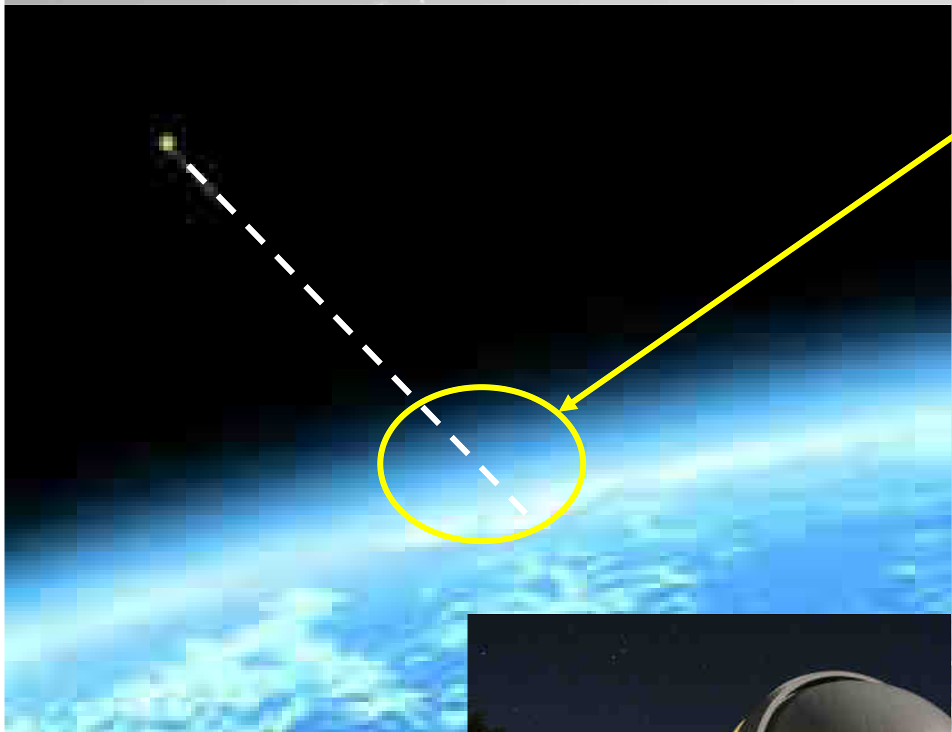

Limitation of Earth based Telescopes

Atmosphere absorbs infrared

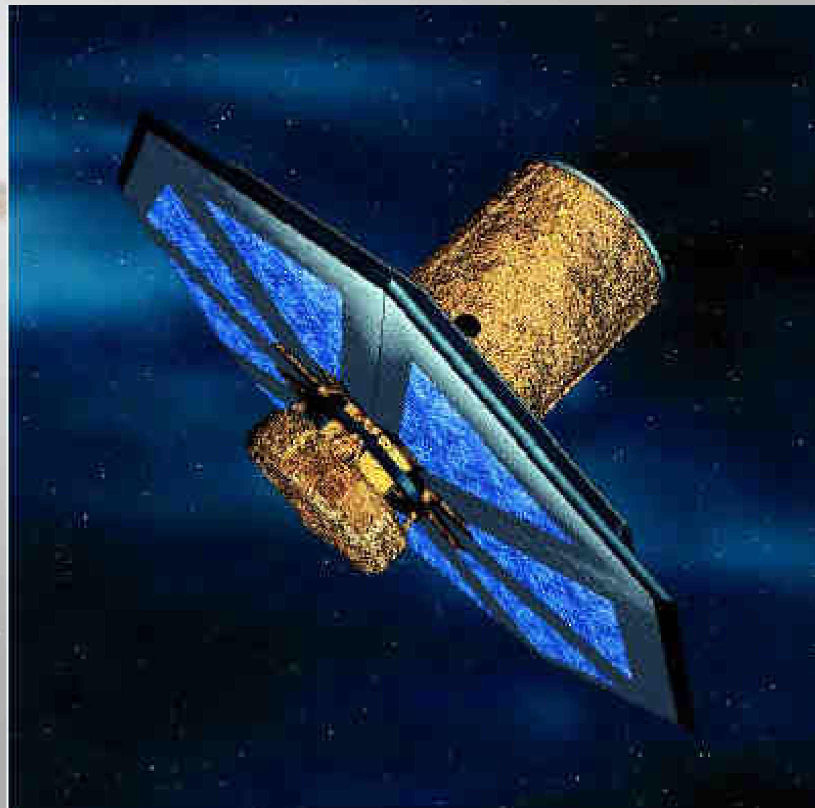

Darwin Mission Description (I)

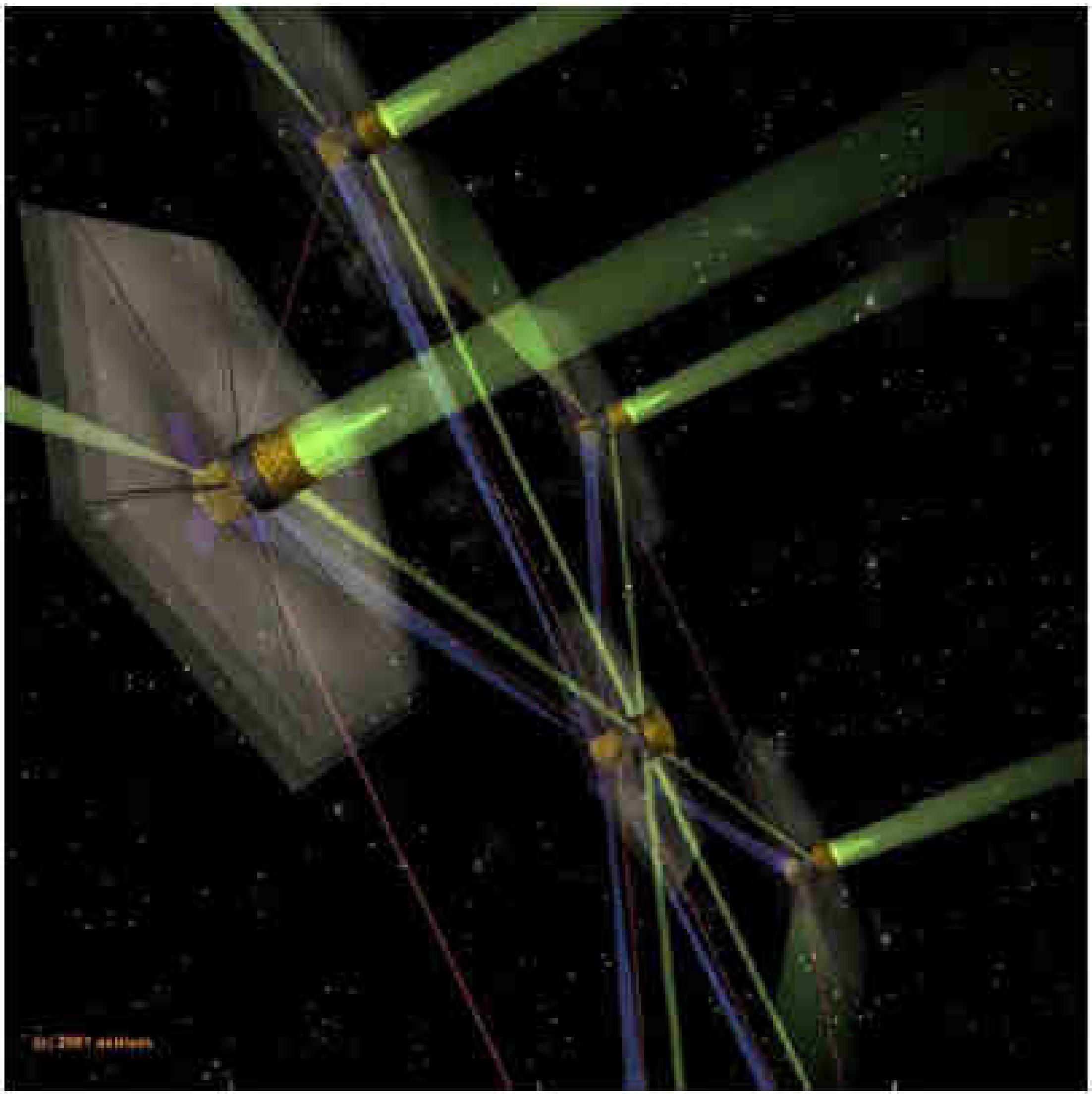

- **ESA** cornerstone **mission**
  - Scheduled launch in 2015
  - Objectives:
    - ➢ Find Earth-like **Exo-planets**
    - ➢ Analyse their atmosphere to detect signs of life

- **Nulling interferometry**:
  - the light collected by the flying telescopes is recombined inside a central hub
    - ➢ from the star interfere destructively
    - ➢ from the planet interfere constructively

- **Constellation** of 3 to 6 Darwin-type satellites

Darwin Mission Description (II)

- **Exo-planets**.
  - ➢ The first one was discovered by Latham et al. in 1989.
  - ➢ and Mayor and Queloz (1995), Butler y Marcy (1996).
  - ➢ Nowadays (2007) we know more than 200 exo-planets in 140 external systems.

Currently we do not know exo-planets with signs or possibilities of life.

Ver difficult to observe. The near stars hides the exo-planets.

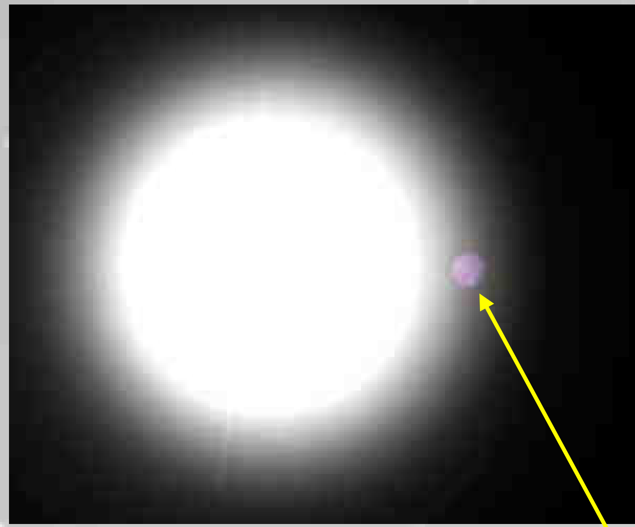

- **Destructive Interferometry**

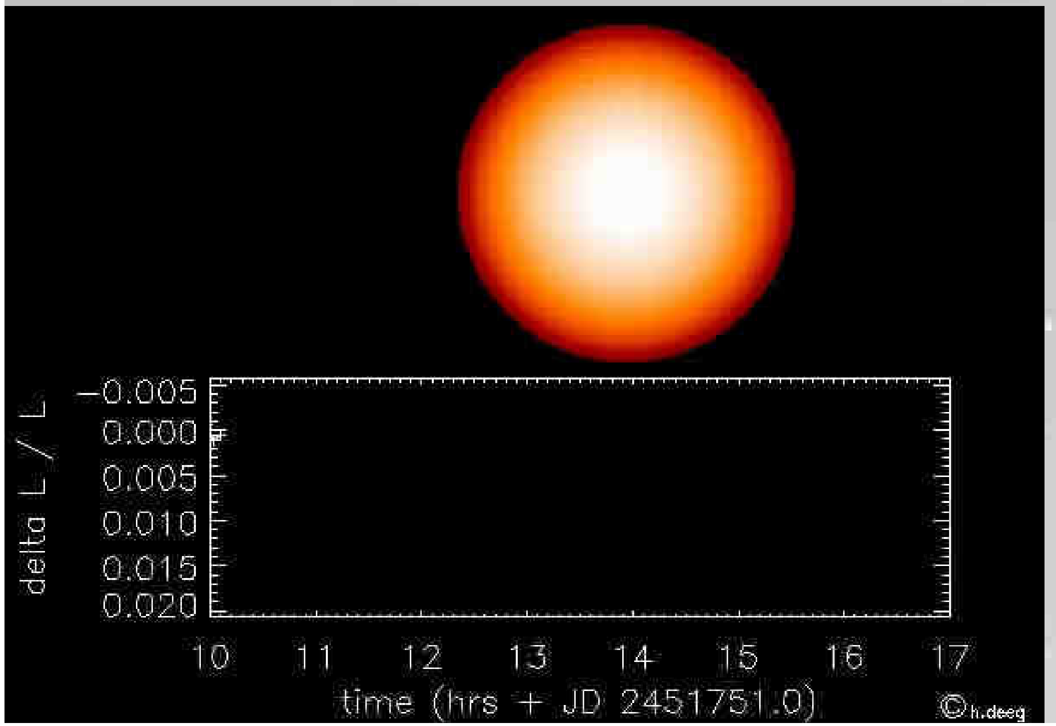

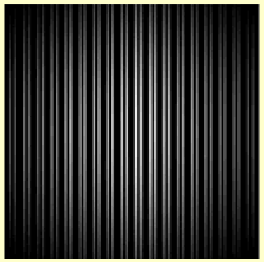

Combining light from the telescopes

In the Hub

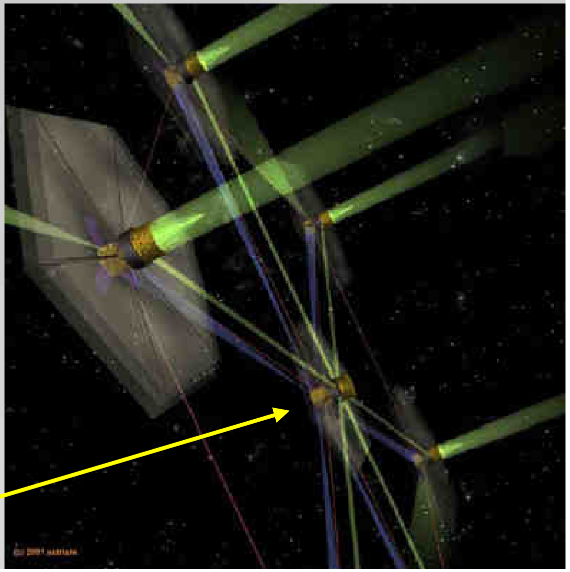

Darwin Satellite (I)

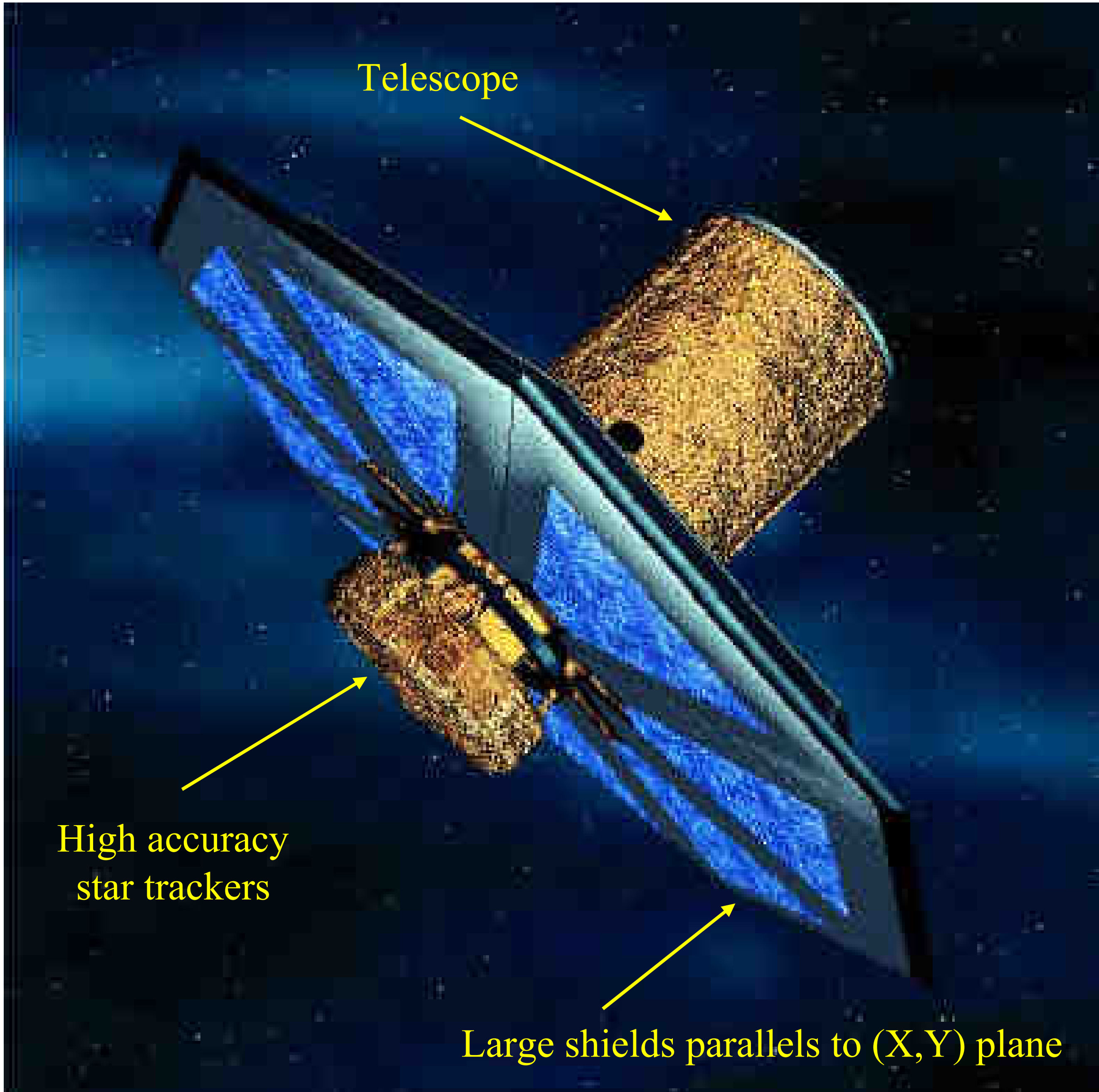

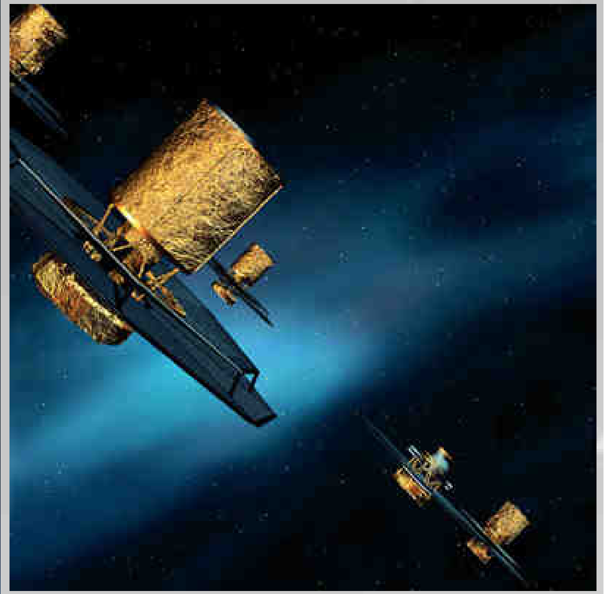

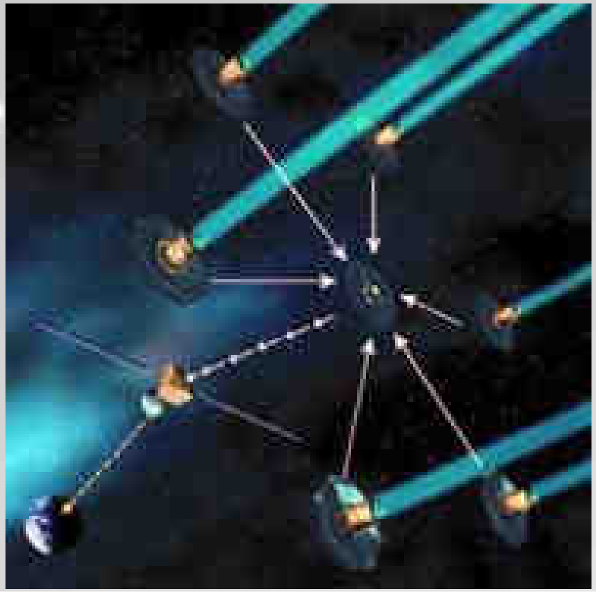

Darwin Satellite (II)

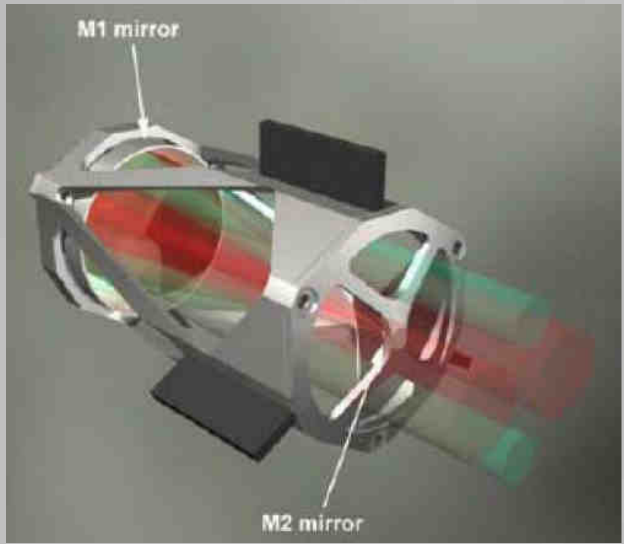

Fine Pointing Metrology (FPM) for 3D fine attitude

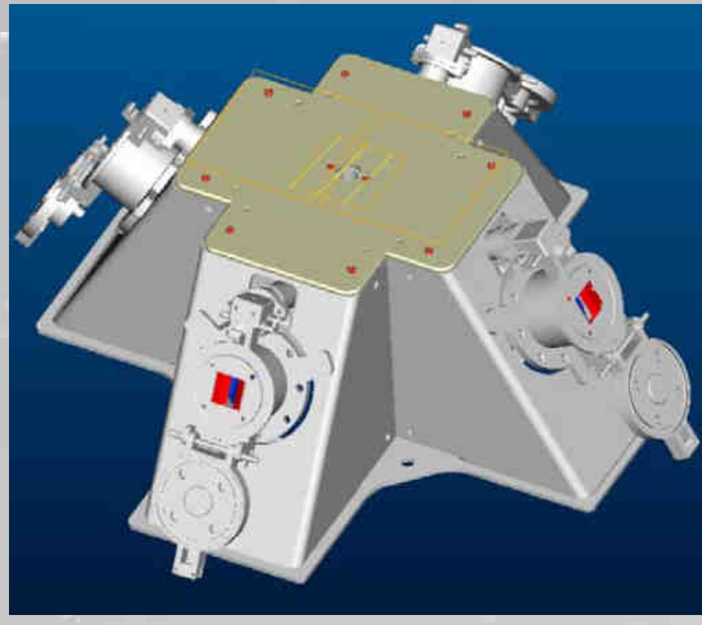

Thrusters and micro-actuators 6D (FEEPS)

–micro Newton ion thrusters + Magnetic field thrusters

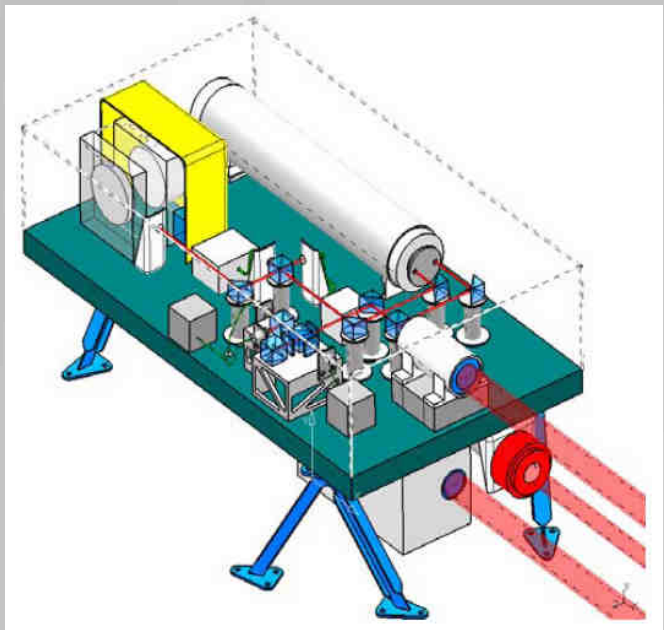

OPD (**Optical Pathlength Difference**) Fringe Tracker for fine position measures

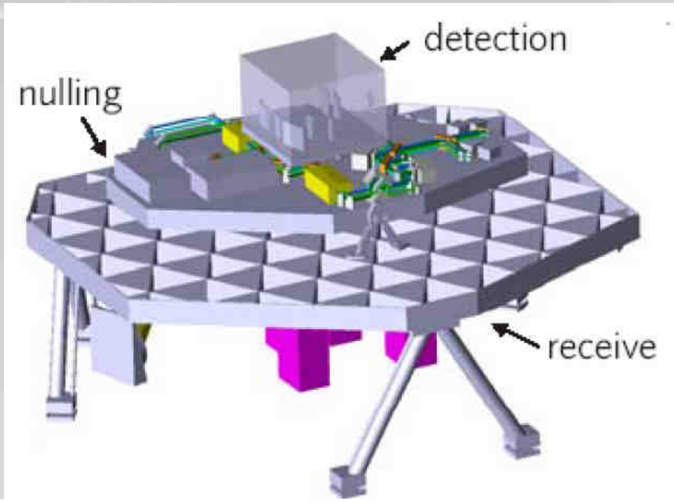

Darwin Satellite (III)

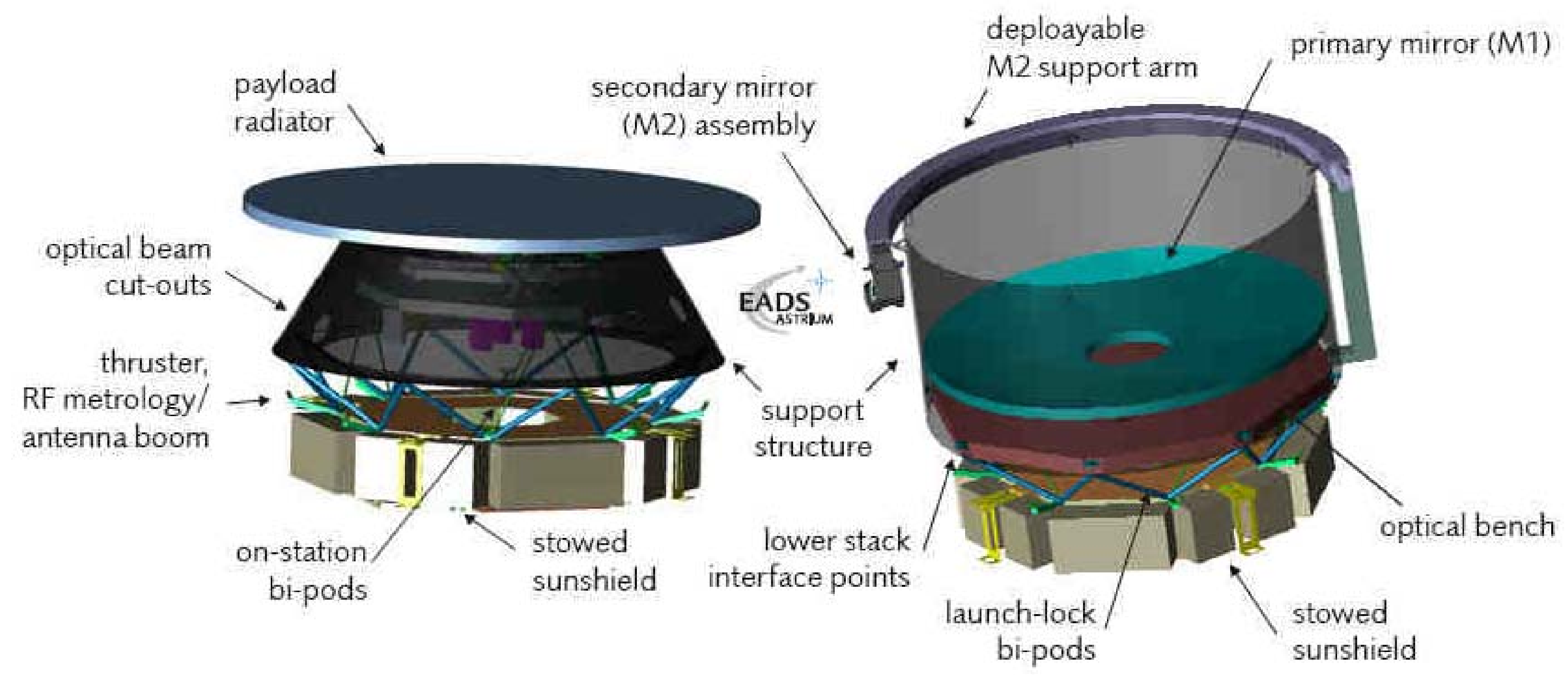

Hub satellite (Combinator)

Darwin satellite (Collector)

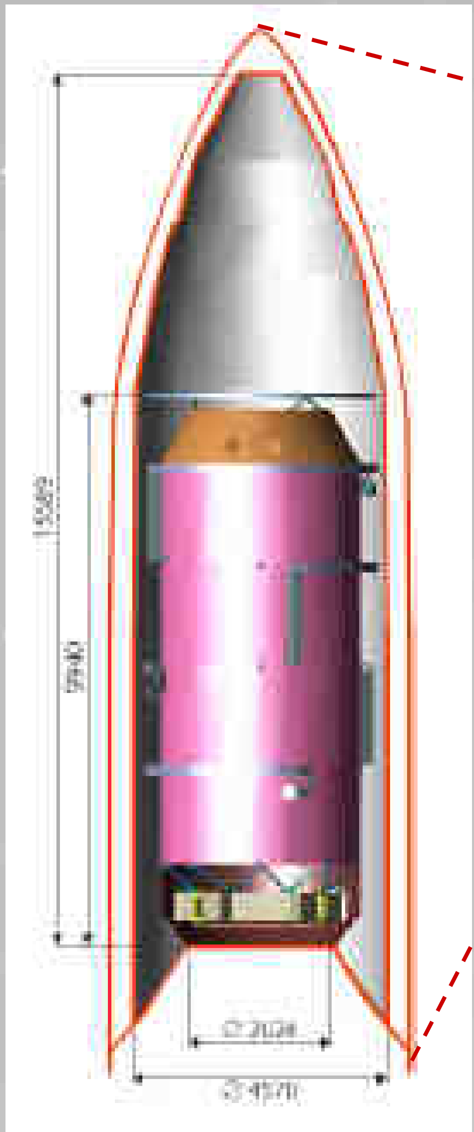

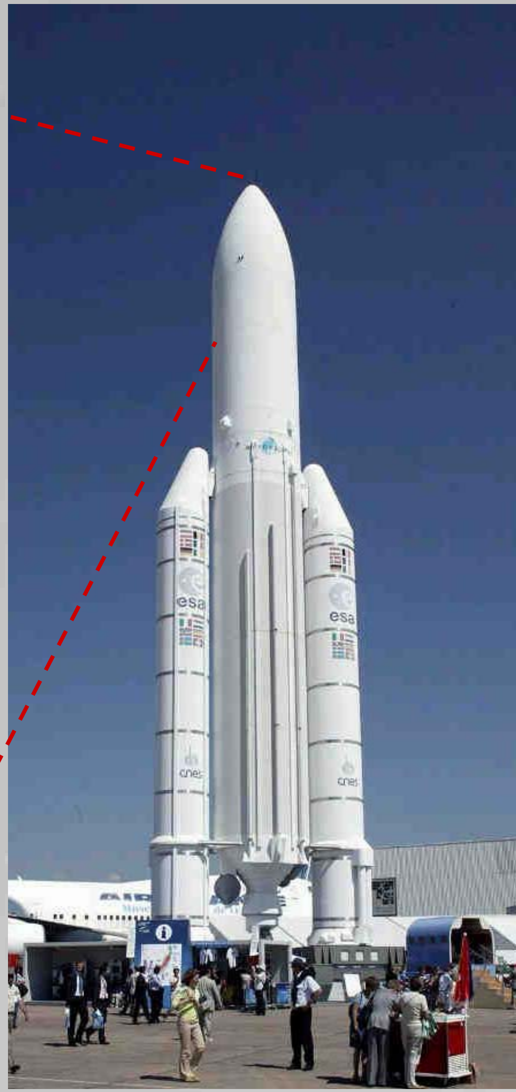

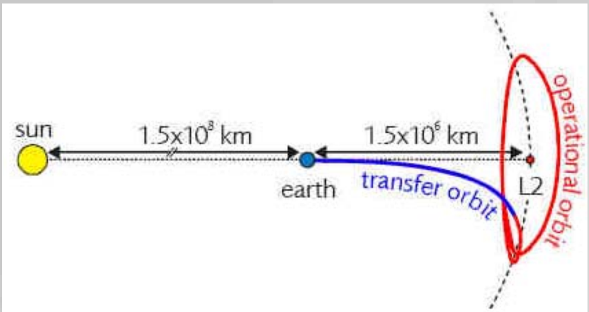

Launcher **ARIANE V**

with 4 Darwin sattelites
and a hub satellite

Heigh: up to 52 m
Diameter: up to 5.4 m
Max. Liftoff mass : 746 tonnes
Max. Payload mass : 9.5 tonnes

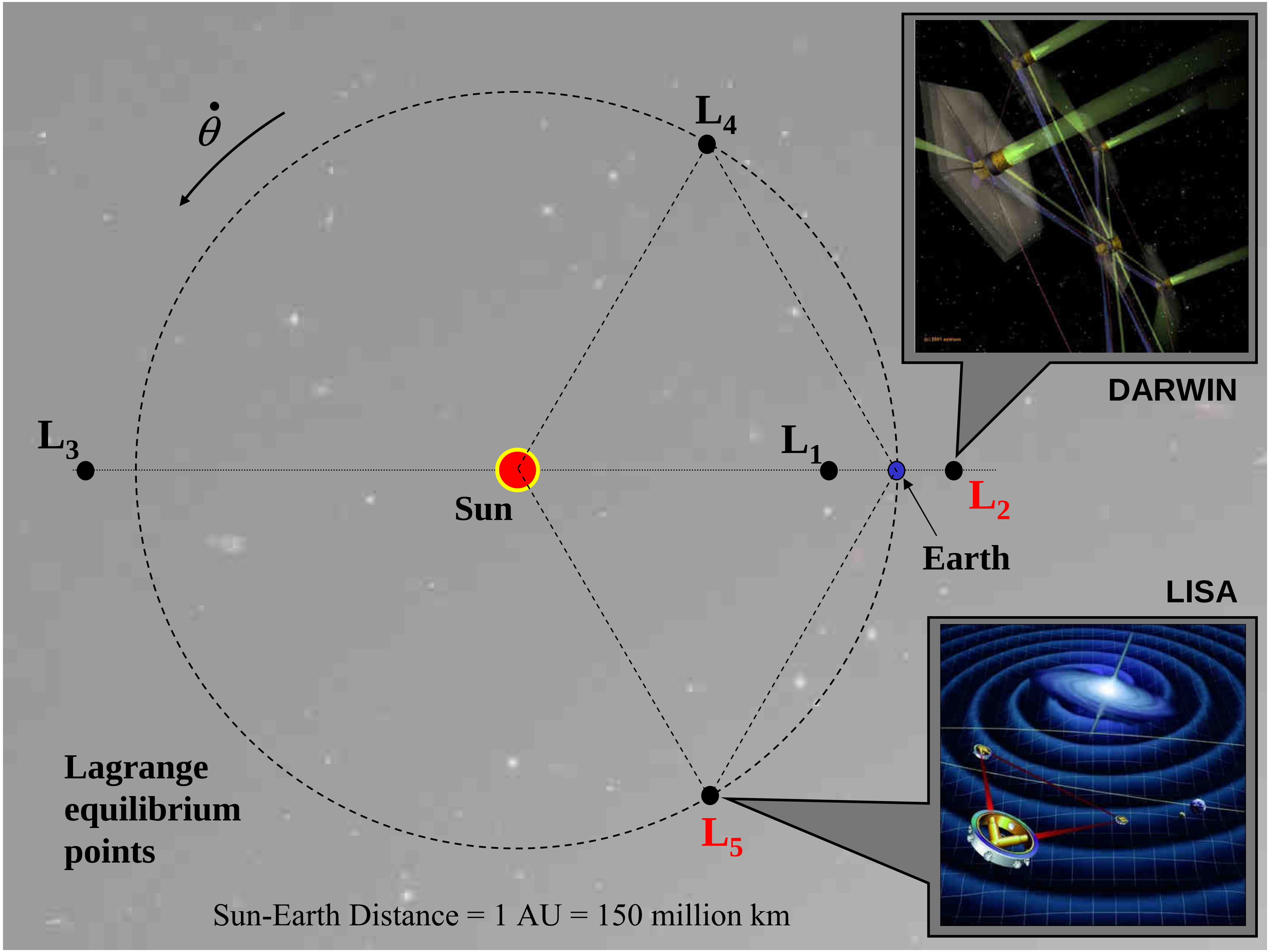

$\dot{\theta}$
L_4
L_3
Sun
L_1
Earth
L_2
L_5
DARWIN
LISA
Lagrange
equilibrium
points
Sun-Earth Distance = 1 AU = 150 million km

Satellite Description (I)

- The large sun-shield protect the instruments from the sun-light

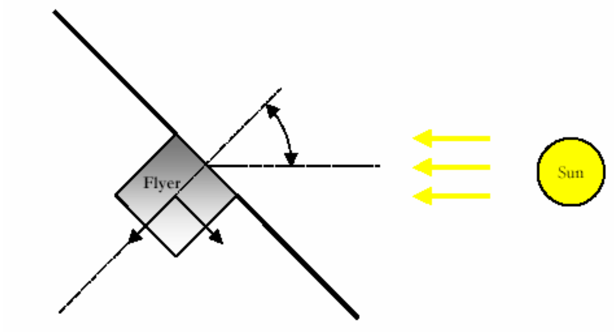

- Sun-shield characteristics:
  - Parallel to (X,Y) plan
  - Modelled with 6 large flexible beams attached to the rigid structure $\Rightarrow$ FLIMSY APPENDAGES

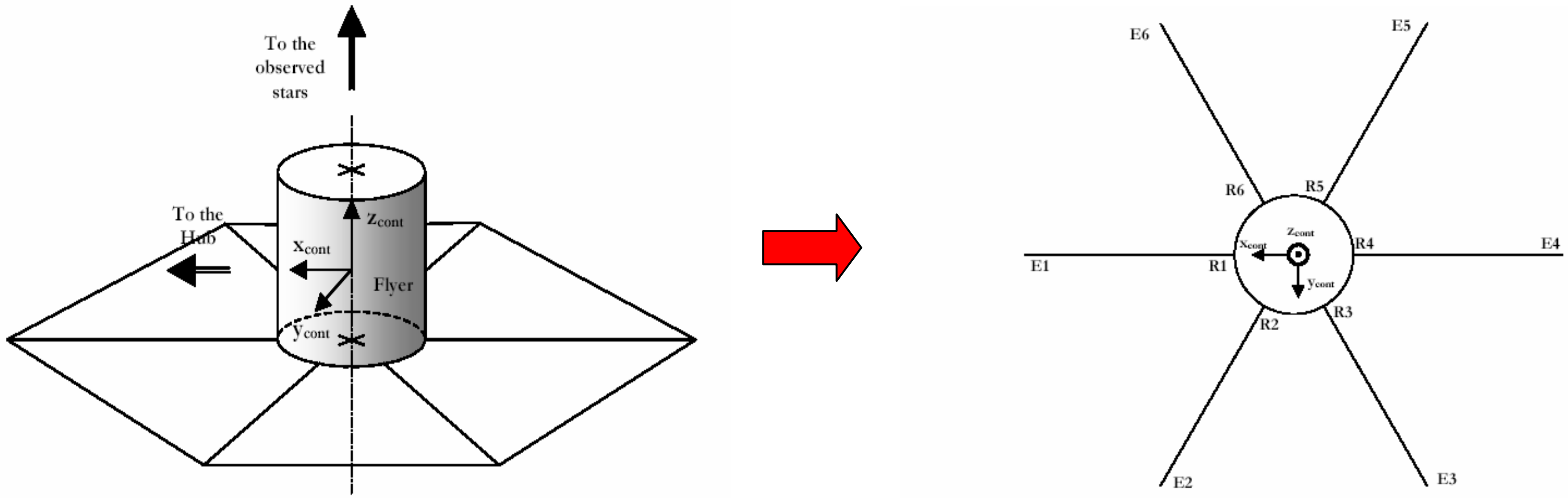

Mario Garcia-Sanz

Satellite Description (II)

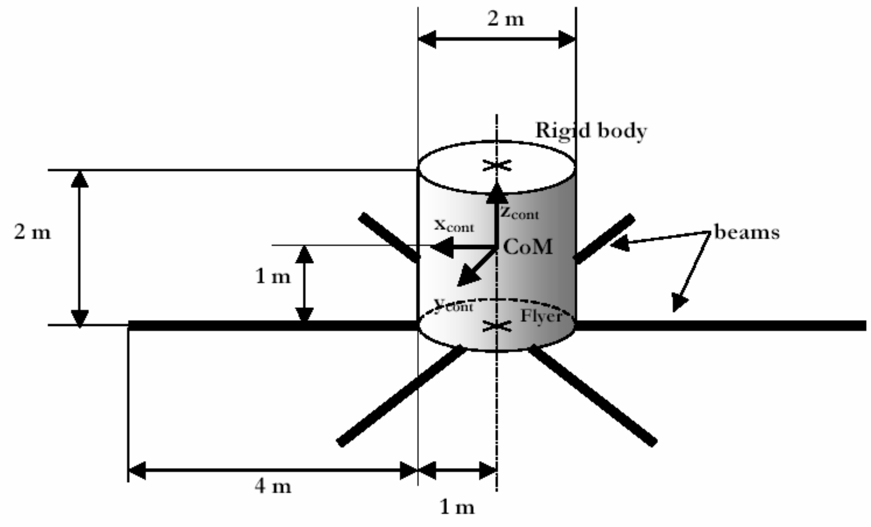

- **Satellite dimensions**
  - body mass : 500 kg
  - cylinder with Zcont as revolution axis. 2 m diameter and 2 m height
  - beam mass : 7 kg * 6 beams = 42 kg
  - length of simple beam : 4 m

- **Flexible modes**
  - Validated with finite elements methods
  - 1st flexible mode has been considered for each beam and along its X and Y axes

Parameter	Uncertainty range
Frequency	[0.05 , 0.5] Hz
Damping	[0.1 , 1] %
Mass	5 %
Inertia	1 %

SYSTEM DYNAMICS UNCERTAINTY
The satellite parameters vary within a certain range of uncertainty

Mario Garcia-Sanz

Satellite Modeling (I)

$$\begin{array}{c} \text{Position} \\ \\ \text{Attitude} \end{array} \quad \begin{bmatrix} x(s) \\ y(s) \\ z(s) \\ \varphi(s) \\ \theta(s) \\ \psi(s) \end{bmatrix} = \begin{bmatrix} p_{11}(s) & p_{12}(s) & p_{13}(s) & p_{14}(s) & p_{15}(s) & p_{16}(s) \\ p_{21}(s) & p_{22}(s) & p_{23}(s) & p_{24}(s) & p_{25}(s) & p_{26}(s) \\ p_{31}(s) & p_{32}(s) & p_{33}(s) & p_{34}(s) & p_{35}(s) & p_{36}(s) \\ p_{41}(s) & p_{42}(s) & p_{43}(s) & p_{44}(s) & p_{45}(s) & p_{46}(s) \\ p_{51}(s) & p_{52}(s) & p_{53}(s) & p_{54}(s) & p_{55}(s) & p_{56}(s) \\ p_{61}(s) & p_{62}(s) & p_{63}(s) & p_{64}(s) & p_{65}(s) & p_{66}(s) \end{bmatrix} \begin{bmatrix} F_x(s) \\ F_y(s) \\ F_z(s) \\ T_\varphi(s) \\ T_\theta(s) \\ T_\psi(s) \end{bmatrix} \quad \begin{array}{c} \text{Force} \\ \\ \text{Torque} \end{array}$$

where every $p_{ij}(s)$, i, j = 1, 2, … 6, is a **50 order** Laplace transfer function with **uncertainty**.

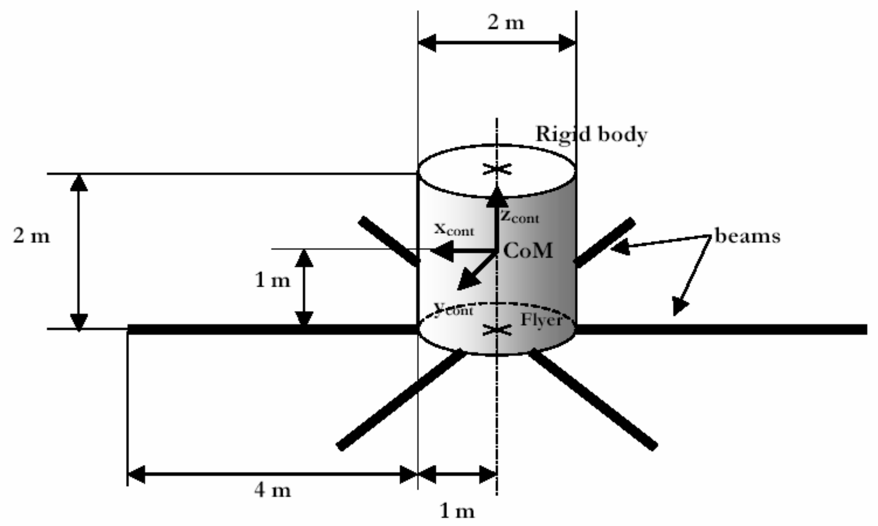

Mario Garcia-Sanz

Satellite Modeling (II)

$$\begin{bmatrix} x(s) \\ y(s) \\ z(s) \\ \varphi(s) \\ \theta(s) \\ \psi(s) \end{bmatrix} = \begin{bmatrix} p_{11}(s) & p_{12}(s) & p_{13}(s) & p_{14}(s) & p_{15}(s) & p_{16}(s) \\ p_{21}(s) & p_{22}(s) & p_{23}(s) & p_{24}(s) & p_{25}(s) & p_{26}(s) \\ p_{31}(s) & p_{32}(s) & p_{33}(s) & p_{34}(s) & p_{35}(s) & p_{36}(s) \\ p_{41}(s) & p_{42}(s) & p_{43}(s) & p_{44}(s) & p_{45}(s) & p_{46}(s) \\ p_{51}(s) & p_{52}(s) & p_{53}(s) & p_{54}(s) & p_{55}(s) & p_{56}(s) \\ p_{61}(s) & p_{62}(s) & p_{63}(s) & p_{64}(s) & p_{65}(s) & p_{66}(s) \end{bmatrix} \begin{bmatrix} F_x(s) \\ F_y(s) \\ F_z(s) \\ T_\varphi(s) \\ T_\theta(s) \\ T_\psi(s) \end{bmatrix}$$

Darwin Flyer 6DOF Dynamics

Bode plots of the plant matrix elements

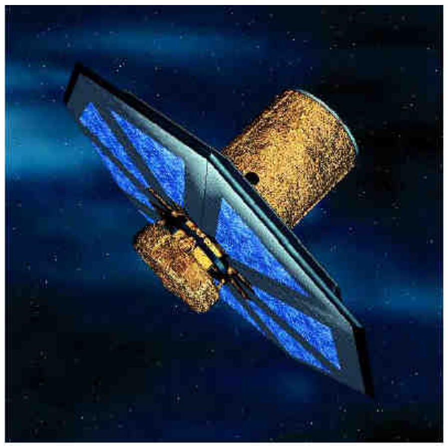

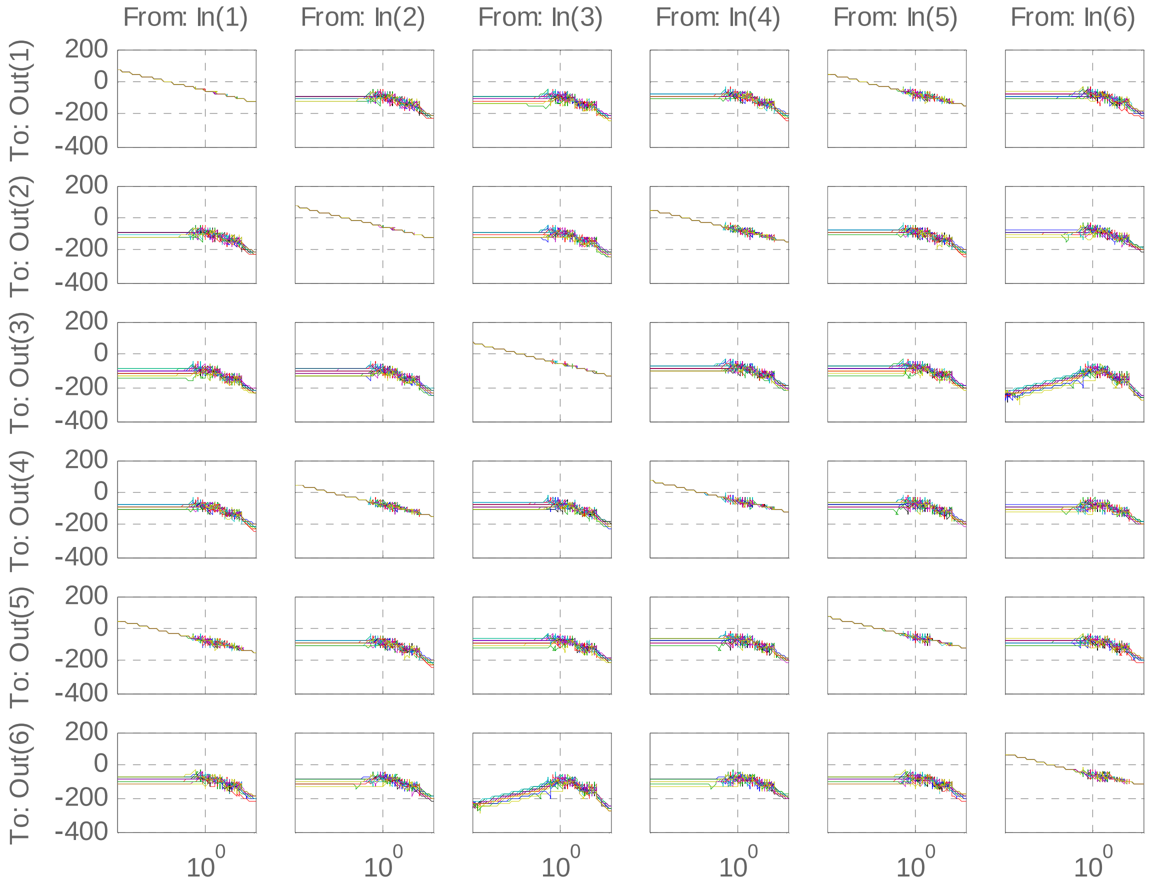

Mario Garcia-Sanz

Specificacions

Darwin-type Flyer Requirements

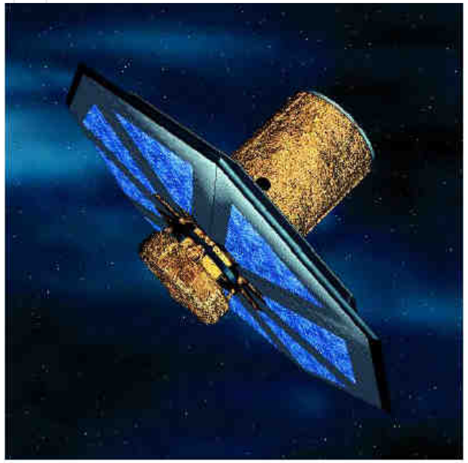

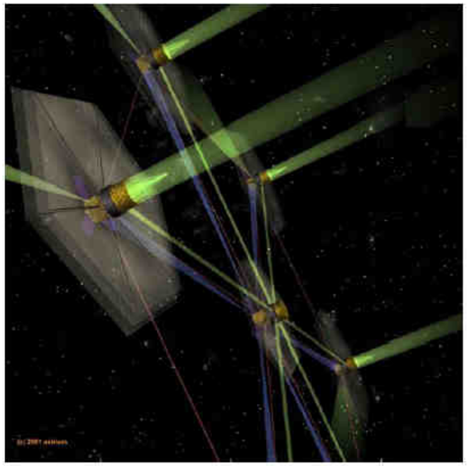

	Objective	Numerical Requirement
Astronomical Requirements	Position accuracy	Maximum absolute value: 1 μm for all axes
		Standard deviation: 0.33 μm for all axes
	Pointing accuracy	Maximum absolute value: 25.5 mas for all axes (3 σ)
		Standard deviation: 8.5 mas for all axes (1 σ)
Engineering Requirements	Bandwidth	~ 0.01 Hz for all axes
	Saturation limits	Maximum force: 150 μN Maximum torque: 150 μNm
	Rejection of high frequency noises (from measurement and actuation)	High roll-off after the bandwidth
Control Requirements	Stability margins	$\max_{\omega} \lvert \boldsymbol{T}(j\omega) \rvert < 2$ $\max_{\omega} \lvert \boldsymbol{S}(j\omega) \rvert < 2$
	Loop interaction	Minimum
	Rejection of flexible modes	Maximum
	Controller complexity and order	Minimum

Mario Garcia-Sanz

Project Objectives

- **Analysis** of the new methodology:

  non-diagonal MIMO QFT robust control design:

- García-Sanz M., Egaña I. (2002).
  Quantitative Non-diagonal Controller Design for Multivariable Systems with Uncertainty.
  Int. J. Robust Nonlinear Control, Vol. 12, No. 4, pp. 321-333.

- García-Sanz M., Egaña I., Barreras M. (2005).
  Design of quantitative feedback theory non-diagonal controllers for use in uncertain multiple-input multiple-output systems.
  IEE Control Theory and Applications. Vol. 152, N. 02, pp. 177-187.

- García-Sanz M., Barreras M. (2006).
  Non-diagonal QFT controller design for a 3-input 3-output industrial Furnace.
  J. of Dynamic Systems, Measurement & Control, *ASME*, Vol. 128, pp. 319-329. USA.

- Garcia-Sanz M., Eguinoa I., Barreras M., Bennani S. (2008).
  Non-diagonal MIMO QFT Controller Design for Darwin-type Spacecraft with large flimsy appendages.
  J.Dynamic Systems, Measurement & Control, ASME,USA.Vol.130, January.

- **Application**: Control of Position + Attitude of a Darwin spacecraft with flexible appendages
- **Comparison** with previous studies (H-infinity and diagonal MIMO QFT)

BENCHMARK SIMULATOR

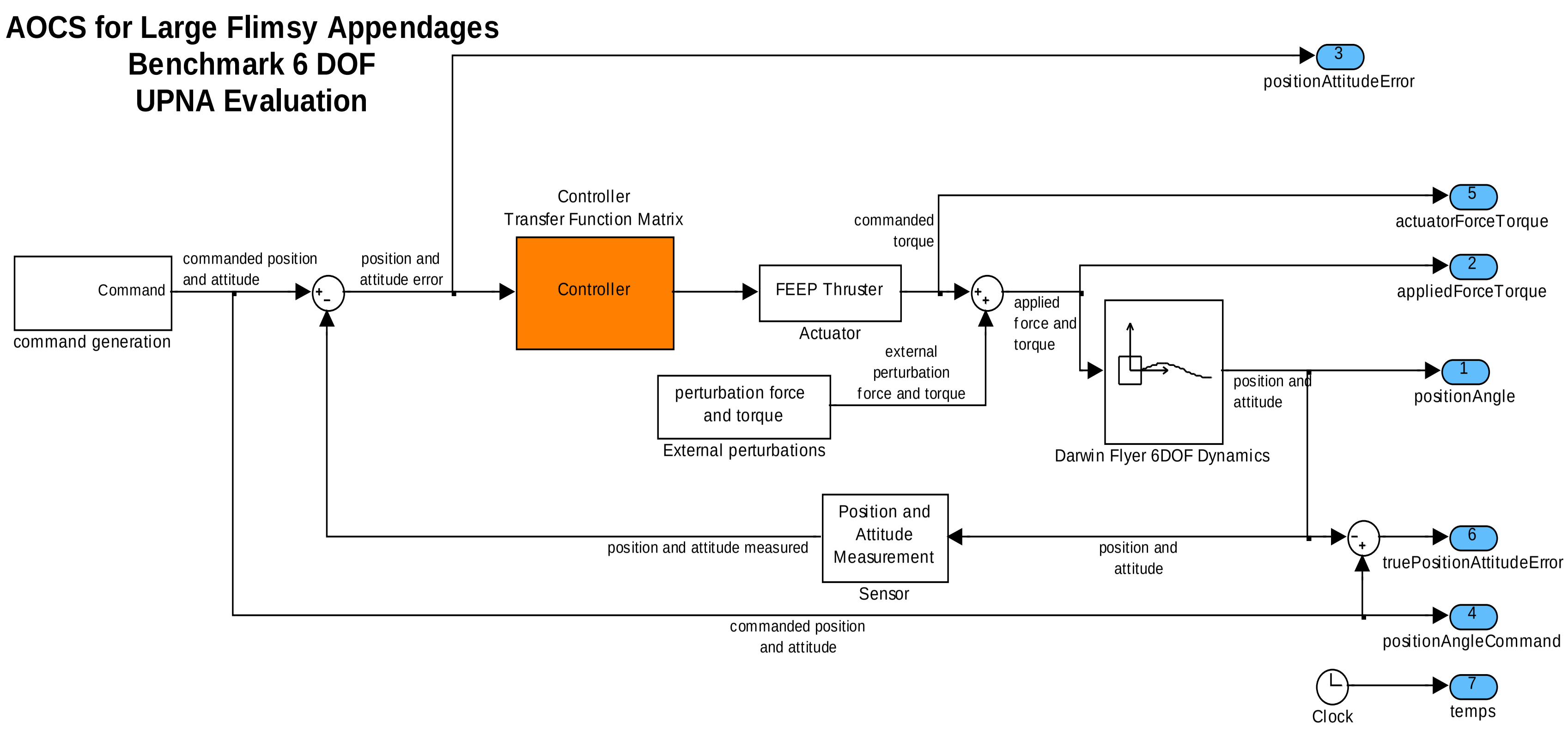

Developed by Astrium Space
for ESA-ESTEC (Holland)

300 different plants due
to uncertainty.
Monte-Carlo analysis

Mario Garcia-Sanz

COUPLING ANALYSIS AND CONTROLLER STRUCTURE (I)

RGA analysis of the Darwin-type satellite dynamic model performed for different frequencies

$$\boldsymbol{RGA}(j\omega) = \begin{bmatrix} \lambda_{11} & \lambda_{12} & \cdots & \lambda_{1n} \\ \lambda_{21} & \lambda_{22} & \cdots & \lambda_{2n} \\ \vdots & \vdots & \cdots & \vdots \\ \lambda_{n1} & \lambda_{n2} & \cdots & \lambda_{nn} \end{bmatrix} = \boldsymbol{P}(j\omega) \otimes (\boldsymbol{P}^{-1}(j\omega))^T$$

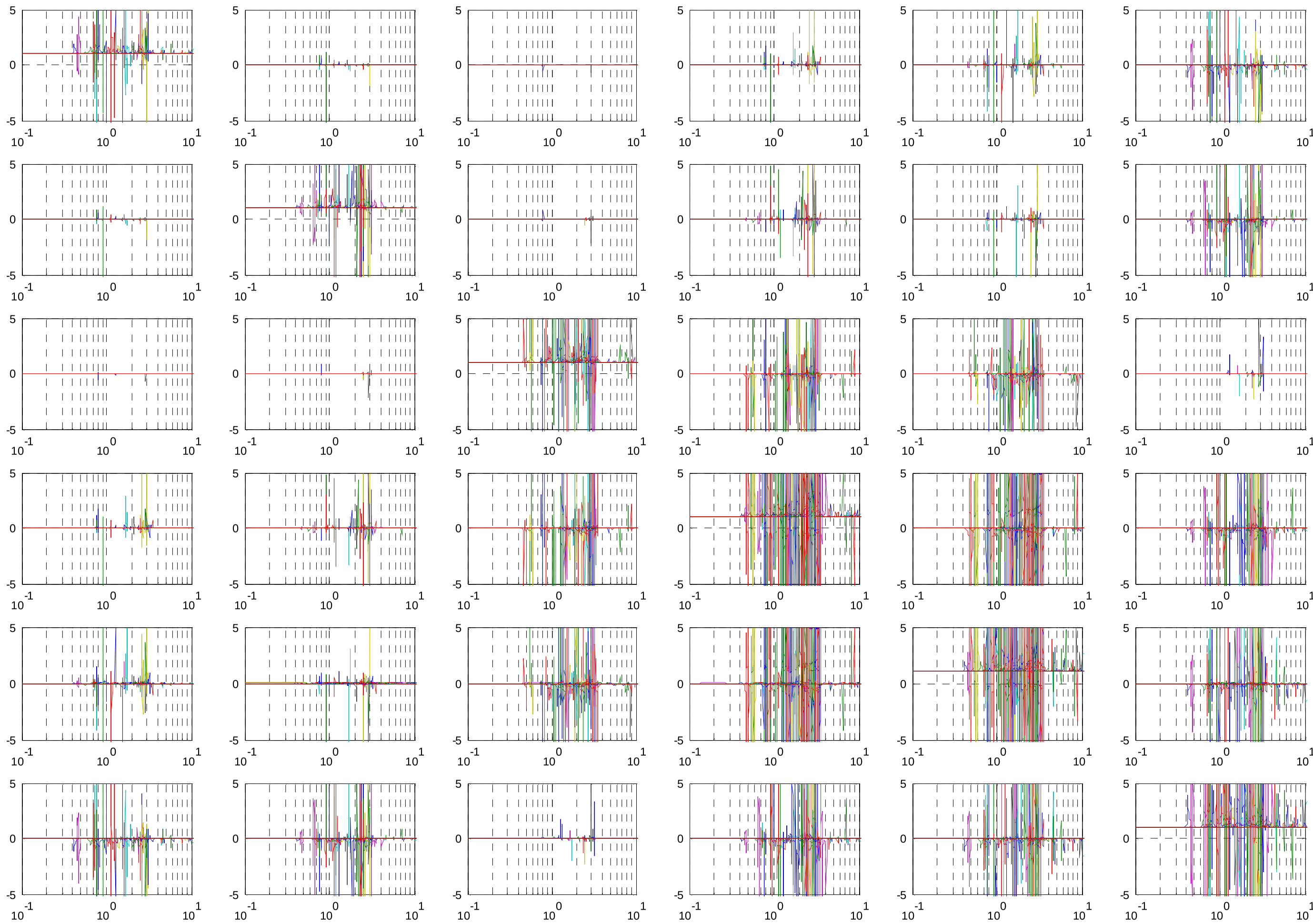

Mario Garcia-Sanz

COUPLING ANALYSIS AND CONTROLLER STRUCTURE (II)

From low frequency up to 0.19 rad/sec
And from 3.51 rad/sec to infinity

$$\left|\boldsymbol{RGA}_{\left(\omega=6.28\cdot10^{-4}\,\text{rad/sec}\right)}\right| = \begin{bmatrix} \boldsymbol{1.0064} & 0 & 0 & 0 & \boldsymbol{0.0064} & 0 \\ 0 & \boldsymbol{1.0064} & 0 & \boldsymbol{0.0064} & 0 & 0 \\ 0 & 0 & \boldsymbol{1} & 0 & 0 & 0 \\ 0 & \boldsymbol{0.0064} & 0 & \boldsymbol{1.0064} & 0 & 0 \\ \boldsymbol{0.0064} & 0 & 0 & 0 & \boldsymbol{1.0064} & 0 \\ 0 & 0 & 0 & 0 & 0 & \boldsymbol{1} \end{bmatrix}$$

$$\left|\boldsymbol{RGA}_{\left(\omega=0.8\,\text{rad/sec}\right)}\right| = \begin{bmatrix} \boldsymbol{1.1674} & 0.0001 & 0.0000 & 0.0012 & 0.3720 & 0.0001 \\ 0.0001 & \boldsymbol{1.0180} & 0.0000 & 0.0305 & 0.0013 & 0.0004 \\ 0.0000 & 0.0000 & \boldsymbol{4.8592} & 0.3468 & \boldsymbol{4.1456} & 0.0000 \\ 0.0012 & 0.0305 & 0.3468 & \boldsymbol{3.2030} & \boldsymbol{2.3865} & 0.0006 \\ 0.3720 & 0.0013 & \boldsymbol{4.1456} & \boldsymbol{2.3865} & \boldsymbol{7.2470} & 0.0008 \\ 0.0001 & 0.0004 & 0.0000 & 0.0006 & 0.0008 & \boldsymbol{1.0009} \end{bmatrix}$$

Other results

$$\left|\boldsymbol{RGA}_{\left(\omega=1\,\text{rad/sec}\right)}\right| = \begin{bmatrix} \boldsymbol{0.9899} & 0.0002 & 0.0000 & 0.0001 & 0.0003 & 0.0102 \\ 0.0002 & \boldsymbol{0.9082} & 0.0000 & 0.0050 & 0.0009 & 0.0963 \\ 0.0000 & 0.0000 & \boldsymbol{3.1307} & \boldsymbol{2.3373} & 0.1110 & 0.0000 \\ 0.0001 & 0.0050 & \boldsymbol{2.3373} & \boldsymbol{12.5674} & \boldsymbol{9.4613} & 0.0690 \\ 0.0003 & 0.0009 & 0.1110 & \boldsymbol{9.4613} & \boldsymbol{10.2042} & 0.0302 \\ 0.0102 & 0.0963 & 0.0000 & 0.0690 & 0.0302 & \boldsymbol{0.7970} \end{bmatrix}$$

Results of the RGA matrix
for various frequencies
(significant values in bold)

Mario Garcia-Sanz

COUPLING ANALYSIS AND CONTROLLER STRUCTURE (III)

First choice →

$$\left| RGA_{(\omega=6.28\cdot10^{-4}\ \mathrm{rad/sec})} \right| = \begin{bmatrix} \mathbf{1.0064} & 0 & 0 & 0 & \mathbf{0.0064} & 0 \\ 0 & \mathbf{1.0064} & 0 & \mathbf{0.0064} & 0 & 0 \\ 0 & 0 & \mathbf{1} & 0 & 0 & 0 \\ 0 & \mathbf{0.0064} & 0 & \mathbf{1.0064} & 0 & 0 \\ \mathbf{0.0064} & 0 & 0 & 0 & \mathbf{1.0064} & 0 \\ 0 & 0 & 0 & 0 & 0 & \mathbf{1} \end{bmatrix}$$

↓

$$G(s) = \begin{bmatrix} g_{11}(s) & 0 & 0 & 0 & g_{15}(s) & 0 \\ 0 & g_{22}(s) & 0 & g_{24}(s) & 0 & 0 \\ 0 & 0 & g_{33}(s) & 0 & 0 & 0 \\ 0 & g_{42}(s) & 0 & g_{44}(s) & 0 & 0 \\ g_{51}(s) & 0 & 0 & 0 & g_{55}(s) & 0 \\ 0 & 0 & 0 & 0 & 0 & g_{66}(s) \end{bmatrix}$$

Control Subsystem	Controller Element	Corresponding Plant Description
SISO: loop 3	g_{33}	Force $_Z \rightarrow$ Position $_Z$
SISO: loop 6	g_{66}	Torque $_Z \rightarrow$ Attitude $_Z$
2x2 MIMO: loops 1 and 5	g_{11}	Force $_X \rightarrow$ Position $_X$
	g_{55}	Torque $_Y \rightarrow$ Attitude $_Y$
	g_{51}	Force $_X \rightarrow$ Attitude $_Y$
	g_{15}	Torque $_Y \rightarrow$ Position $_X$
2x2 MIMO: loops 2 and 4	g_{22}	Force $_Y \rightarrow$ Position $_Y$
	g_{44}	Torque $_X \rightarrow$ Attitude $_X$
	g_{42}	Force $_Y \rightarrow$ Attitude $_X$
	g_{24}	Torque $_X \rightarrow$ Position $_Y$

Mario Garcia-Sanz

COUPLING ANALYSIS AND CONTROLLER STRUCTURE (IV)

If requirements are not fulfilled, Second choice:

$$\boldsymbol{G}(s)=\begin{bmatrix} g_{11}(s) & 0 & 0 & 0 & g_{15}(s) & 0 \\ 0 & g_{22}(s) & 0 & g_{24}(s) & 0 & 0 \\ 0 & 0 & g_{33}(s) & g_{34}(s) & g_{35}(s) & 0 \\ 0 & g_{42}(s) & g_{43}(s) & g_{44}(s) & g_{45}(s) & 0 \\ g_{51}(s) & 0 & g_{53}(s) & g_{54}(s) & g_{55}(s) & 0 \\ 0 & 0 & 0 & 0 & 0 & g_{66}(s) \end{bmatrix}$$

According to:

$$\left|\boldsymbol{RGA}_{\ (\omega=0.8\ \mathrm{rad/sec})}\right| = \begin{bmatrix} \boldsymbol{1.1674} & 0.0001 & 0.0000 & 0.0012 & 0.3720 & 0.0001 \\ 0.0001 & \boldsymbol{1.0180} & 0.0000 & 0.0305 & 0.0013 & 0.0004 \\ 0.0000 & 0.0000 & \boldsymbol{4.8592} & 0.3468 & \boldsymbol{4.1456} & 0.0000 \\ 0.0012 & 0.0305 & 0.3468 & \boldsymbol{3.2030} & \boldsymbol{2.3865} & 0.0006 \\ 0.3720 & 0.0013 & \boldsymbol{4.1456} & \boldsymbol{2.3865} & \boldsymbol{7.2470} & 0.0008 \\ 0.0001 & 0.0004 & 0.0000 & 0.0006 & 0.0008 & \boldsymbol{1.0009} \end{bmatrix}$$

$$\left|\boldsymbol{RGA}_{\ (\omega=6.28\cdot 10^{-4}\ \mathrm{rad/sec})}\right| = \begin{bmatrix} \boldsymbol{1.0064} & 0 & 0 & 0 & \boldsymbol{0.0064} & 0 \\ 0 & \boldsymbol{1.0064} & 0 & \boldsymbol{0.0064} & 0 & 0 \\ 0 & 0 & \boldsymbol{1} & 0 & 0 & 0 \\ 0 & \boldsymbol{0.0064} & 0 & \boldsymbol{1.0064} & 0 & 0 \\ \boldsymbol{0.0064} & 0 & 0 & 0 & \boldsymbol{1.0064} & 0 \\ 0 & 0 & 0 & 0 & 0 & \boldsymbol{1} \end{bmatrix}$$

$$\left|\boldsymbol{RGA}_{\ (\omega=1\ \mathrm{rad/sec})}\right| = \begin{bmatrix} \boldsymbol{0.9899} & 0.0002 & 0.0000 & 0.0001 & 0.0003 & 0.0102 \\ 0.0002 & \boldsymbol{0.9082} & 0.0000 & 0.0050 & 0.0009 & 0.0963 \\ 0.0000 & 0.0000 & \boldsymbol{3.1307} & \boldsymbol{2.3373} & 0.1110 & 0.0000 \\ 0.0001 & 0.0050 & \boldsymbol{2.3373} & \boldsymbol{12.5674} & \boldsymbol{9.4613} & 0.0690 \\ 0.0003 & 0.0009 & 0.1110 & \boldsymbol{9.4613} & \boldsymbol{10.2042} & 0.0302 \\ 0.0102 & 0.0963 & 0.0000 & 0.0690 & 0.0302 & \boldsymbol{0.7970} \end{bmatrix}$$

Mario Garcia-Sanz

ROBUST SPECIFICATIONS (I)

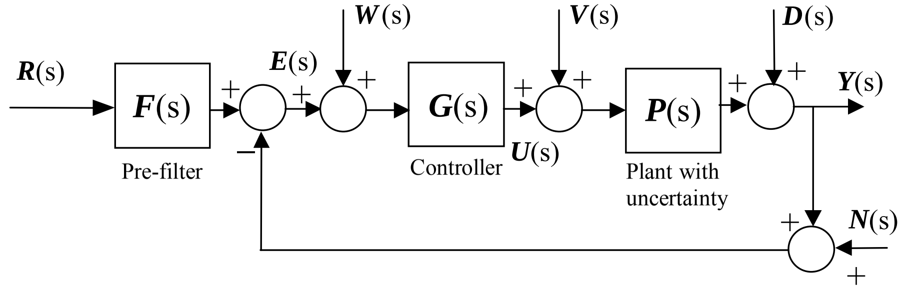

Transfer functions and specification models	*Type*	*Description*
$\lvert T_1(j\omega)\rvert = \left\lvert\frac{L(j\omega)}{1+L(j\omega)}\right\rvert = \left\lvert\frac{U(j\omega)}{V(j\omega)}\right\rvert = \left\lvert\frac{Y(j\omega)}{N(j\omega)}\right\rvert = \left\lvert\frac{Y(j\omega)}{W(j\omega)}\right\rvert \le \delta_1(\omega),\ \omega\in\Omega_1$	1	- Robust stability - Sensor noise attenuation - Attenuation of external perturbations and flexible modes
$\lvert T_2(j\omega)\rvert = \left\lvert\frac{1}{1+L(j\omega)}\right\rvert = \left\lvert\frac{Y(j\omega)}{D(j\omega)}\right\rvert = \left\lvert\frac{E(j\omega)}{N(j\omega)}\right\rvert \le \delta_2(\omega),\ \ \omega\in\Omega_2$	2	- Robust sensitivity - Sensor noise attenuation
$\lvert T_3(j\omega)\rvert = \left\lvert\frac{P(j\omega)}{1+L(j\omega)}\right\rvert = \left\lvert\frac{Y(j\omega)}{V(j\omega)}\right\rvert = \left\lvert\frac{E(j\omega)}{V(j\omega)}\right\rvert \le \delta_3(\omega),\ \ \omega\in\Omega_3$	3	- Robust disturbance rejection at plant input
$\lvert T_4(j\omega)\rvert = \left\lvert\frac{G(j\omega)}{1+L(j\omega)}\right\rvert = \left\lvert\frac{U(j\omega)}{D(j\omega)}\right\rvert = \left\lvert\frac{U(j\omega)}{N(j\omega)}\right\rvert = \left\lvert\frac{U(j\omega)}{W(j\omega)}\right\rvert = \left\lvert\frac{U(j\omega)}{R(j\omega)F(j\omega)}\right\rvert \le \delta_4(\omega),\ \omega\in\Omega_4$	4	- Robust control effort attenuation of actuator noise, sensor noise and external perturbations

ROBUST SPECIFICATIONS (II)

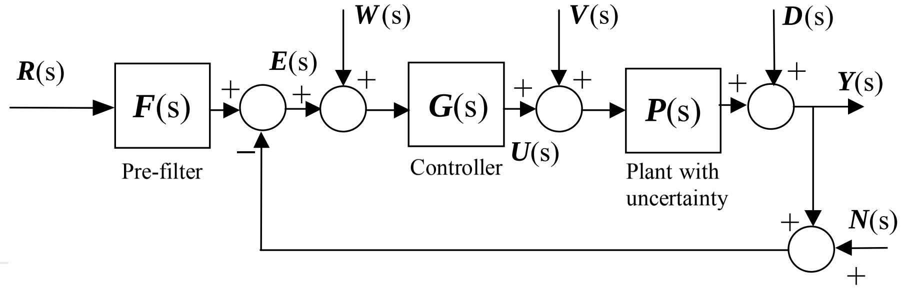

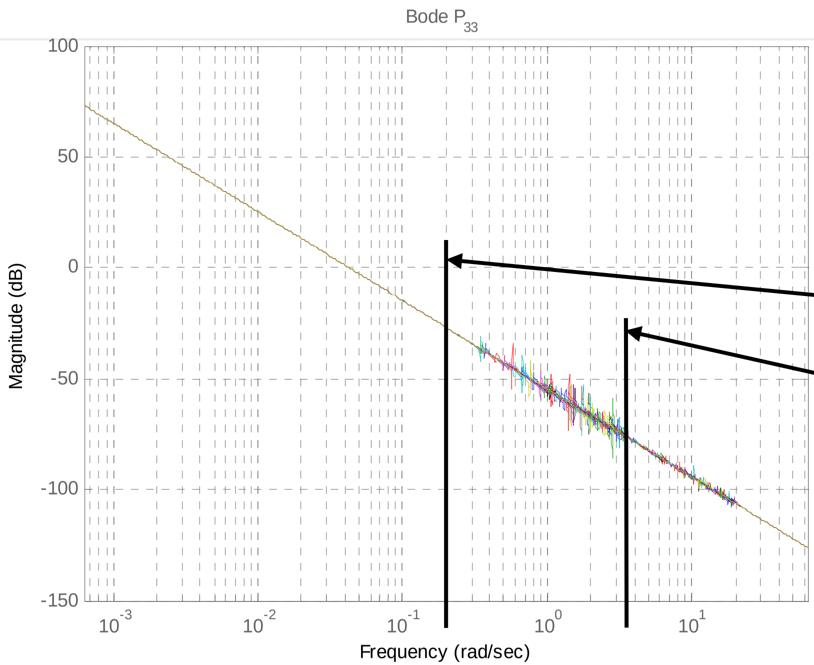

10^{-4} = 0.0001 Hz = 0.00062 rad/s

$10^{-1.5}$ = 0.0316 Hz = 0.2 rad/s

$10^{-0.25}$ = 0.562 Hz = 3.53 rad/s

10^{1} = 10 Hz = 62.8 rad/s

Frequencies of interest (Hz)	
freq1	logspace(-4, -1.5, 4)
freq2 (Problematic range of frequencies)	logspace(-1.5, -0.25, 12)
freq3	logspace(-0.25, 1, 3)

Mario Garcia-Sanz

SISO DESIGNS

Classical QFT robust control design for SISO subsystems:

– Loop 3

– Loop 6

Steps 1a and 1b

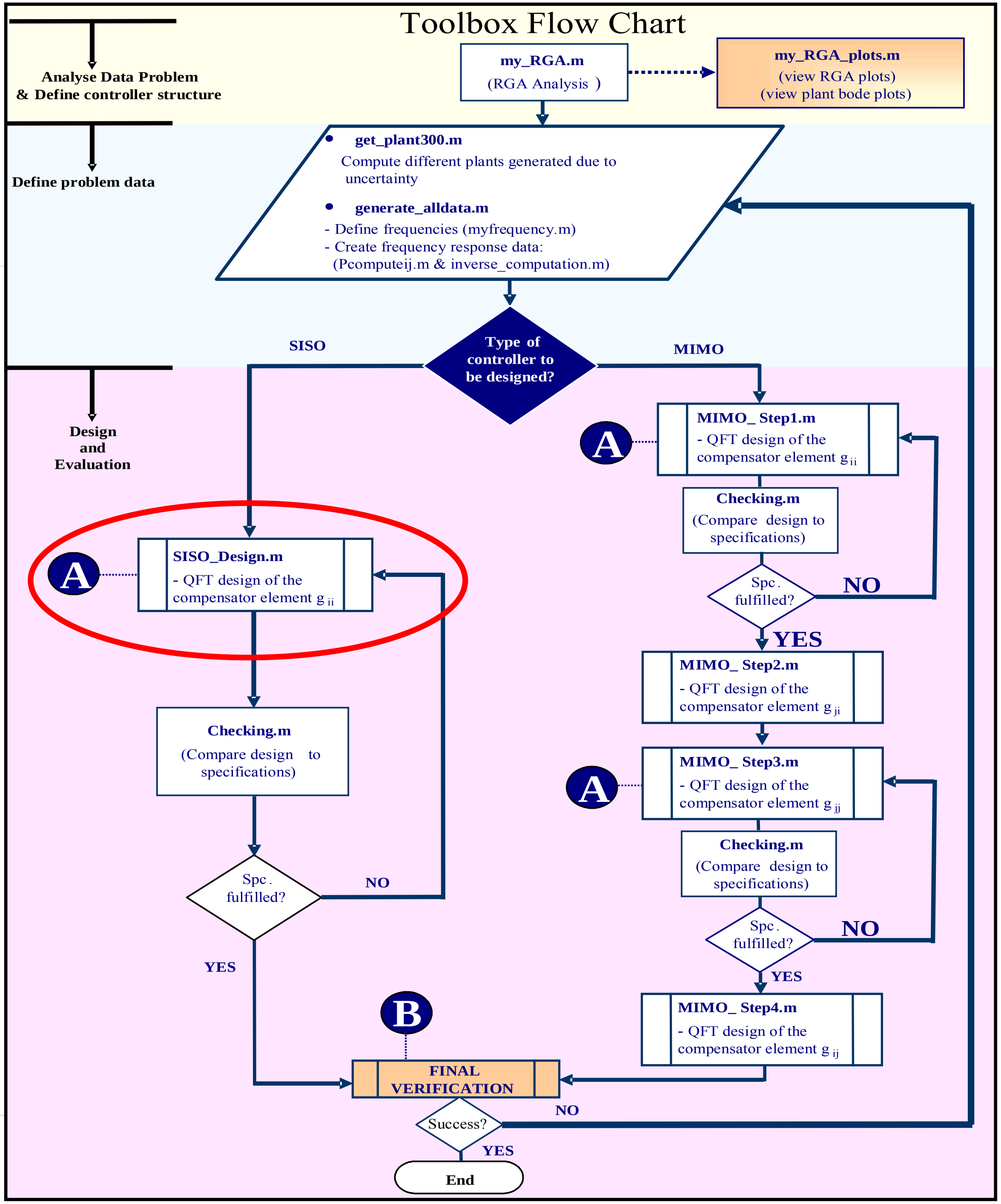

Step 1a) : design of the diagonal controller $g_{33}(s)$

Robust Performance Specifications

Robust stability (Type 1)

$$\left| \frac{P(s)\,G(s)}{1+P(s)\,G(s)} \right| = |T(s)| \le 1.85$$

Robust sensitivity (Type 2)

$$\left| \frac{1}{1+P(s)\,G(s)} \right| = |S(s)| \le 2$$

Robust disturbance rejection at plant input (Type 3)

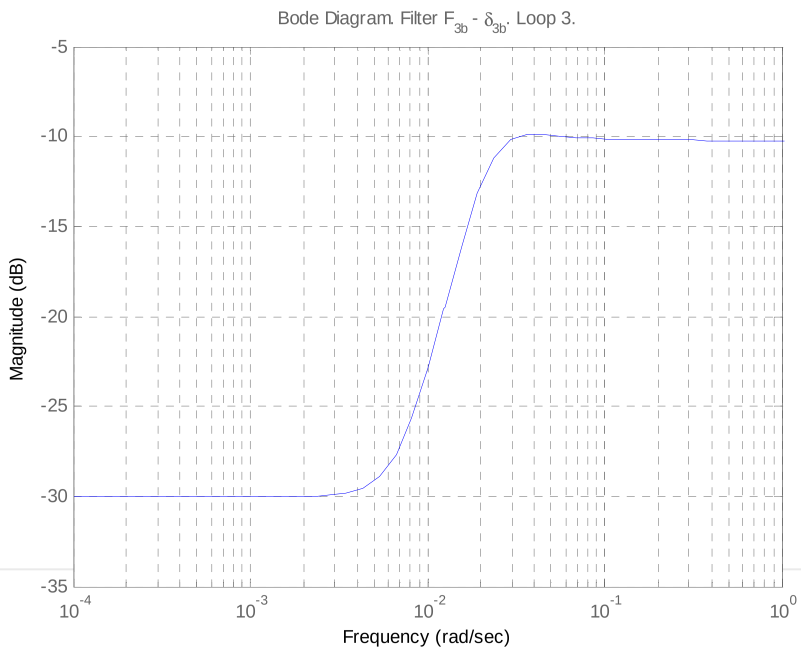

Robust control effort attenuation (Type 4)

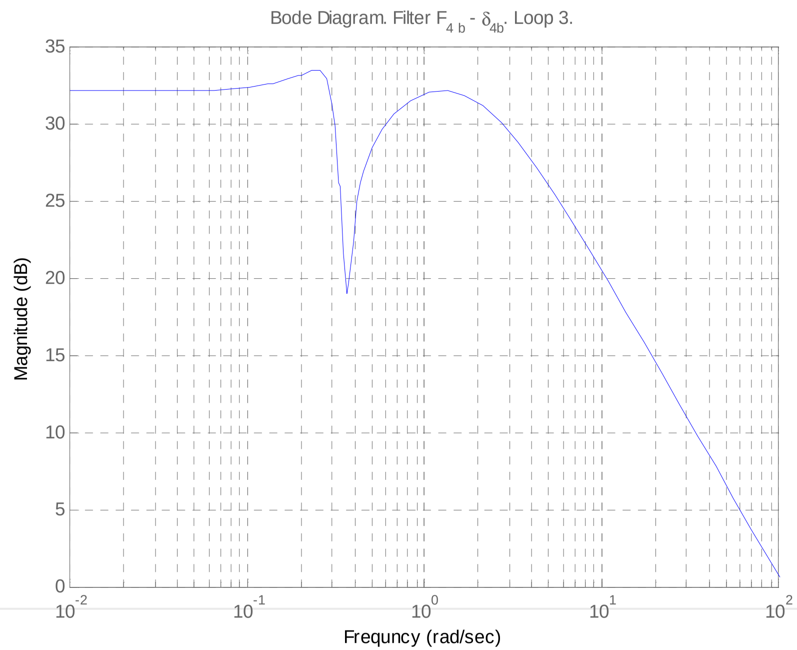

Mario Garcia-Sanz

Step 1a) : design of the diagonal controller $g_{33}(s)$

Templates of the plant $p_{33}(s)$

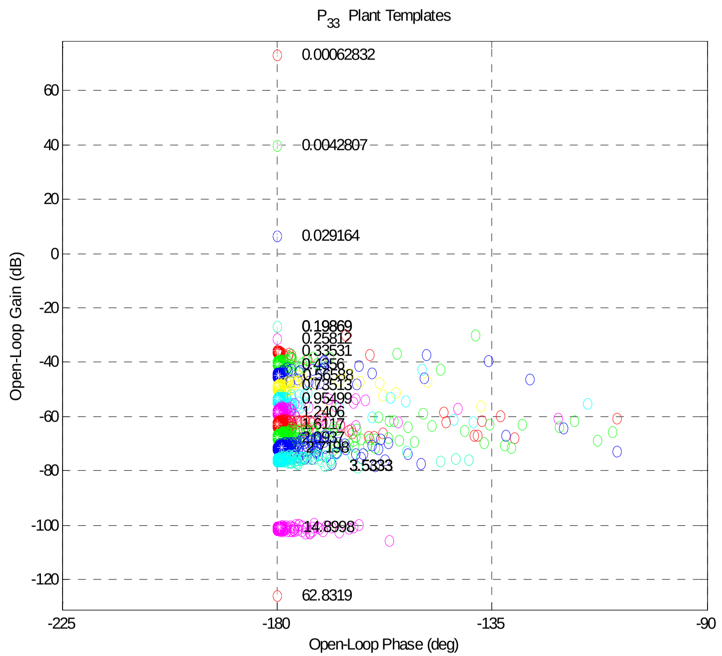

Loop-shaping $L_{33}(s)=p_{33}(s)\ g_{33}(s)$

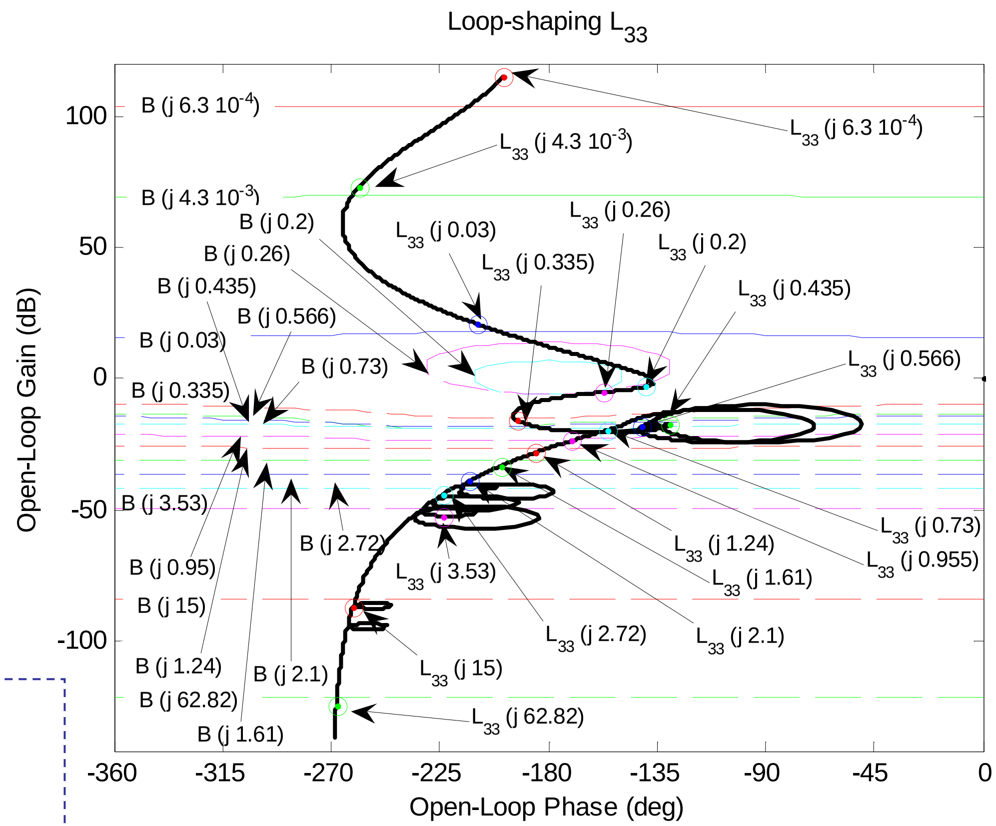

The subsystem is found to be **stable** according to the sufficient stability conditions (a and b).

Step 1b) : design of the diagonal controller $g_{66}(s)$

Robust Performance Specifications

Robust stability (Type 1)

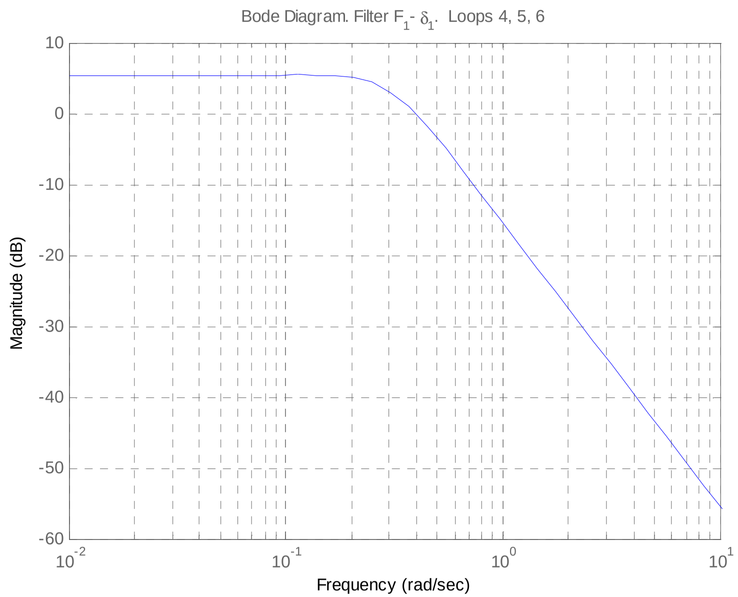

Robust sensitivity (Type 2)

$$\left| \frac{1}{1+\boldsymbol{P}(s)\,\boldsymbol{G}(s)} \right| = |\boldsymbol{S}(s)| \leq 2$$

Robust disturbance rejection
at plant input (Type 3)

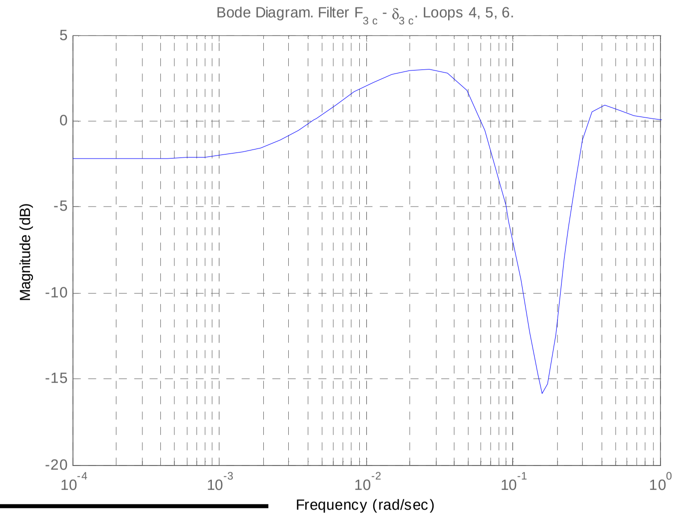

Robust control effort attenuation (Type 4)

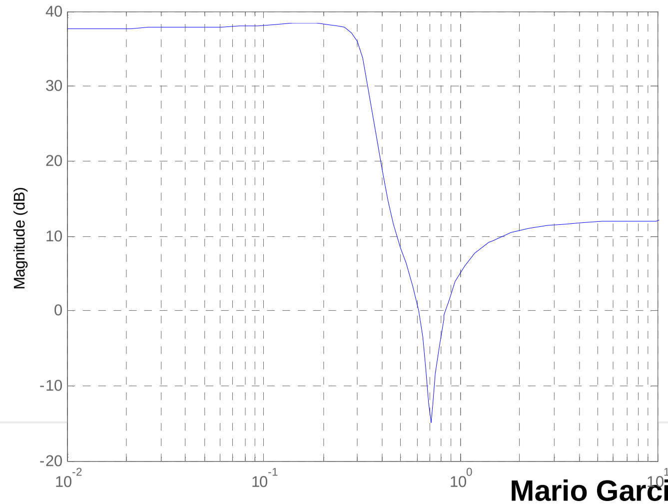

Mario Garcia-Sanz

Step 1b) : design of the diagonal controller $g_{66}(s)$

Templates of the plant $p_{66}(s)$

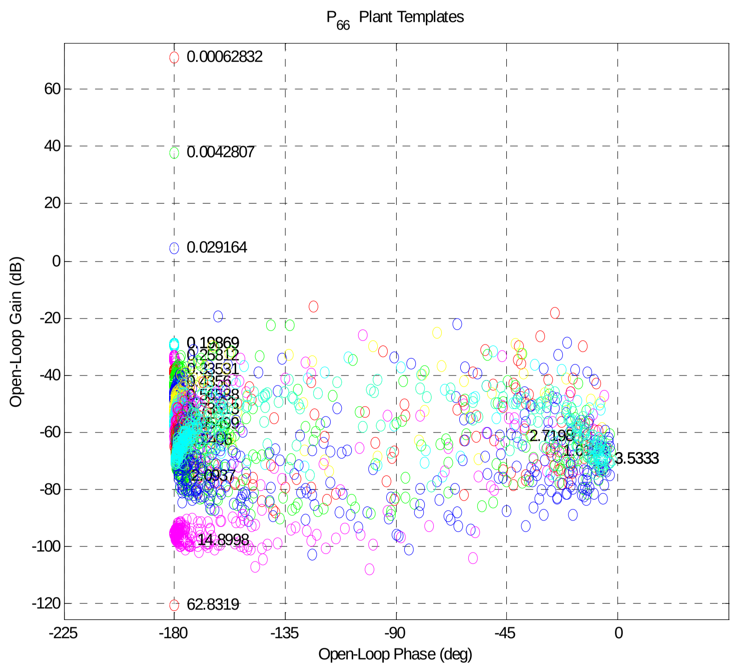

Loop-shaping $L_{66}(s)=p_{66}(s)\ g_{66}(s)$

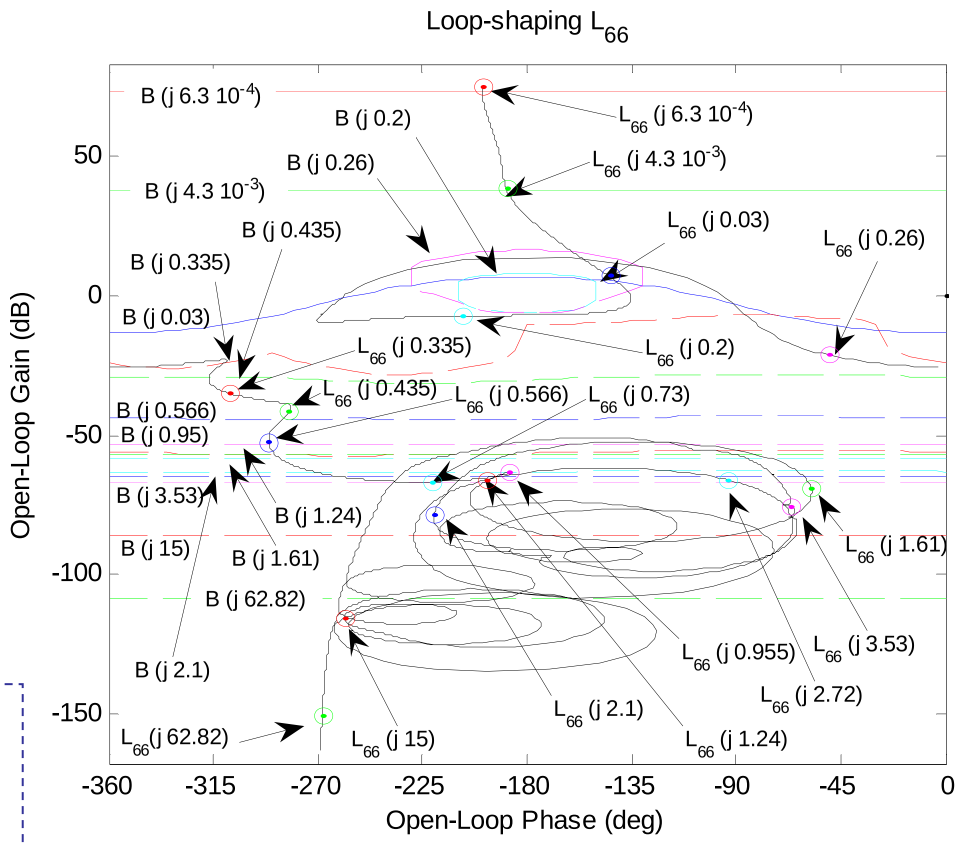

The subsystem is found to be **stable** according to the sufficient stability conditions (a and b).

MIMO DESIGNS

Non-diagonal MIMO QFT design methodology for MIMO subsystems:

- – Loops 1 and 5
- – Loops 2 and 4

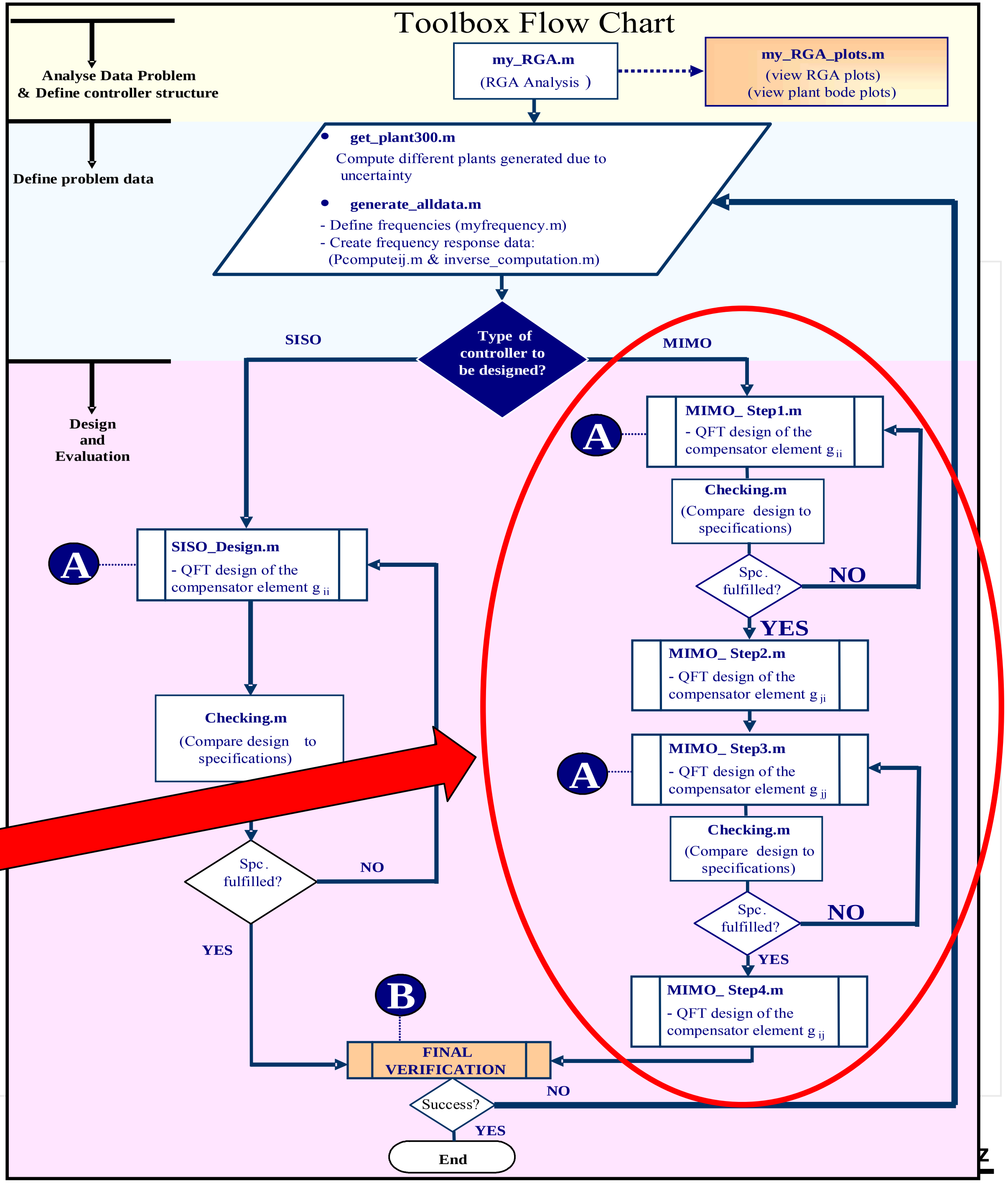

Steps 2 a and 2 b

$$G = \begin{bmatrix} g_{11} & 0 \\ g_{51} & 0 \end{bmatrix} \Rightarrow \begin{bmatrix} g_{11} & g_{15} \\ g_{51} & g_{55} \end{bmatrix}$$

MIMO DESIGNS

Step 2a) : MIMO subsystem loops 1 and 5

Design of the diagonal controller $g_{11}(s)$

Robust Performance Specifications

Robust stability (Type 1)

$$\left| \frac{P(s)\,G(s)}{1+P(s)\,G(s)} \right| = |T(s)| \le 1.85$$

Robust sensitivity (Type 2)

$$\left| \frac{1}{1+P(s)\,G(s)} \right| = |S(s)| \le 2$$

Robust disturbance rejection at plant input (Type 3)

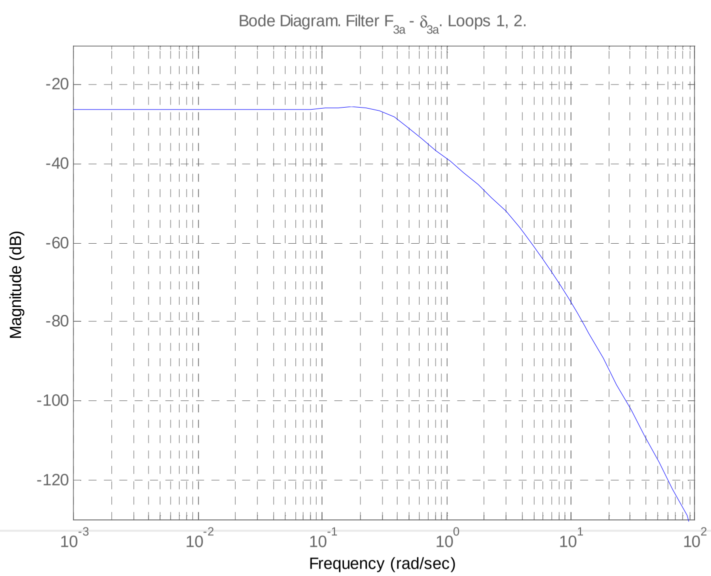

Robust control effort attenuation (Type 4)

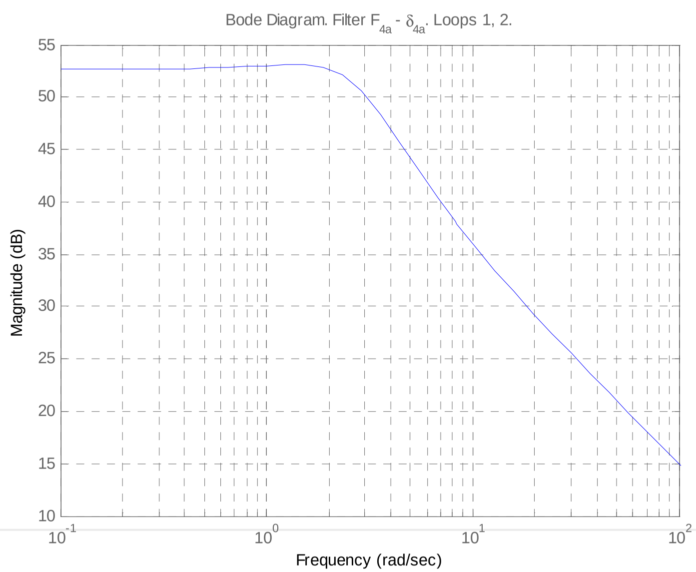

Mario Garcia-Sanz

$$G = \begin{bmatrix} g_{11} & 0 \\ g_{51} & 0 \end{bmatrix} \Rightarrow \begin{bmatrix} g_{11} & g_{15} \\ g_{51} & g_{55} \end{bmatrix}$$

MIMO DESIGNS

Step 2a) : MIMO subsystem loops 1 and 5

Design of the diagonal controller $g_{11}(s)$

Templates of the plant $(p_{11}^{*e}(s))^{-1}$

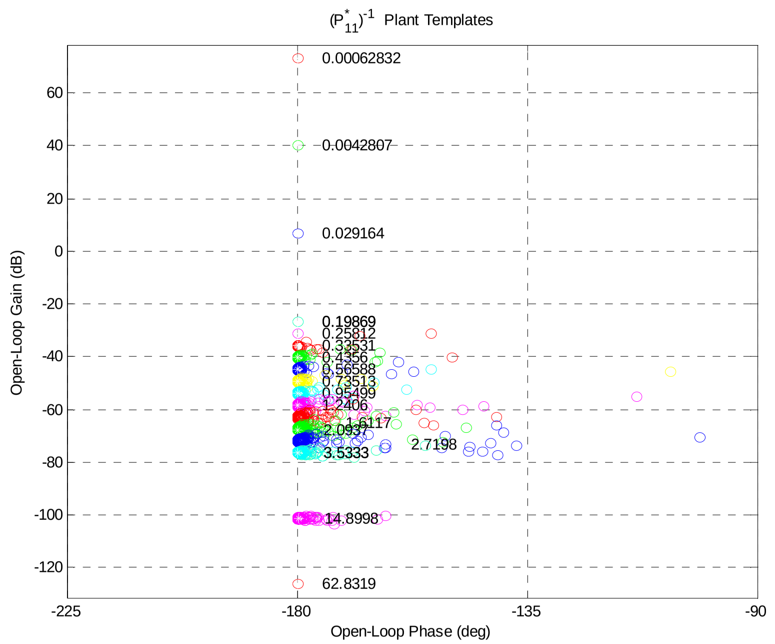

Loop-shaping $L_{11}(s)= (p_{11}^{*e}(s))^{-1}\, g_{11}(s)$

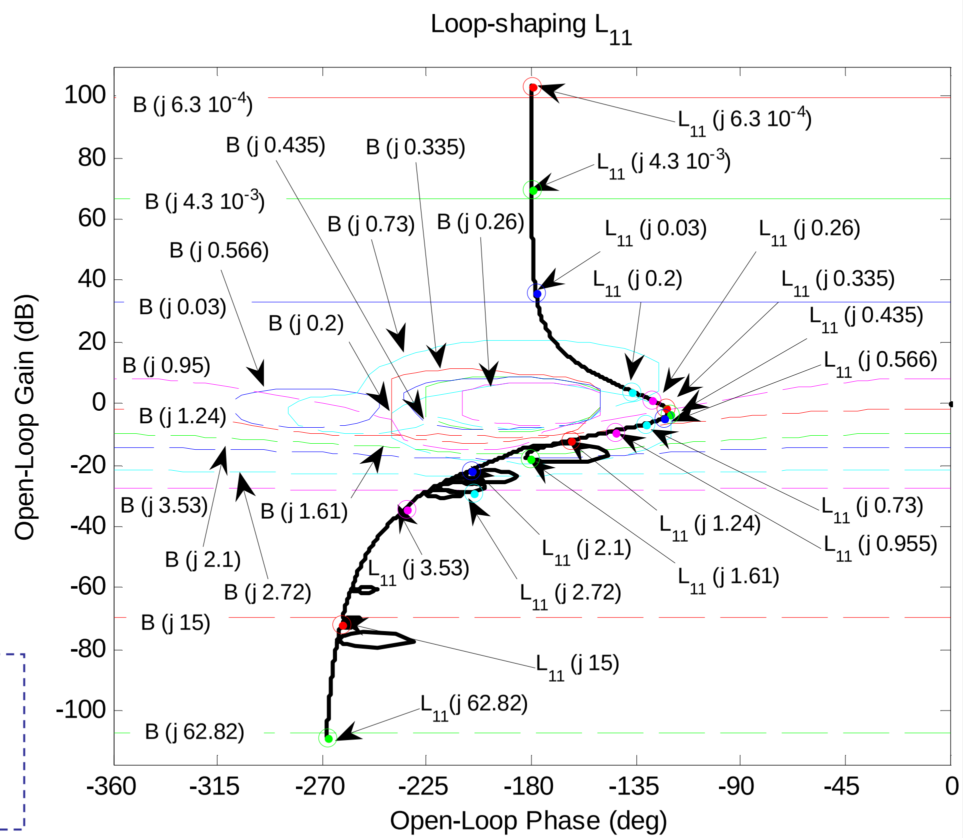

The subsystem is found to be **stable** according to the sufficient stability conditions (a and b).

Mario Garcia-Sanz

$$G=\begin{bmatrix} g_{11} & 0 \\ g_{51} & 0 \end{bmatrix} \Rightarrow \begin{bmatrix} g_{11} & g_{15} \\ g_{51} & g_{55} \end{bmatrix}$$

MIMO DESIGNS

Step 2a) : MIMO subsystem loops 1 and 5

Design the off-diagonal controller $g_{51}(s)$

- Element designed to reduce the coupling
- Calculated according to the expression: $\longrightarrow$ $g_{51}^{opt}(s) = -p_{51}^{*\,N}(s)$

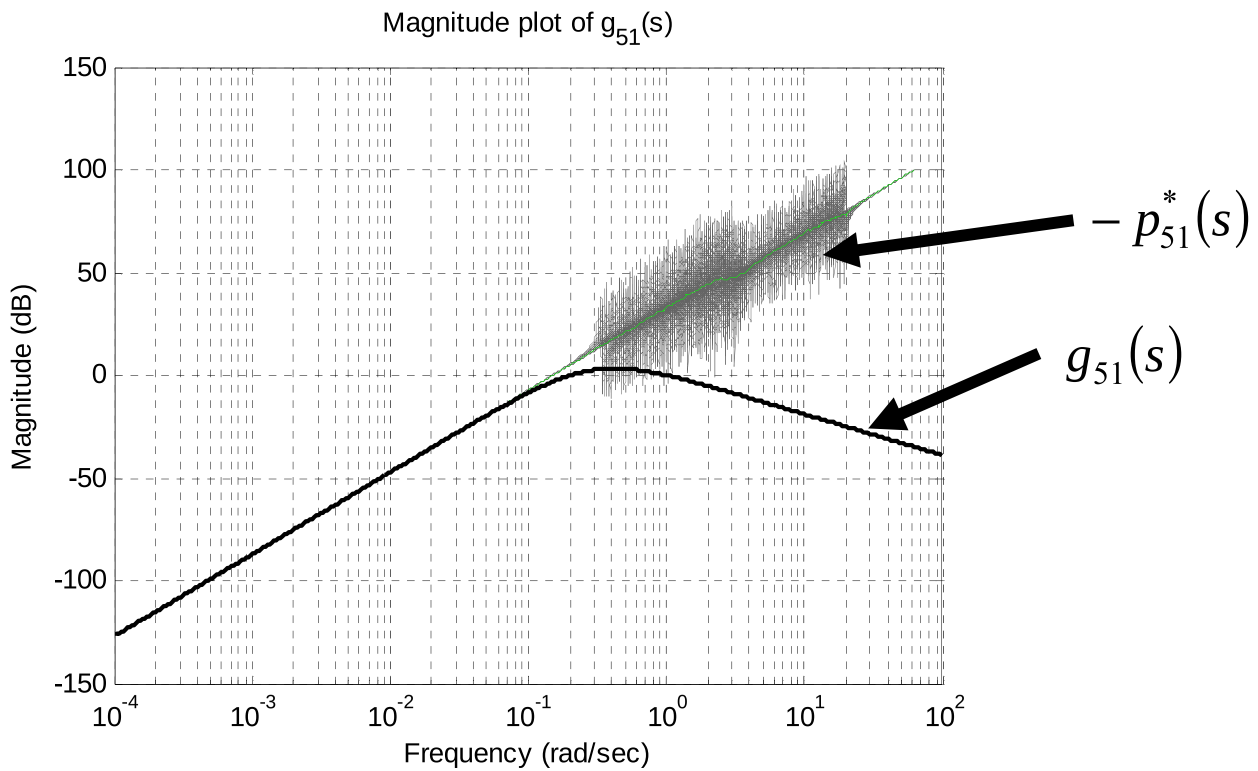

Mario Garcia-Sanz

$$G=\begin{bmatrix} g_{11} & 0 \\ g_{51} & 0 \end{bmatrix} \Rightarrow \begin{bmatrix} g_{11} & g_{15} \\ g_{51} & g_{55} \end{bmatrix}$$

MIMO DESIGNS

Step 2a) : MIMO subsystem loops 1 and 5

Design the diagonal controller $g_{55}(s)$

Controller element designed for the **equivalent plant** computed with :

$$\left[p_{55}^{*e}(s)\right]_2=\left[p_{55}^{*e}(s)\right]_1-\frac{\left(\left[p_{51}^{*e}(s)\right]_1+\left[g_{51}(s)\right]_1\right)\left(\left[p_{15}^{*e}(s)\right]_1\right)}{\left[p_{11}^{*e}(s)\right]_1+\left[g_{11}(s)\right]_1}$$

Robust Performance Specifications

Robust stability (Type 1)

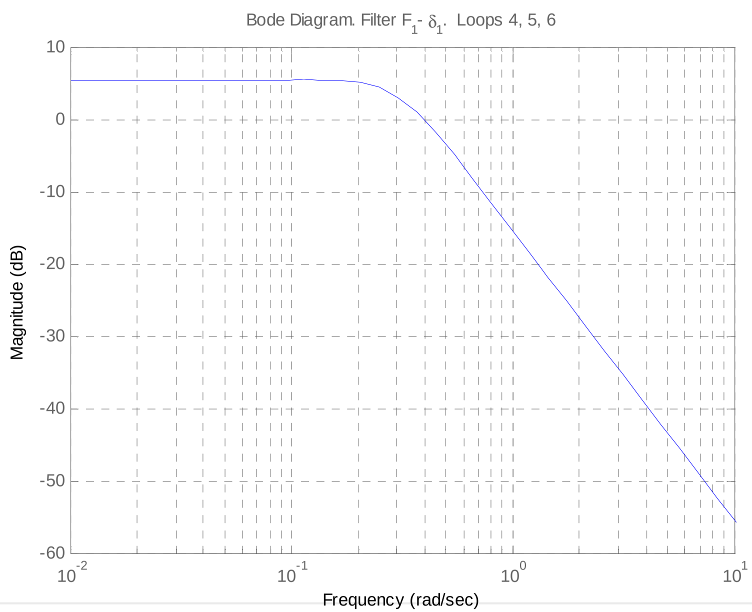

Robust sensitivity (Type 2)

$$\left|\frac{1}{1+\boldsymbol{P}(s)\,\boldsymbol{G}(s)}\right|=\left|\boldsymbol{S}(s)\right|\leq 2$$

Mario Garcia-Sanz

$$G = \begin{bmatrix} g_{11} & 0 \\ g_{51} & 0 \end{bmatrix} \Rightarrow \begin{bmatrix} g_{11} & g_{15} \\ g_{51} & g_{55} \end{bmatrix}$$

MIMO DESIGNS

Step 2a) : MIMO subsystem loops 1 and 5

Design the diagonal controller $g_{55}(s)$

Robust disturbance rejection
at plant input (Type 3)

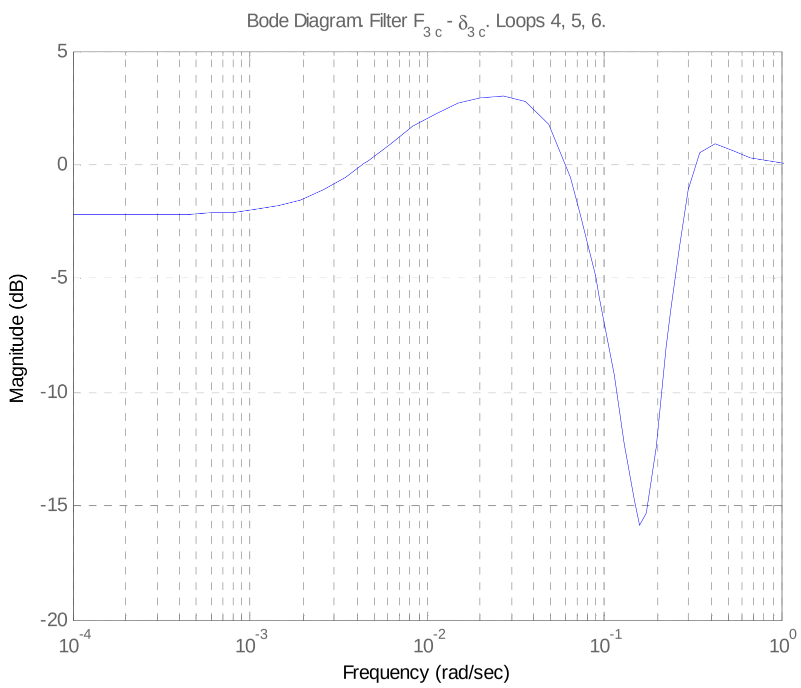

Robust control effort attenuation (Type 4)

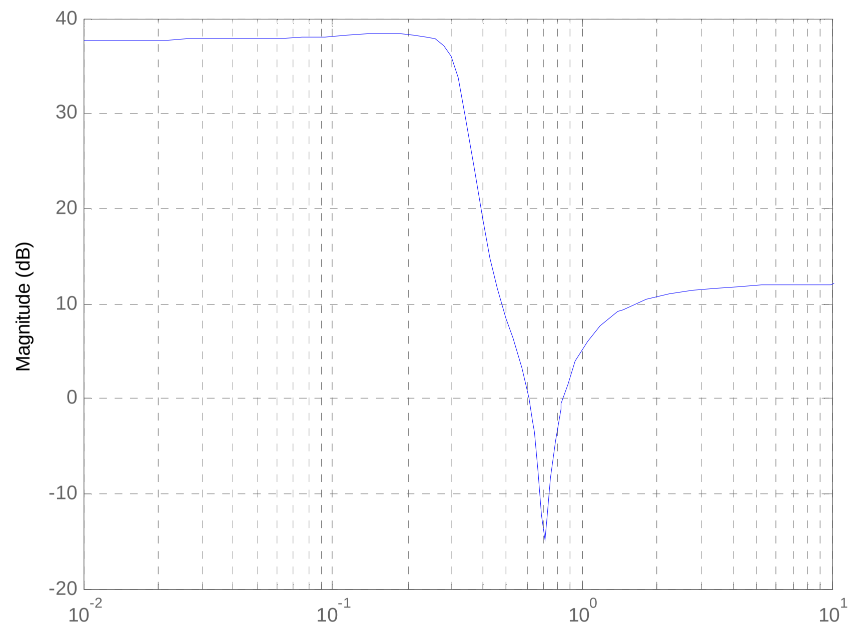

Mario Garcia-Sanz

$$G=\begin{bmatrix} g_{11} & 0 \\ g_{51} & 0 \end{bmatrix} \Rightarrow \begin{bmatrix} g_{11} & g_{15} \\ g_{51} & g_{55} \end{bmatrix}$$

MIMO DESIGNS

Step 2a) : MIMO subsystem loops 1 and 5

Design the diagonal controller $g_{55}(s)$

Templates of the plant $(p_{55}{}^{*e}(s))^{-1}$

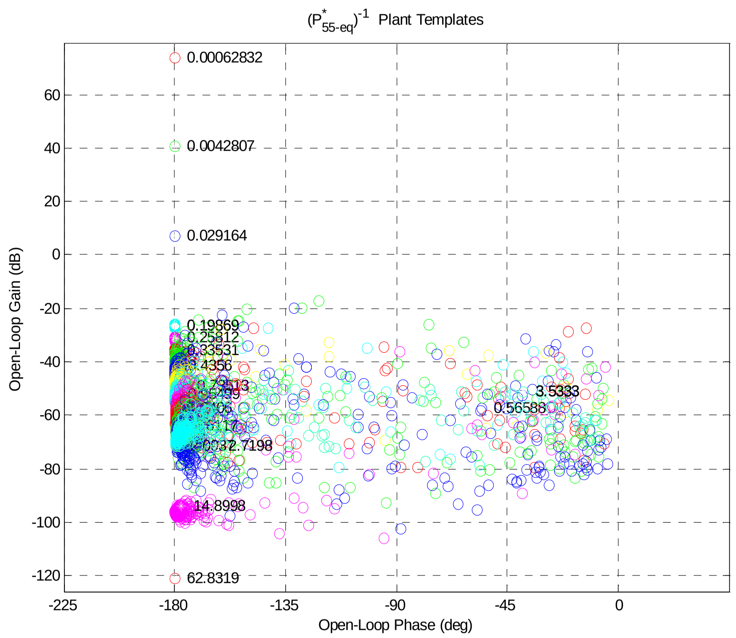

Loop-shaping $L_{55}(s)= (p_{55}{}^{*e}(s))^{-1}\, g_{55}(s)$

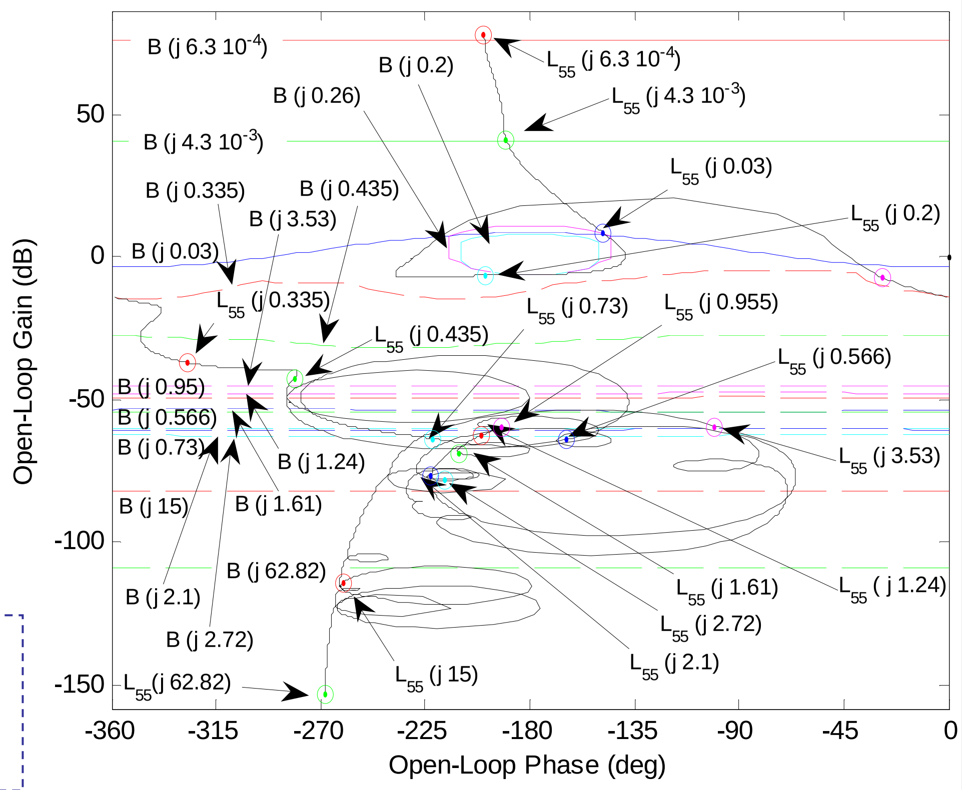

The subsystem is found to be **stable** according to the sufficient stability conditions (a and b).

Mario Garcia-Sanz

$$G=\begin{bmatrix} g_{11} & 0 \\ g_{51} & 0 \end{bmatrix} \Rightarrow \begin{bmatrix} g_{11} & g_{15} \\ g_{51} & g_{55} \end{bmatrix}$$

MIMO DESIGNS

Step 2a) : MIMO subsystem loops 1 and 5

Design the off-diagonal controller $g_{15}(s)$

- Element designed to reduce the coupling
- Calculated according to the expression: → $g_{15}^{opt}(s) = -p_{15}^{*\,N}(s)$

↓

But due to requirement of minimum controller complexity and order → $g_{15}(s)=0$

The 2x2 MIMO subsystem is found to be **stable** according to the sufficient stability conditions (c and d).

Finally, it is also checked that **no additional RHP zeros** have been introduced by the compensator

$$G=\begin{bmatrix} g_{22} & 0 \\ g_{42} & 0 \end{bmatrix} \Rightarrow \begin{bmatrix} g_{22} & g_{24} \\ g_{42} & g_{44} \end{bmatrix}$$

MIMO DESIGNS

Step 2b) : MIMO subsystem loops 2 and 4

Design of the diagonal controller $g_{22}(s)$

Robust Performance Specifications

Robust stability (Type 1)

$$\left| \frac{P(s)G(s)}{1+P(s)G(s)} \right| = |T(s)| \le 1.85$$

Robust sensitivity (Type 2)

$$\left| \frac{1}{1+P(s)G(s)} \right| = |S(s)| \le 2$$

Robust disturbance rejection
at plant input (Type 3)

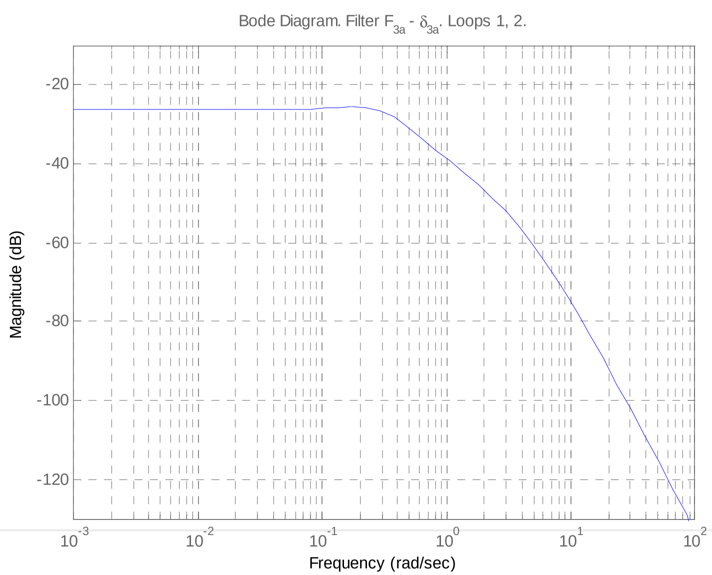

Robust control effort attenuation (Type 4)

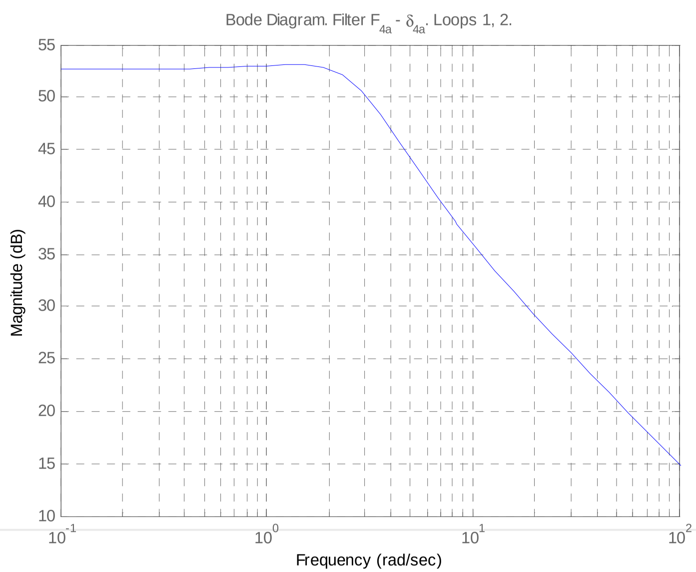

Mario Garcia-Sanz

MIMO DESIGNS

Step 2b) : MIMO subsystem loops 2 and 4

$$G = \begin{bmatrix} g_{22} & 0 \\ g_{42} & 0 \end{bmatrix} \Rightarrow \begin{bmatrix} g_{22} & g_{24} \\ g_{42} & g_{44} \end{bmatrix}$$

Design of the diagonal controller $g_{22}(s)$

Templates of the plant $(p_{22}{}^{*e}(s))^{-1}$

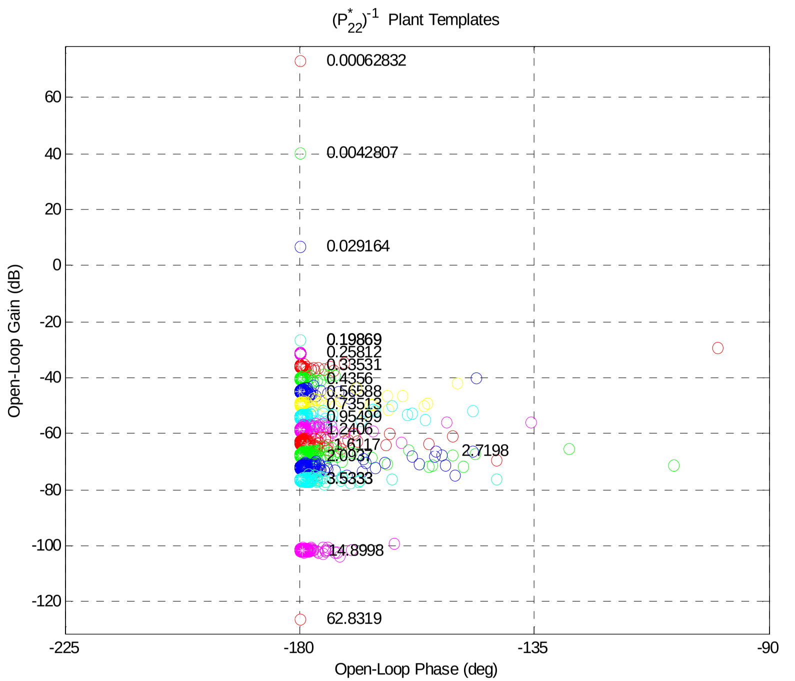

Loop-shaping $L_{22}(s) = (p_{22}{}^{*e}(s))^{-1}\, g_{22}(s)$

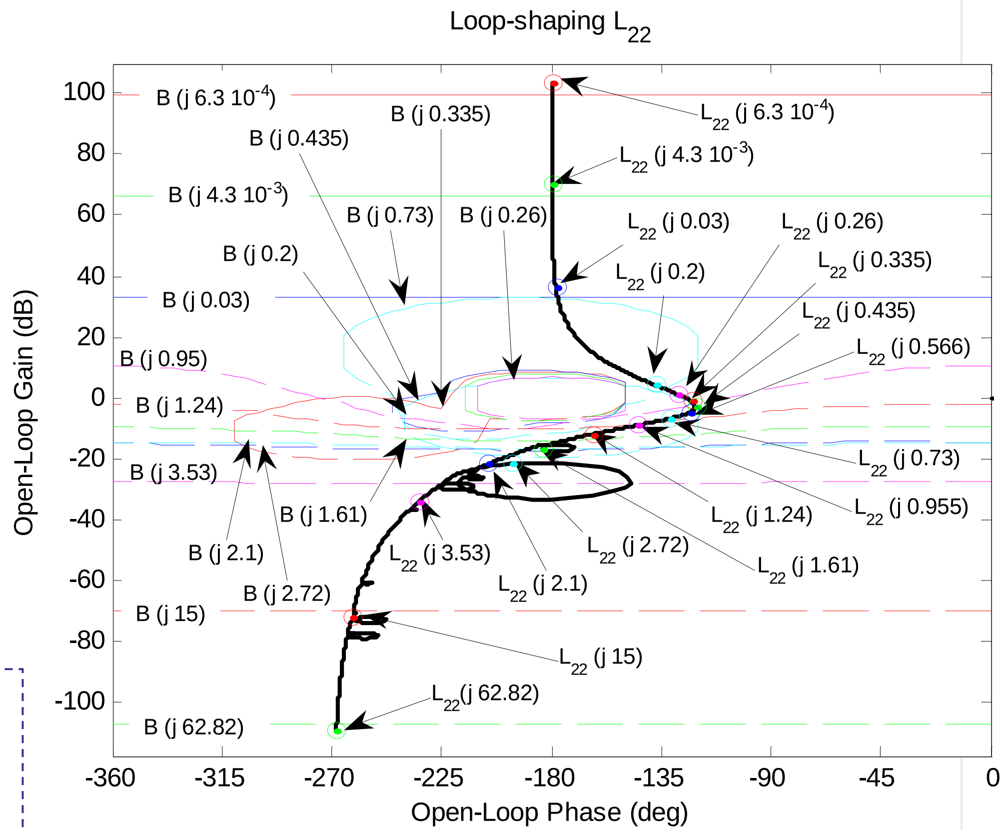

The subsystem is found to be **stable** according to the sufficient stability conditions (a and b).

Mario Garcia-Sanz

$$G=\begin{bmatrix} g_{22} & 0 \\ g_{42} & 0 \end{bmatrix} \Rightarrow \begin{bmatrix} g_{22} & g_{24} \\ g_{42} & g_{44} \end{bmatrix}$$

MIMO DESIGNS

Step 2b) : MIMO subsystem loops 2 and 4

Design the off-diagonal controller $g_{42}(s)$

- Element designed to reduce the coupling
- Calculated according to the expression: $\longrightarrow$ $g_{42}^{opt}(s) = -{p_{42}^{*}}^{N}(s)$

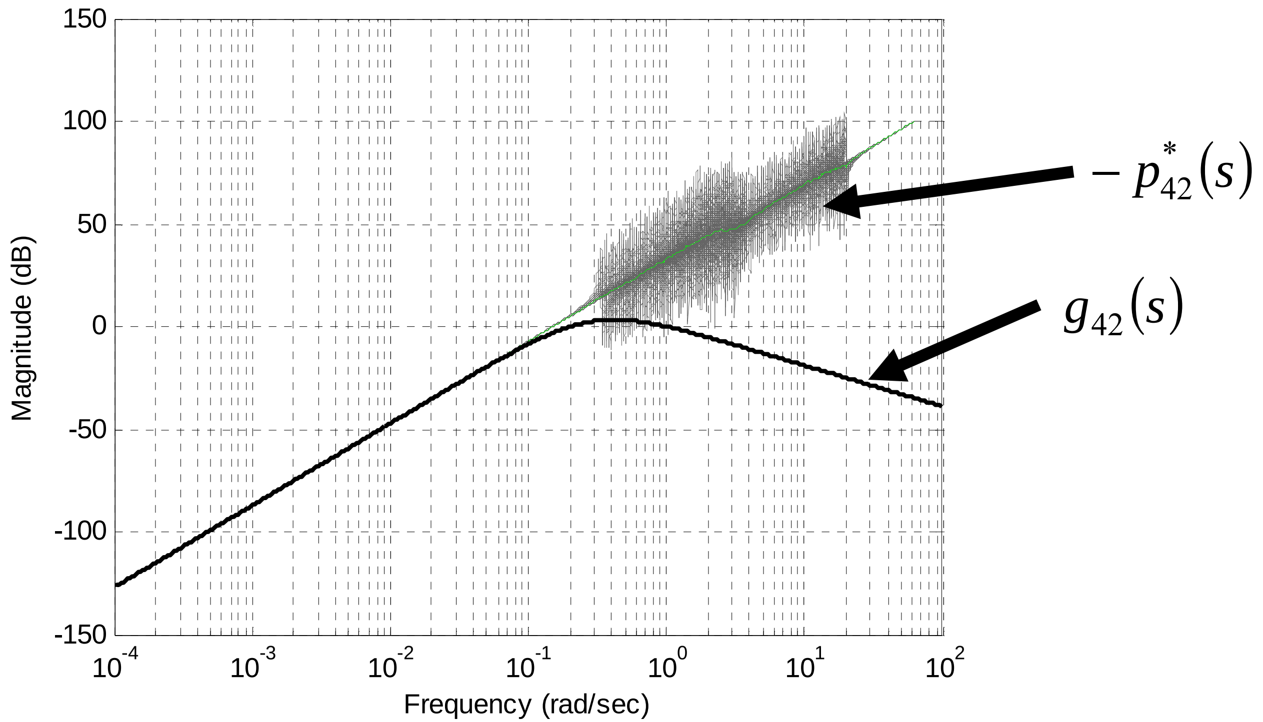

Mario Garcia-Sanz

$$G = \begin{bmatrix} g_{22} & 0 \\ g_{42} & 0 \end{bmatrix} \Rightarrow \begin{bmatrix} g_{22} & g_{24} \\ g_{42} & g_{44} \end{bmatrix}$$

MIMO DESIGNS

Step 2b) : MIMO subsystem loops 2 and 4

Design of the diagonal controller $g_{44}(s)$

Controller element designed for the **equivalent plant** computed with :

$$\left[p_{44}^{*e}(s)\right]_2 = \left[p_{44}^{*e}(s)\right]_1 - \frac{\left(\left[p_{42}^{*e}(s)\right]_1 + [g_{42}(s)]_1\right)\left(\left[p_{24}^{*e}(s)\right]_1\right)}{\left[p_{22}^{*e}(s)\right]_1 + [g_{22}(s)]_1}$$

Robust Performance Specifications

Robust stability (Type 1)

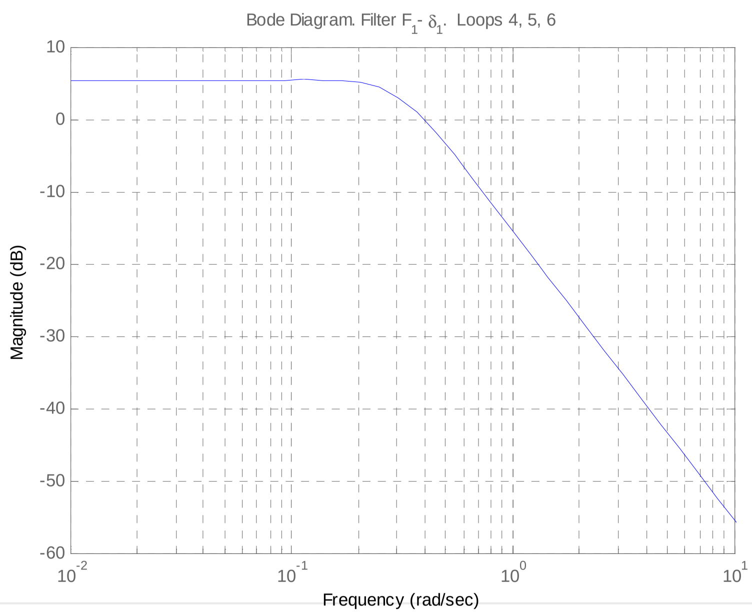

Robust sensitivity (Type 2)

$$\left| \frac{1}{1 + \boldsymbol{P}(s)\,\boldsymbol{G}(s)} \right| = \left|\boldsymbol{S}(s)\right| \le 2$$

Mario Garcia-Sanz

MIMO DESIGNS

$$G = \begin{bmatrix} g_{22} & 0 \\ g_{42} & 0 \end{bmatrix} \Rightarrow \begin{bmatrix} g_{22} & g_{24} \\ g_{42} & g_{44} \end{bmatrix}$$

Step 2b) : MIMO subsystem loops 2 and 4

Design of the diagonal controller $g_{44}(s)$

Robust disturbance rejection at plant input (Type 3)

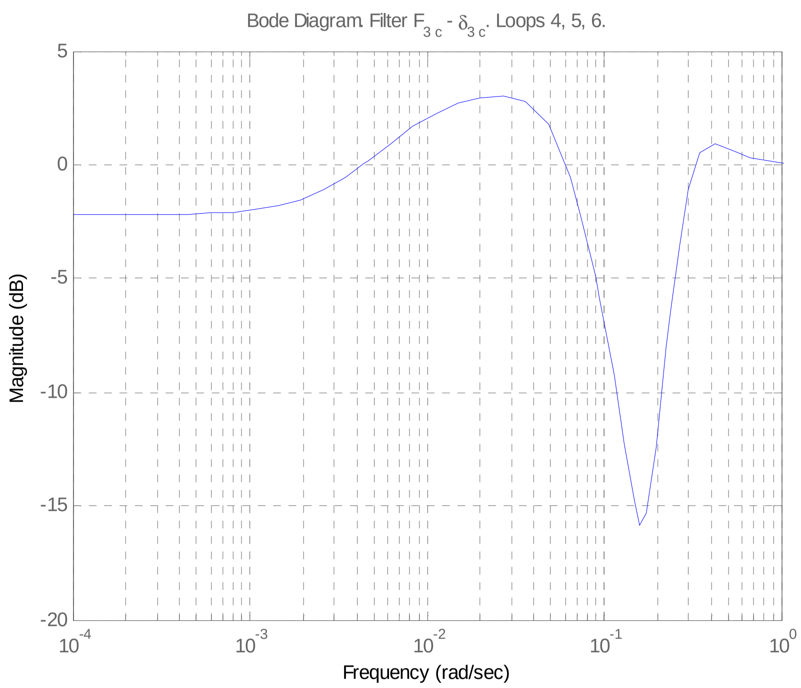

Robust control effort attenuation (Type 4)

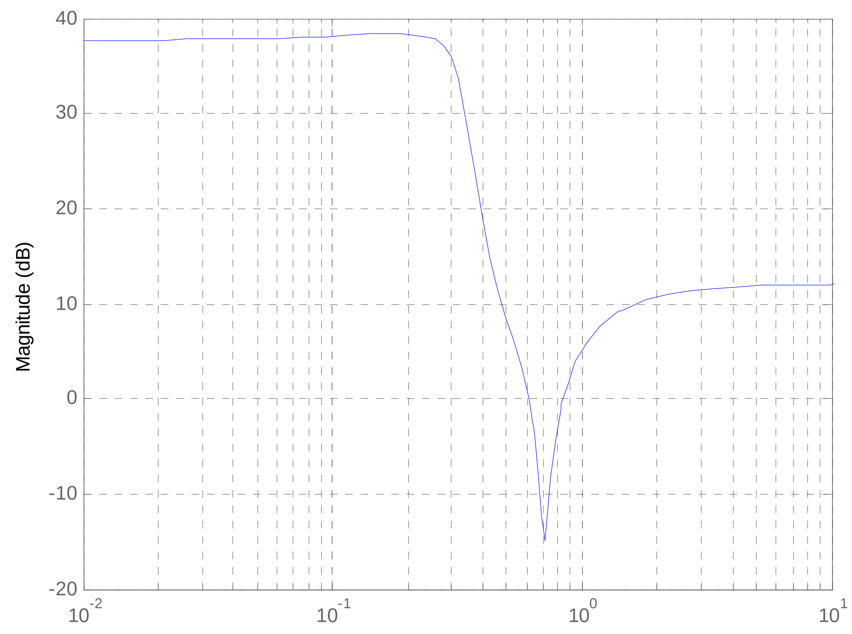

Mario Garcia-Sanz

MIMO DESIGNS

$$G = \begin{bmatrix} g_{22} & 0 \\ g_{42} & 0 \end{bmatrix} \Rightarrow \begin{bmatrix} g_{22} & g_{24} \\ g_{42} & g_{44} \end{bmatrix}$$

Step 2b) : MIMO subsystem loops 2 and 4

Design of the diagonal controller $g_{44}(s)$

Templates of the plant $(p_{44}^{*e}(s))^{-1}$

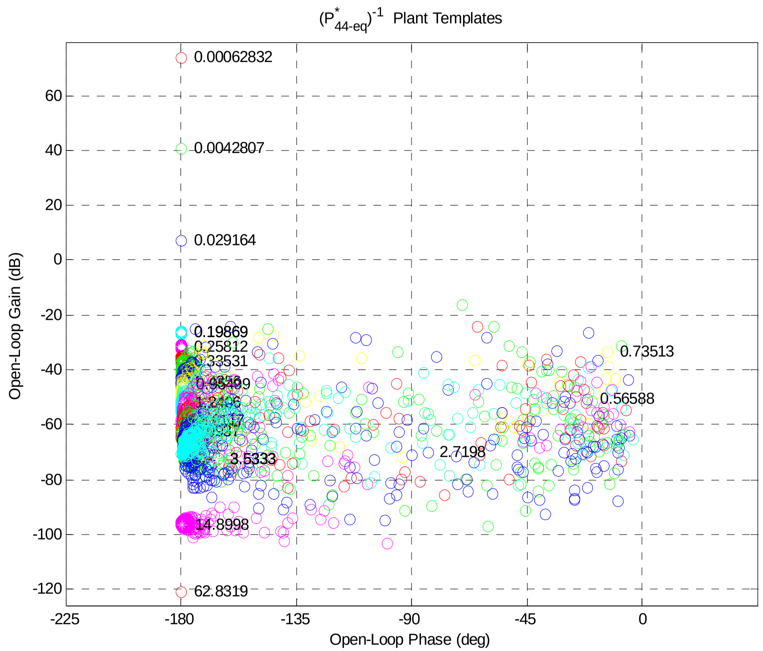

Loop-shaping $L_{44}(s)= (p_{44}^{*e}(s))^{-1}\, g_{44}(s)$

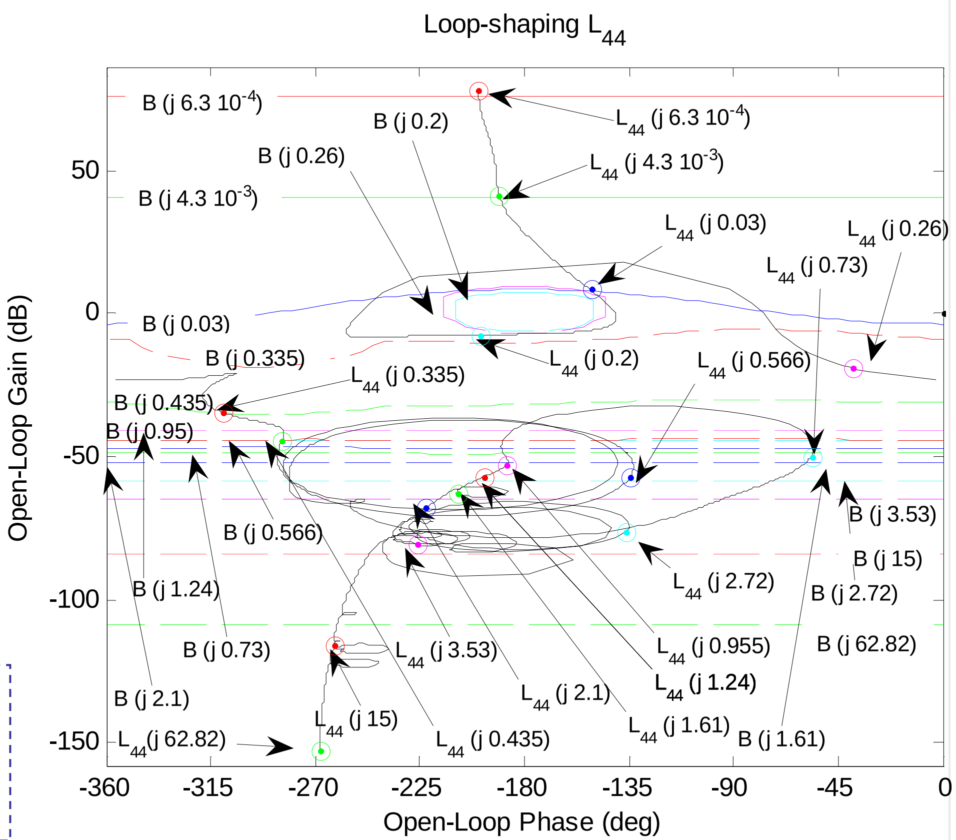

The subsystem is found to be **stable** according to the sufficient stability conditions (a and b).

Mario Garcia-Sanz

$$G = \begin{bmatrix} g_{22} & 0 \\ g_{42} & 0 \end{bmatrix} \Rightarrow \begin{bmatrix} g_{22} & g_{24} \\ g_{42} & g_{44} \end{bmatrix}$$

Step 2b) : MIMO subsystem loops 2 and 4

Design the off-diagonal controller $g_{24}(s)$

- Element designed to reduce the coupling
- Calculated according to the expression: $\longrightarrow$ $g_{24}^{opt}(s) = -p_{24}^{*\,N}(s)$

But due to requirement of minimum controller complexity and order $\longrightarrow$ $g_{24}(s) = 0$

The 2x2 MIMO subsystem is found to be **stable** according to the sufficient stability conditions (c and d).

Finally, it is also checked that **no additional RHP zeros** have been introduced by the compensator

Controller evaluation and comparison (I)

- **Non-diagonal MIMO QFT** (introduced here)
- H-infinity (provided by ESA)
- Diagonal MIMO QFT (for comparision)

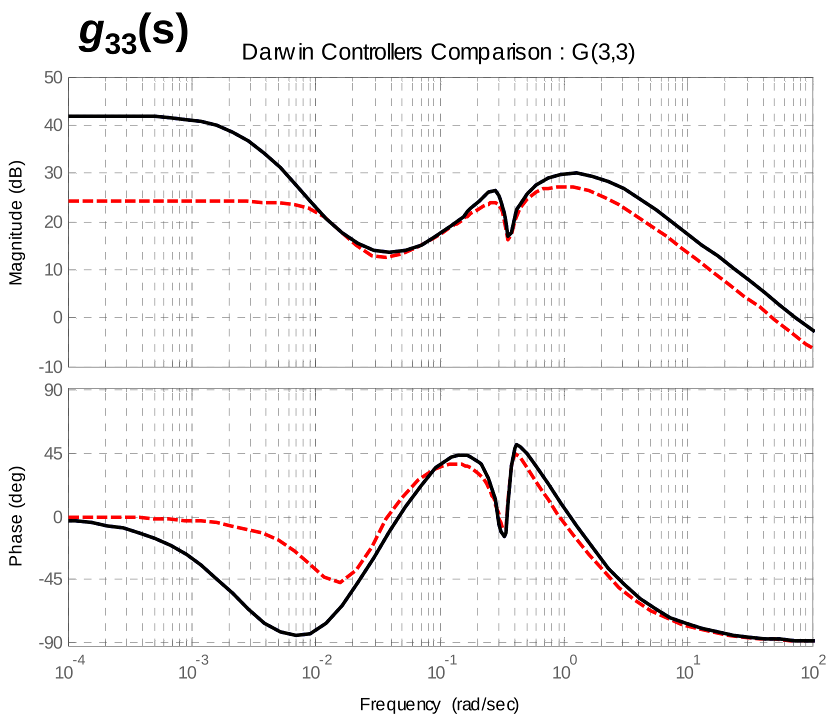

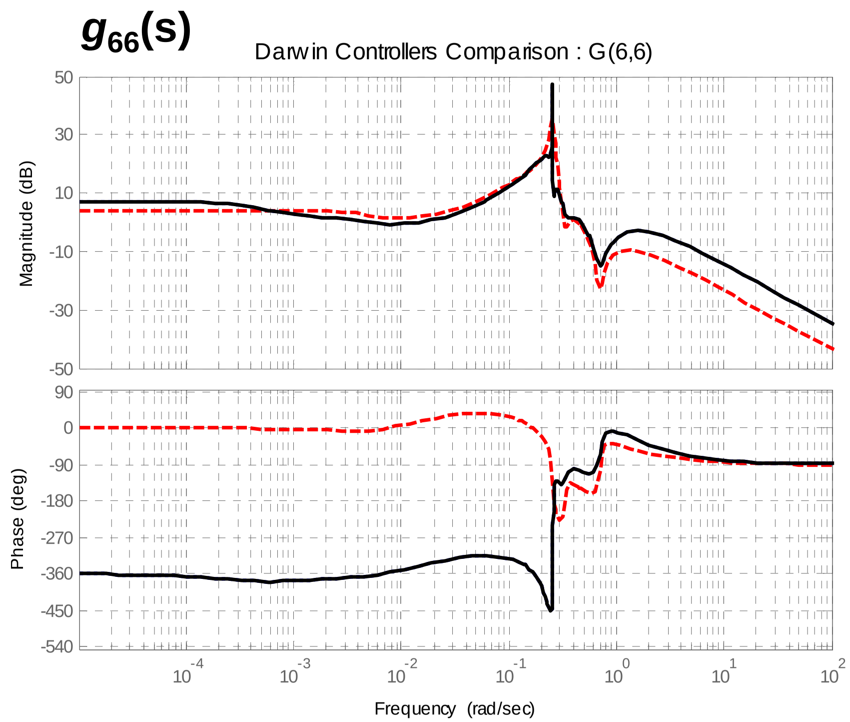

Bode Diagram Compensators:

Non-diagonal and Diagonal MIMO QFT in solid line,
H-infinity in dashed line.
(a) $g33(s)$, (b) $g66(s)$

Mario Garcia-Sanz

Controller evaluation and comparison (II)

- **Non-diagonal MIMO QFT** (introduced here)
- H-infinity (provided by ESA)
- Diagonal MIMO QFT (for comparision)

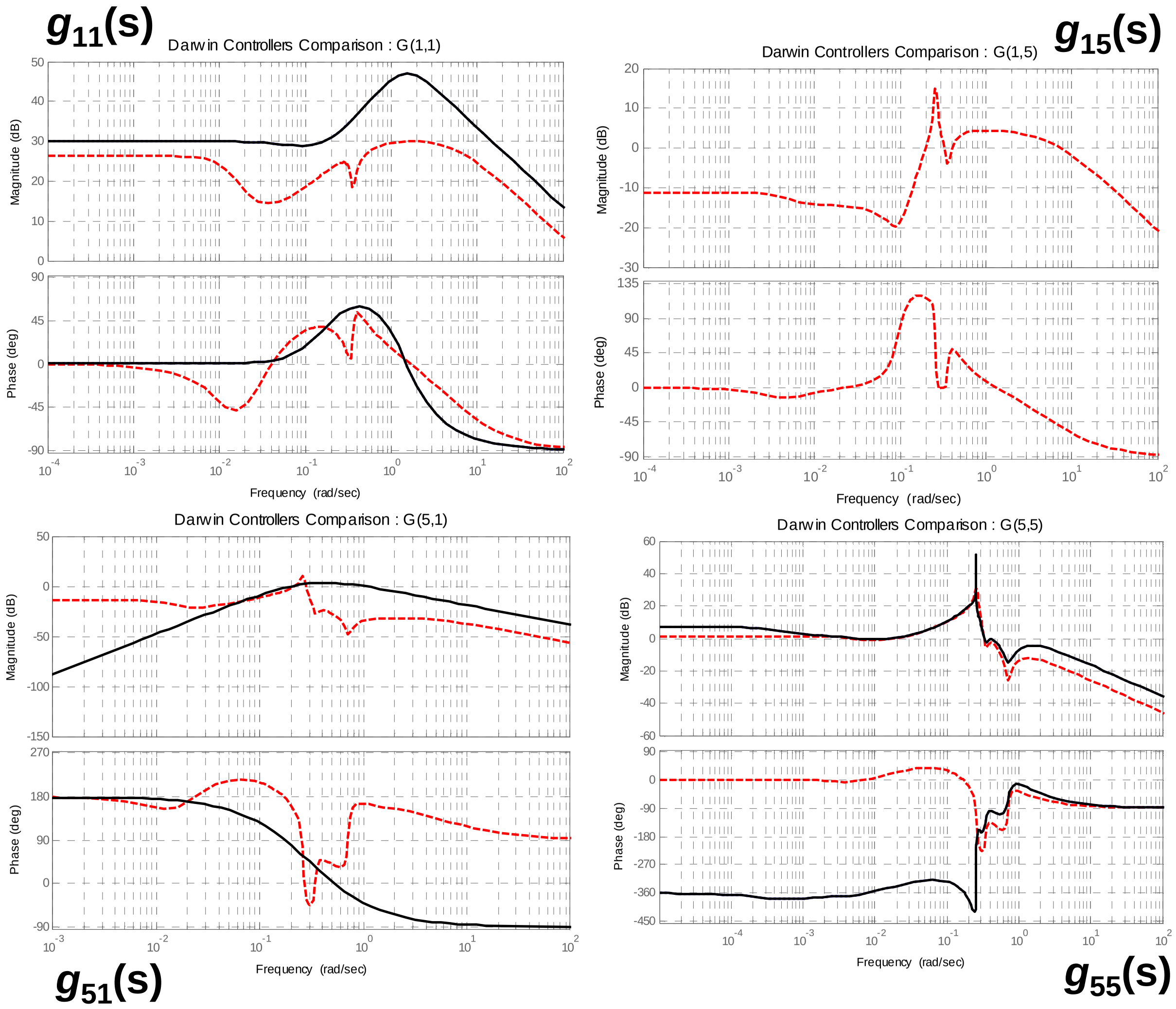

Bode Diagram Compensators:

Non-diagonal MIMO QFT in solid line

[also diagonal MIMO QFT for $g11(s)$ and $g55(s)$],

H-infinity in dashed line.

(a) $g11(s)$, (b) $g15(s)$, (c) $g51(s)$, (d) $g55(s)$

Mario Garcia-Sanz

Controller evaluation and comparison (III)

- **Non-diagonal MIMO QFT** (introduced here)
- H-infinity (provided by ESA)
- Diagonal MIMO QFT (for comparision)

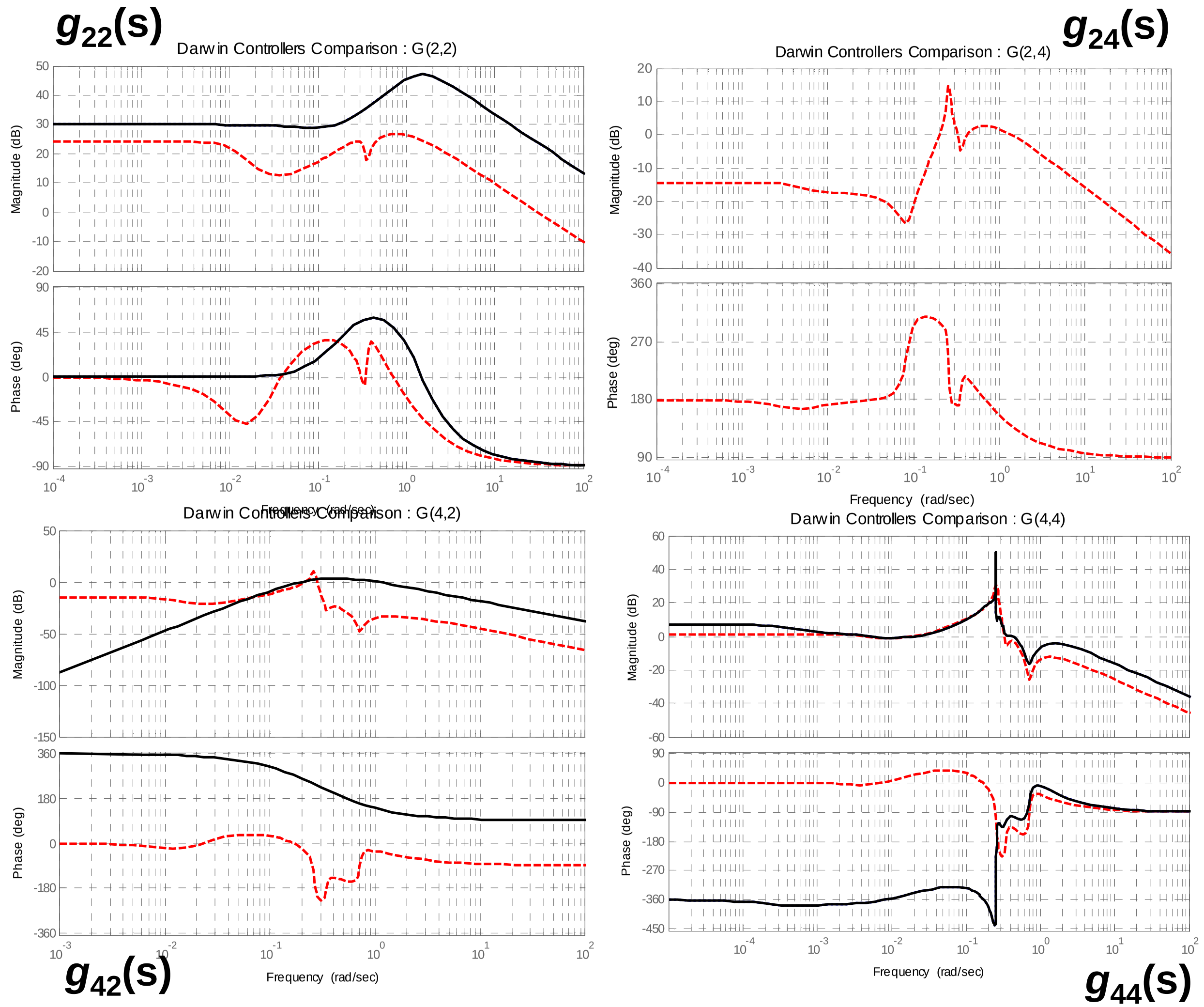

Bode Diagram Compensators:

Non-diagonal MIMO QFT in solid line

[also diagonal MIMO QFT for $g22(s)$ and $g44(s)$],

H-infinity in dashed line.

(a) $g22(s)$, (b) $g24(s)$, (c) $g42(s)$, (d) $g44(s)$

Mario Garcia-Sanz

Controller evaluation and comparison (IV)

- **Non-diagonal MIMO QFT** (introduced here)
- H-infinity (provided by ESA)
- Diagonal MIMO QFT (for comparision)

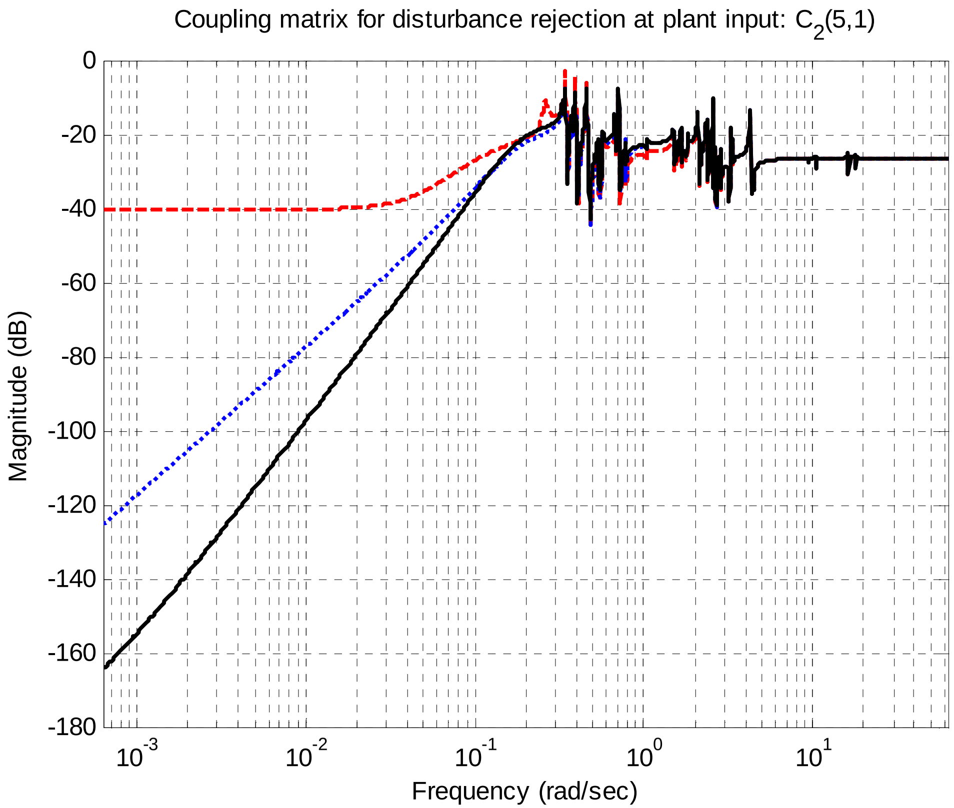

Element (5,1)
of the coupling matrix *C2*:

non-diagonal MIMO QFT in solid line

diagonal MIMO QFT in dotted line

H-infinity in dashed line

$$\left| c_{2ij} \right|_{g_{ij}=g_{ij}^{opt}} = \left| \psi_{ij}\, \Delta_{ij} \right|$$

$$\psi_{ij} = \frac{p_{ij}^{*N}}{\left(1+\Delta_{jj}\right) p_{jj}^{*N} + g_{jj}}$$

For $\omega \in [0, 0.1]$ rad/sec: $C_2(5,1)_{\text{non-diag QFT}} < C_2(5,1)_{\text{diag QFT}} < C_2(5,1)_{\text{H-infinity}}$,
which explains results under low frequency external disturbances

Mario Garcia-Sanz

Controller evaluation and comparison (V)

- **Non-diagonal MIMO QFT** (introduced here)
- H-infinity (provided by ESA)
- Diagonal MIMO QFT (for comparision)

Non-diagonal MIMO QFT has **8 elements** of **order**: from **3** to **14**.

$$\mathbf{G}(s)=\begin{bmatrix} g_{11}(s) & 0 & 0 & 0 & 0 & 0 \\ 0 & g_{22}(s) & 0 & 0 & 0 & 0 \\ 0 & 0 & g_{33}(s) & 0 & 0 & 0 \\ 0 & g_{42}(s) & 0 & g_{44}(s) & 0 & 0 \\ g_{51}(s) & 0 & 0 & 0 & g_{55}(s) & 0 \\ 0 & 0 & 0 & 0 & 0 & g_{66}(s) \end{bmatrix}$$

H-infinity expressed as transfer functions has **36 elements** of **order 42**.

$$\mathbf{G}(s)=\begin{bmatrix} g_{11}(s) & g_{12}(s) & g_{13}(s) & g_{14}(s) & g_{15}(s) & g_{16}(s) \\ g_{21}(s) & g_{22}(s) & g_{23}(s) & g_{24}(s) & g_{25}(s) & g_{26}(s) \\ g_{31}(s) & g_{32}(s) & g_{33}(s) & g_{34}(s) & g_{35}(s) & g_{36}(s) \\ g_{41}(s) & g_{42}(s) & g_{43}(s) & g_{44}(s) & g_{45}(s) & g_{46}(s) \\ g_{51}(s) & g_{52}(s) & g_{53}(s) & g_{54}(s) & g_{55}(s) & g_{56}(s) \\ g_{61}(s) & g_{62}(s) & g_{63}(s) & g_{64}(s) & g_{65}(s) & g_{66}(s) \end{bmatrix}$$

Diagonal MIMO QFT has **6 elements** of **order**: from **5** to **14**.

$$\mathbf{G}(s)=\begin{bmatrix} g_{11}(s) & 0 & 0 & 0 & 0 & 0 \\ 0 & g_{22}(s) & 0 & 0 & 0 & 0 \\ 0 & 0 & g_{33}(s) & 0 & 0 & 0 \\ 0 & 0 & 0 & g_{44}(s) & 0 & 0 \\ 0 & 0 & 0 & 0 & g_{55}(s) & 0 \\ 0 & 0 & 0 & 0 & 0 & g_{66}(s) \end{bmatrix}$$

Controller	Number of Multiplications	Number of Sums
Non-diagonal MIMO QFT	**130**	**124**
H-infinity	2994	2988
Diagonal MIMO QFT	116	110

Mario Garcia-Sanz

Benchmark Simulator (I)

- **Non-diagonal MIMO QFT** (introduced here)
- H-infinity (provided by ESA)
- Diagonal MIMO QFT (for comparision)

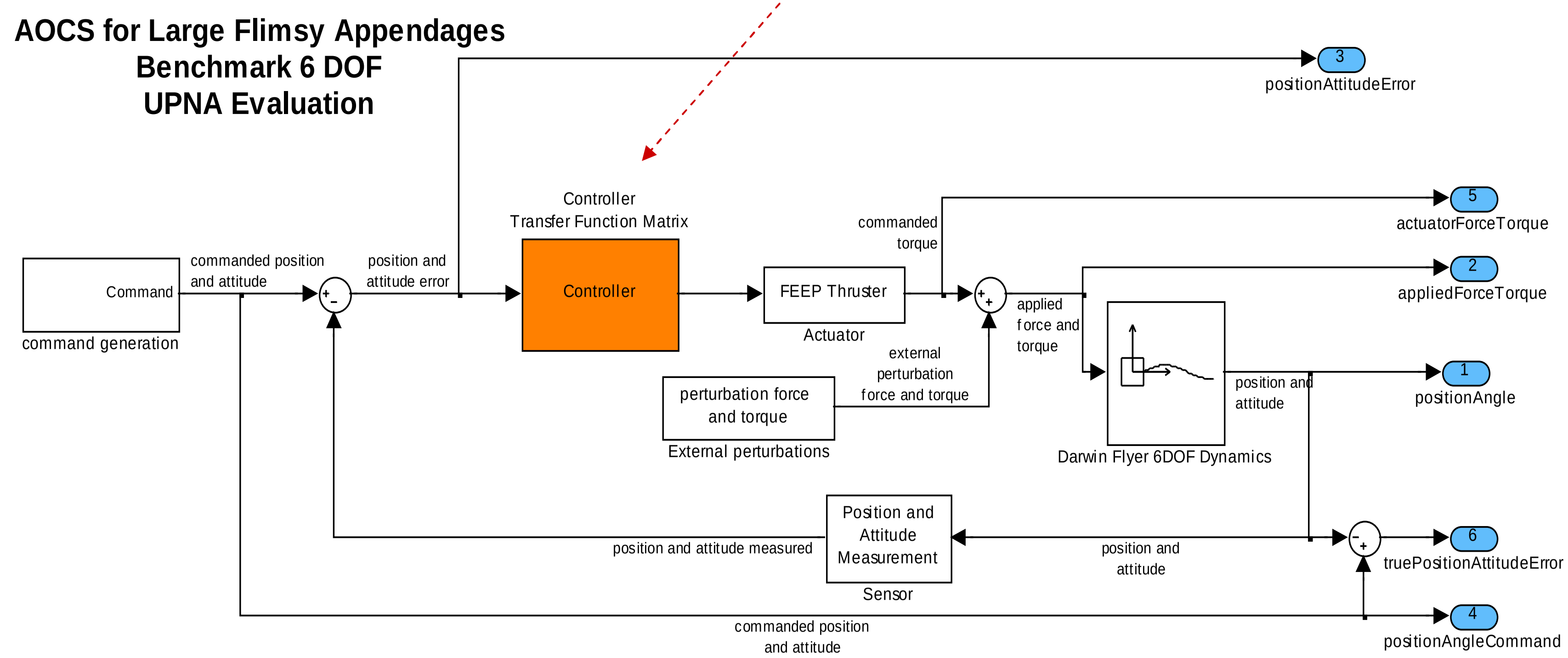

Two benchmark:

B1.- *Developed by Astrium Space for ESA-ESTEC*

B2.- *B1 + Low freq. disturbances*

300 different plants due to uncertainty. Monte-Carlo analysis

Sampling frequency: 1 Hz

Mario Garcia-Sanz

Benchmark Simulator (II)

Position and attitude sensors

- **Non-diagonal MIMO QFT** (introduced here)
- H-infinity (provided by ESA)
- Diagonal MIMO QFT (for comparision)

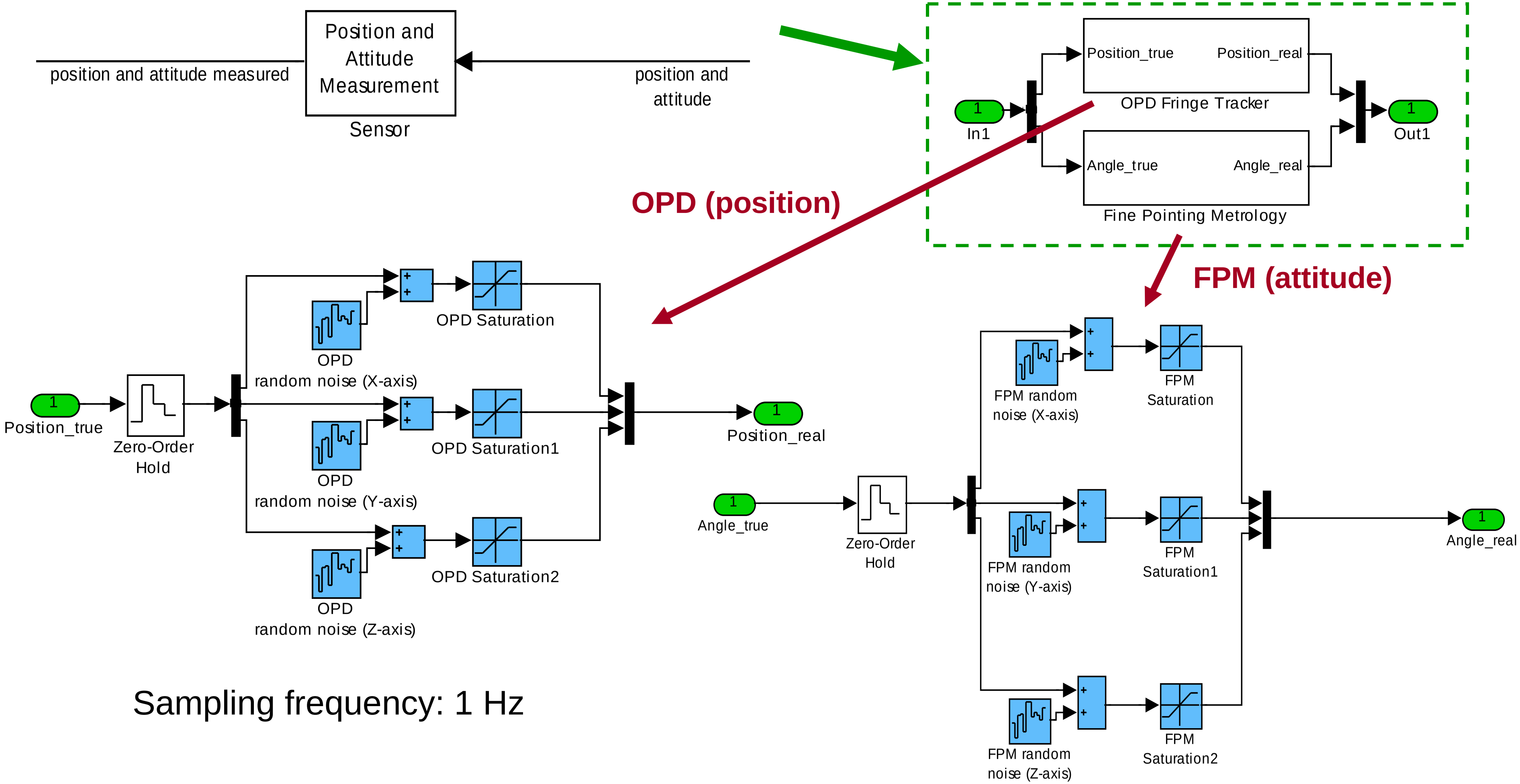

Sampling frequency: 1 Hz

Mario Garcia-Sanz

Benchmark Simulator (III)

FEEP Thrusters Actuators

- **Non-diagonal MIMO QFT** (introduced here)
- H-infinity (provided by ESA)
- Diagonal MIMO QFT (for comparision)

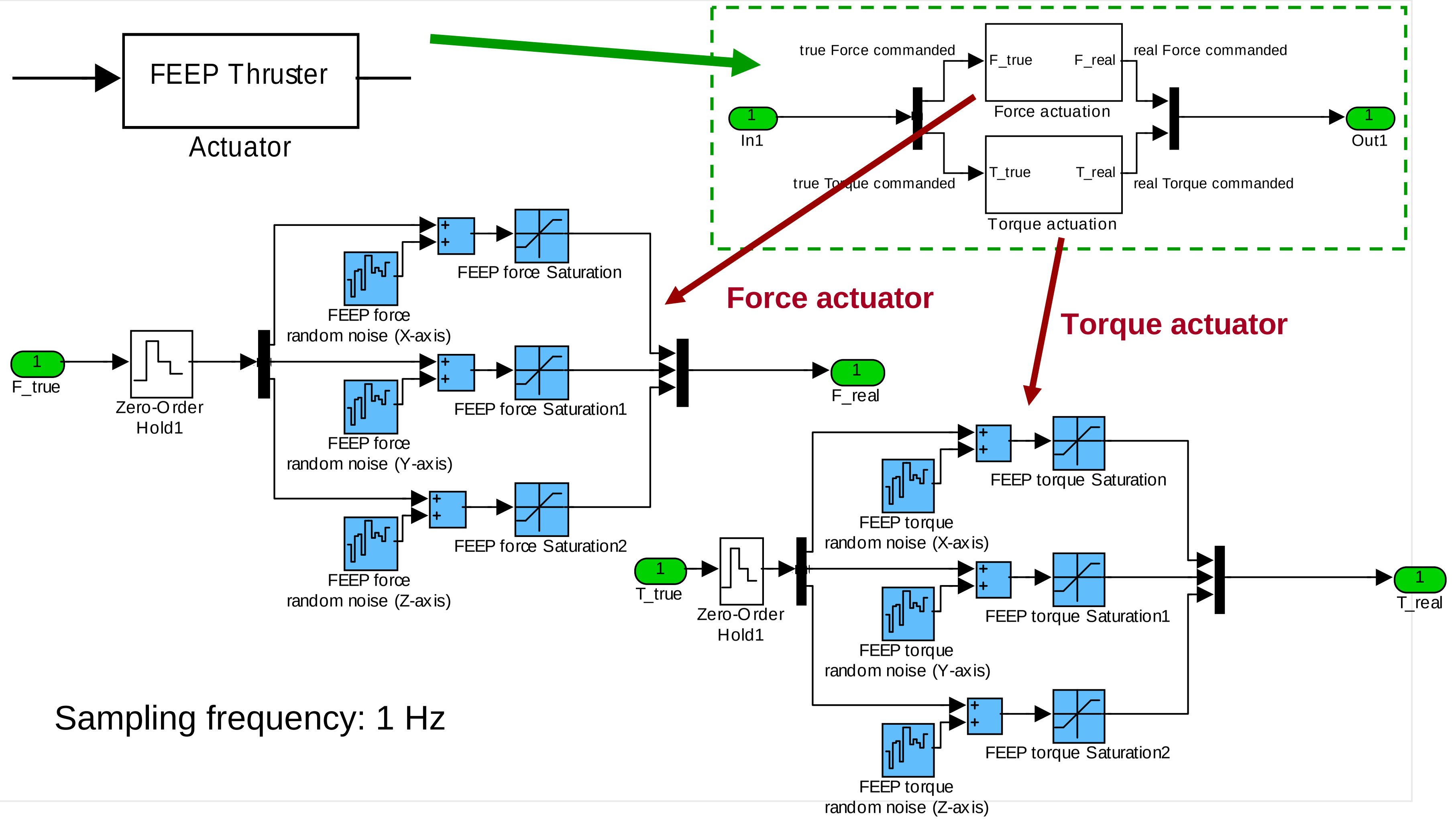

Mario Garcia-Sanz

Benchmark Simulator (IV)

External Perturbations at the plant input

- **Non-diagonal MIMO QFT** (introduced here)
- H-infinity (provided by ESA)
- Diagonal MIMO QFT (for comparision)

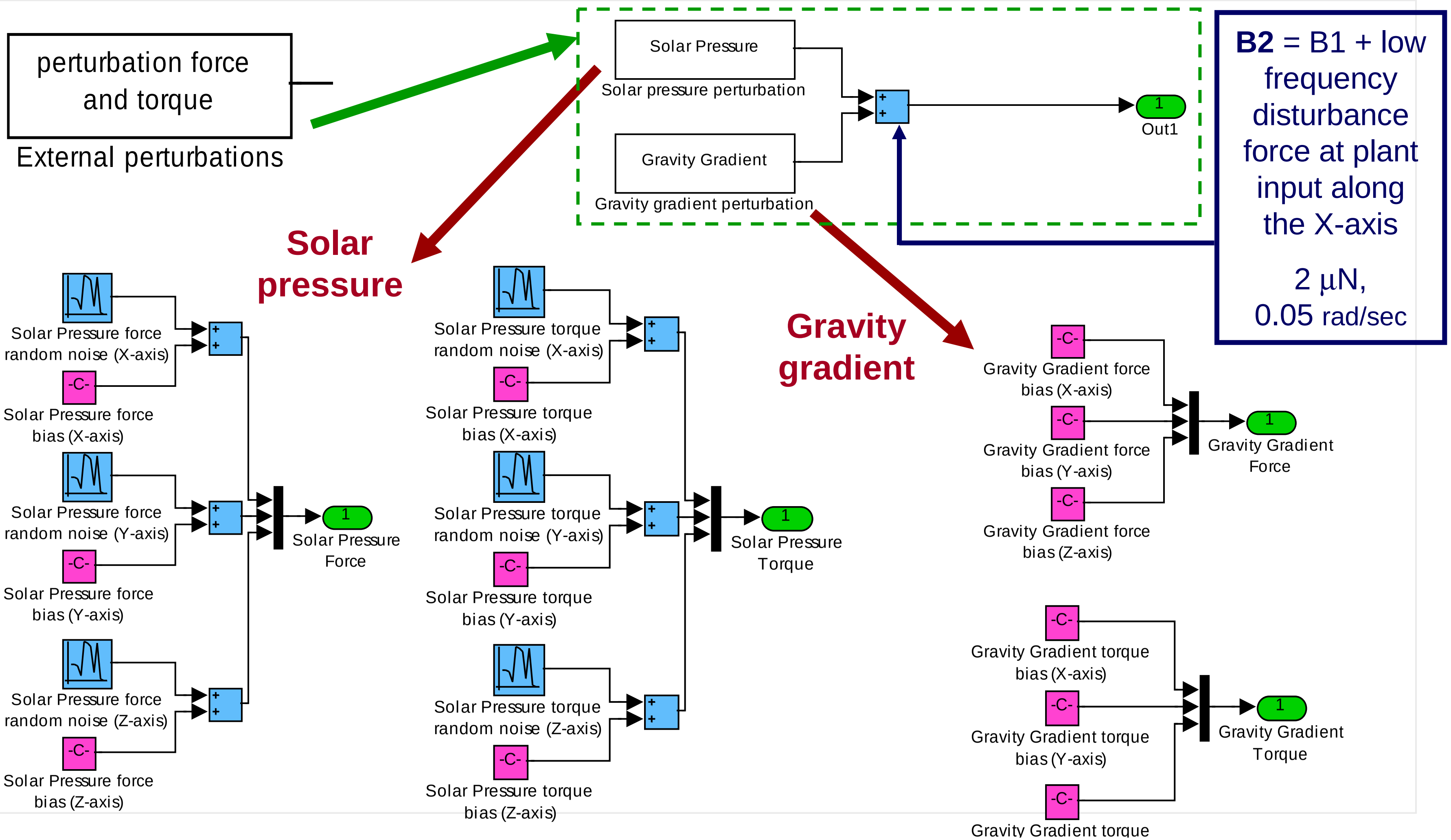

Mario Garcia-Sanz

Time-domain Analysis. Results (I)

Position and attitude responses

- **Non-diagonal MIMO QFT** (introduced here)
- H-infinity (provided by ESA)
- Diagonal MIMO QFT (for comparision)

Position outputs for several run cases

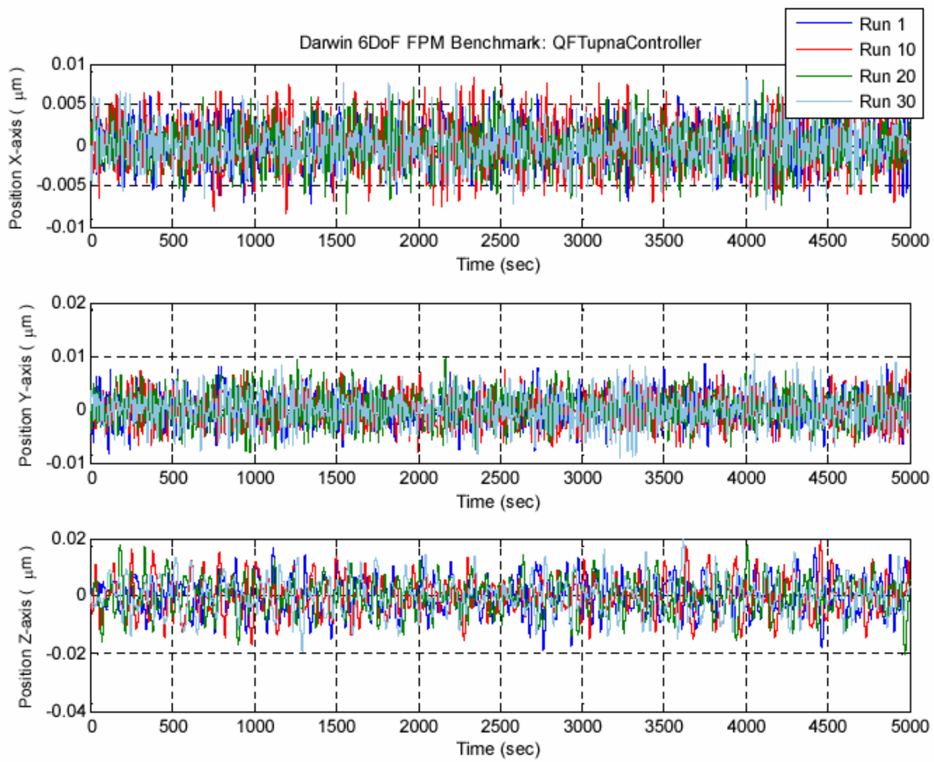

Attitude outputs for several run cases

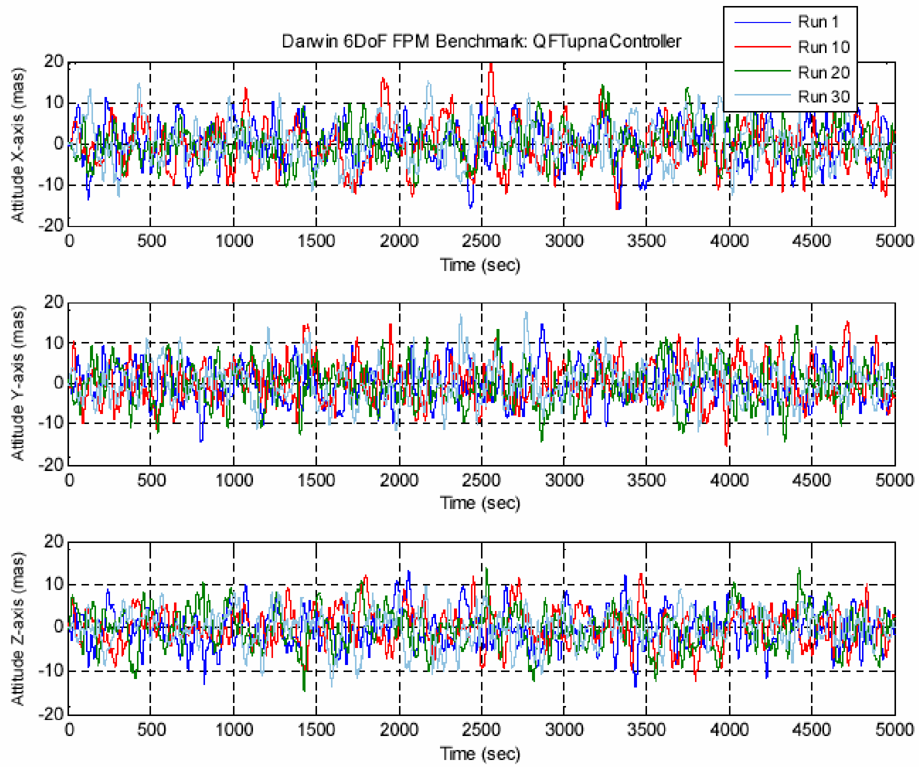

Mario Garcia-Sanz

Time-domain Analysis. Results (II)

- **Non-diagonal MIMO QFT** (introduced here)
- H-infinity (provided by ESA)
- Diagonal MIMO QFT (for comparision)

Evaluation Criteria

For each controller:

the **greatest value** over the 300 uncertain cases is shown for:

- **Position errors**: the maximum
  the standard deviation

- **Attitude errors**: the maximum
  the standard deviation

- Actuator commands: the maximum

in all axes.

Mario Garcia-Sanz

Time-domain Analysis. Results (III)

	Specification	Requirement	Benchmark	Non-diagonal MIMO QFT Controller	Diagonal MIMO QFT Controller	H-infinity Controller
1	Maximum Position Error X (μm)	< 1 μm	B1	**0.0131**	**0.0131**	0.0293
			B2	**0.0816**	**0.0816**	0.511
2	Maximum Position Error Y (μm)	< 1 μm	B1	**0.0120**	**0.0120**	0.0299
			B2	**0.0120**	**0.0120**	0.0299
3	Maximum Position Error Z (μm)	< 1 μm	B1	**0.0288**	**0.0288**	0.0292
			B2	**0.0288**	**0.0288**	0.0292
4	Maximum Attitude Error X (mas)	< 25.5 mas	B1	**25.27**	25.31	25.95
			B2	**25.27**	25.31	25.95
5	Maximum Attitude Error Y (mas)	< 25.5 mas	B1	**22.91**	22.99	23.21
			B2	**22.55**	23.75	28.91
6	Maximum Attitude Error Z (mas)	< 25.5 mas	B1	**21.15**	**21.15**	22.84
			B2	**21.15**	**21.15**	22.84

Time-domain Analysis. Results (IV)

	Specification	Requirement	Benchmark	Non-diagonal MIMO QFT Controller	Diagonal MIMO QFT Controller	H-infinity Controller
7	Std. Deviation of Position Error X (μm)	< 0.33 μm	B1	**0.00275**	0.00276	0.00686
			B2	**0.0511**	**0.0511**	0.341
8	Std. Deviation of Position Error Y (μm)	< 0.33 μm	B1	**0.00265**	0.00266	0.00722
			B2	**0.00265**	0.00266	0.00722
9	Std. Deviation of Position Error Z (μm)	< 0.33 μm	B1	**0.00668**	**0.00668**	0.00691
			B2	**0.00668**	**0.00668**	0.00691
10	Std. Deviation of Attitude Error X (mas)	< 8.5 mas	B1	**5.57**	**5.57**	5.68
			B2	**5.57**	**5.57**	5.68
11	Std. Deviation of Attitude Error Y (mas)	< 8.5 mas	B1	**5.76**	**5.76**	6.01
			B2	**5.80**	5.85	8.23
12	Std. Deviation of Attitude Error Z (mas)	< 8.5 mas	B1	**4.83**	**4.83**	5.00
			B2	**4.83**	**4.83**	5.00

Time-domain Analysis. Results (V)

	Specification	Requirement	Benchmark	Non-diagonal MIMO QFT Controller	Diagonal MIMO QFT Controller	H-infinity Controller
13	Max. Actuator Force Command X (N)	< 1.5e-4 N	B1	1.94e-6	1.94e-6	**7.42e-7**
			B2	3.94e-6	3.94e-6	**3.31e-6**
14	Max. Actuator Force Command Y (N)	< 1.5e-4 N	B1	1.86e-6	1.86e-6	**6.68e-7**
			B2	1.86e-6	1.86e-6	**6.68e-7**
15	Max. Actuator Force Command Z (N)	< 1.5e-4 N	B1	5.94e-7	5.94e-7	**5.61e-7**
			B2	5.94e-7	5.94e-7	**5.61e-7**
16	Max. Actuator Torque Command X (Nm)	< 1.5e-4 N m	B1	**8.68e-7**	8.71e-7	1.03e-6
			B2	**8.68e-7**	8.71e-7	1.03e-6
17	Max. Actuator Torque Command Y (Nm)	< 1.5e-4 N m	B1	**1.05e-6**	**1.05e-6**	1.15e-6
			B2	**1.06e-6**	**1.06e-6**	1.16e-6
18	Max. Actuator Torque Command Z (Nm)	< 1.5e-4 N m	B1	**1.08e-6**	**1.08e-6**	1.27e-6
			B2	**1.08e-6**	**1.08e-6**	1.27e-6

Mario Garcia-Sanz

4.3.- Conclusions

- A **Non-diagonal MIMO QFT** Controller Design methodology
  to design fully populated matrix controllers
  to solve:
  - the reference tracking problem
  - the external disturbance rejection problem at both, plant input and output,
  - in the presence of model plant uncertainty,

  has been presented.

- The technique has been **validated** with a Darwin-type spacecraft
  with flexible appendages

4.4.- Some References

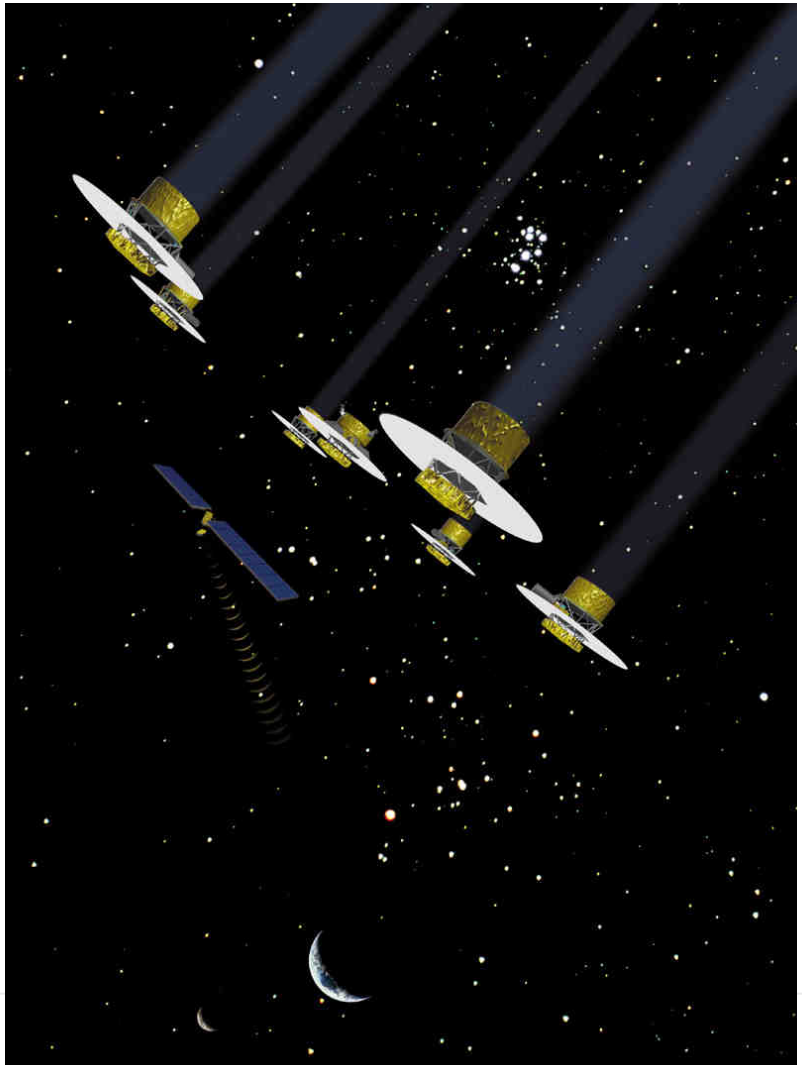

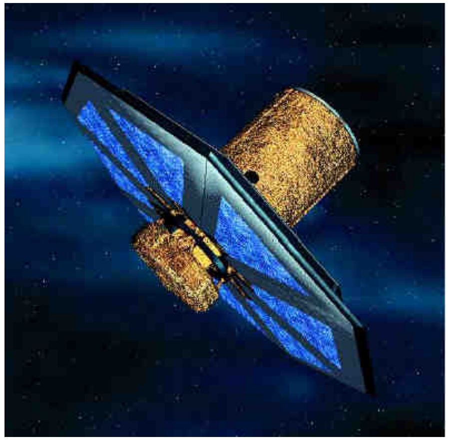

ESA-ESTEC
Noordwijk (Holland)

- ⇨ *Complex MIMO model*
- ⇨ *Demanding Spec.*
- ⇨ *Comparison: H-infinity, Diagonal MIMO QFT, Non-diagonal MIMO QFT*

Ref: M. Garcia-Sanz, I. Eguinoa, M. Barreras, S. Bennani

"Non-diagonal MIMO QFT Controller Design for Darwin-type Spacecraft with large flimsy appendages".

Journal of Dynamic Systems, Measurement and Control, **ASME,** USA. Vol. 130, January 2008**.**

***Special Issue:* COOPERATIVE CONTROL OF MULTIPLE SPACECRAFT FLYING IN FORMATION**

M. Garcia-Sanz (Guest Editor)

IET Control Theory and Applications, Vol. 1, Issue 2 , March 2007, UK.

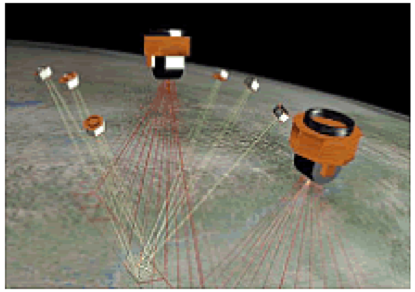

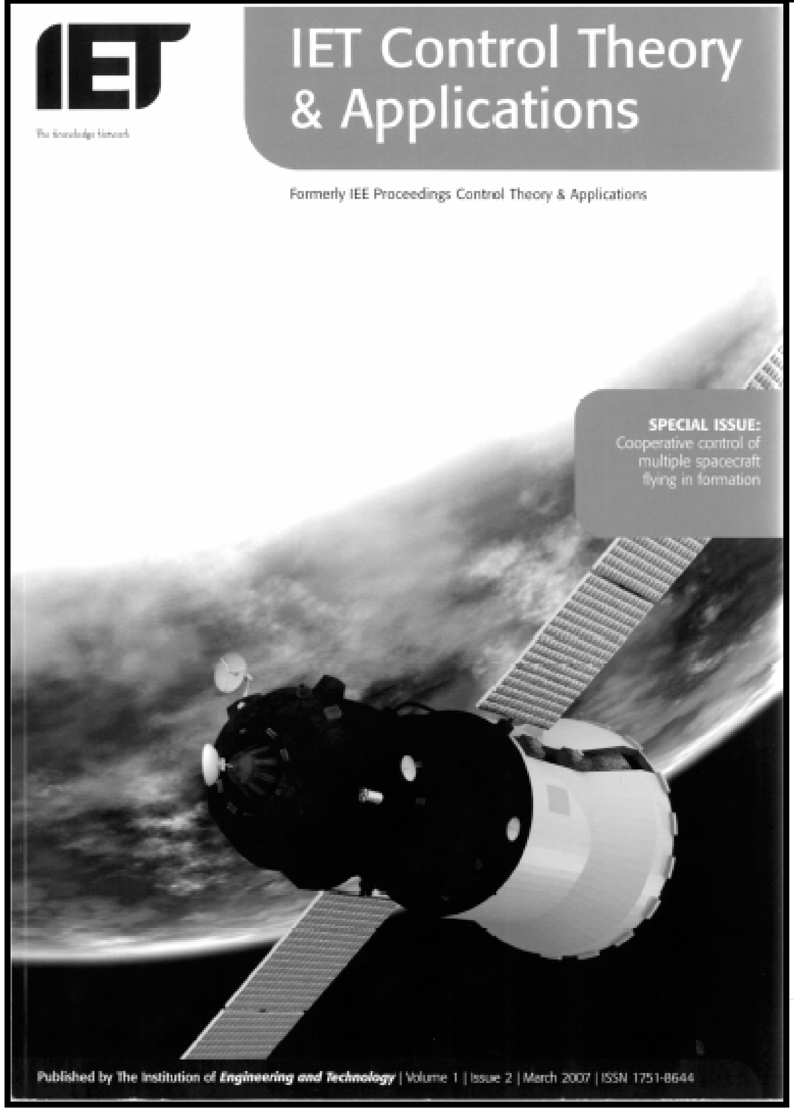

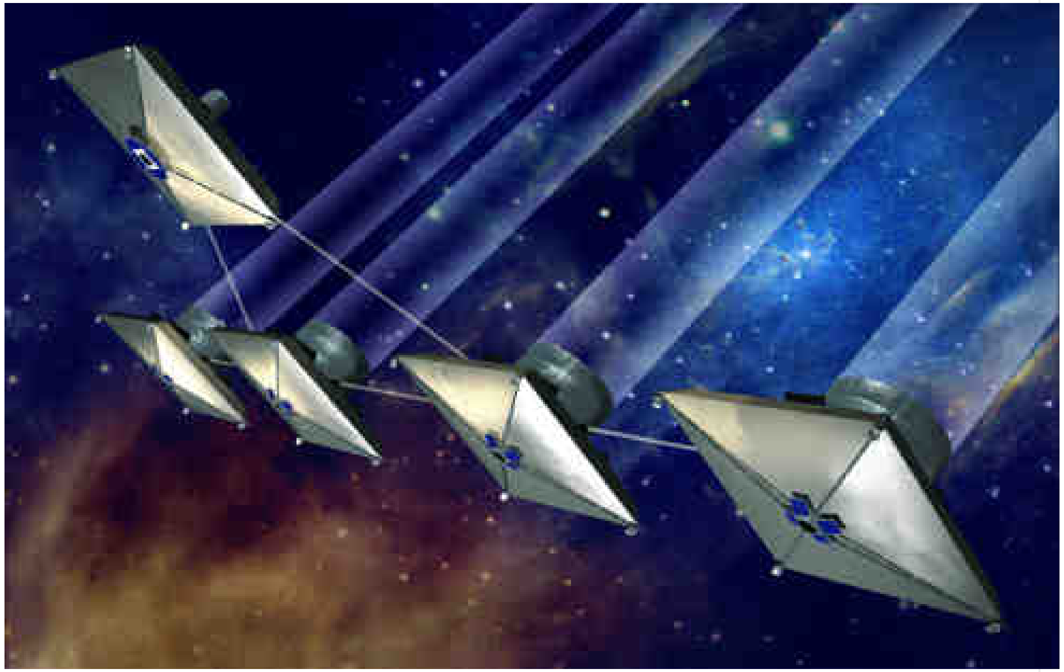

LOAD-SHARING ROBUST CONTROL OF SPACECRAFT FORMATIONS: Deep Space and Low Earth Elliptic Orbits

M. Garcia-Sanz, F. Y. Hadaegh

IET Control Theory and Applications, Vol. 1, Issue 2 , pp. 475-484, March 2007, UK

Outline

1.- QFT Controller Design Technique Fundamentals

2.- Real-world QFT control applications and examples

3.- Non-diagonal MIMO QFT controller design methodologies

4.- Application: Robust QFT control for a MIMO Spacecraft with flexible sunshield

5.- Switching robust control: Beyond the linear limitations.

6.- Example: Switching control for Unmanned Vehicles

5.- Switching robust control: Beyond the linear limitations

Classical linear limitations of feedback systems

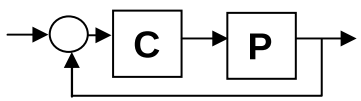

- Bode integrals 1945,
- Freudenberg, Looze 80…

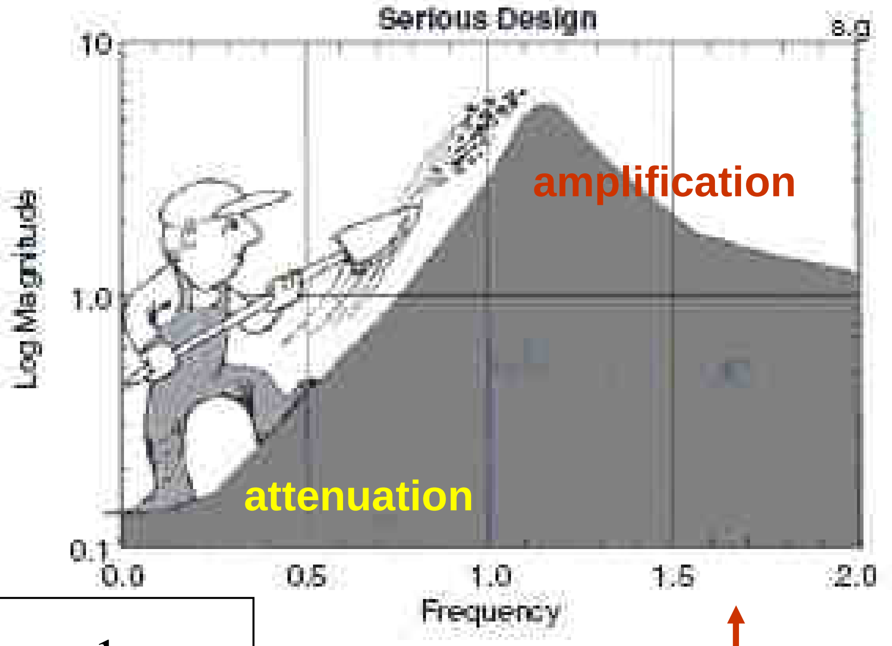

$$\frac{1}{\pi}\int_0^{\infty}\frac{1}{\omega^2}\log_e\left|T(j\omega)\right|d\omega=-\tfrac{1}{2}K_v^{-1}+\tfrac{1}{2}\tau+\sum_{z_i\in CRHP}\frac{1}{z_i}$$

where $K_v=\lim_{s\to 0}\{sC(s)P(s)\}$ *is the system velocity constant,* τ *is the time delay in the loop, and* z_i *are the zeros in the loop.*

$$T(s)=1-S(s)=\frac{C(s)P(s)}{1+C(s)P(s)}$$

Complementary Sensitivity

Sensitivity

"waterbed effect"

$$S(s)=\frac{1}{1+C(s)P(s)}$$

$$\int_{\omega=0}^{\omega=\infty}\log_e\left|S(j\omega)\right|d\omega=\pi\left(\sum_{p_i\in CRHP}p_i\right)-\frac{\pi}{2}k_{HF}$$

where $p_i\in CRHP$ are the poles of L(s)=C(s)P(s) in the closed right half plane (with units of radians/sec), and $k_{HF}=\lim_{s\to\infty}\{sL(s)\}$

Mario Garcia-Sanz

Example: X-29

NASA Dryden Flight Research Center Photo Collection
http://www.dfrc.nasa.gov/gallery/photo/index.html
NASA Photo: EC87-0182 Date: July 24, 1987 Photo by: NASA

X-29 in Banked Flight

Unstable

(pole RHP)

Non-minimum phase

(zero RHP)

Linear limitations

<u>In practice</u>:

-Objective Phase Margin = 45º

- Result ONLY Phase Margin = 39º

Mario Garcia-Sanz

To go beyond the linear limitations:

García-Sanz M., Elso J. (2008). **Beyond the linear limitations by combining switching and QFT: Application to wind turbines pitch control systems**. *Int. J. Robust Nonlinear Control*, Vol. 18, N.12.

SWITCHING

Nonlinear control

Even for linear systems

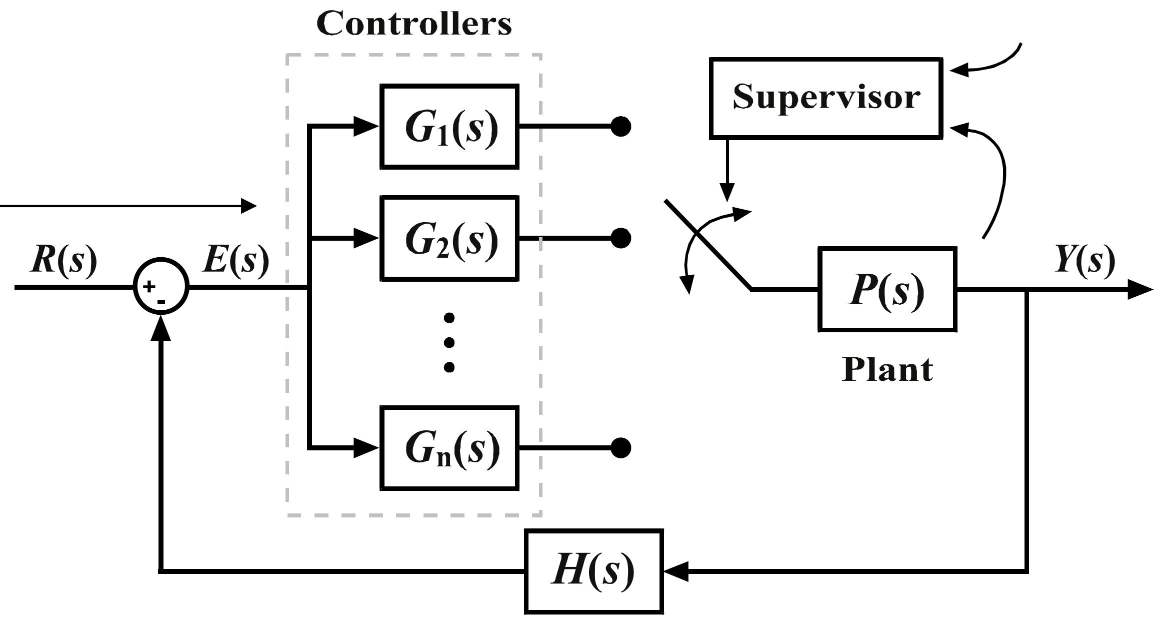

<u>Problem</u> to be solved:

system **stability** is not assured *a priori*,
even if the switching is made between stable controllers

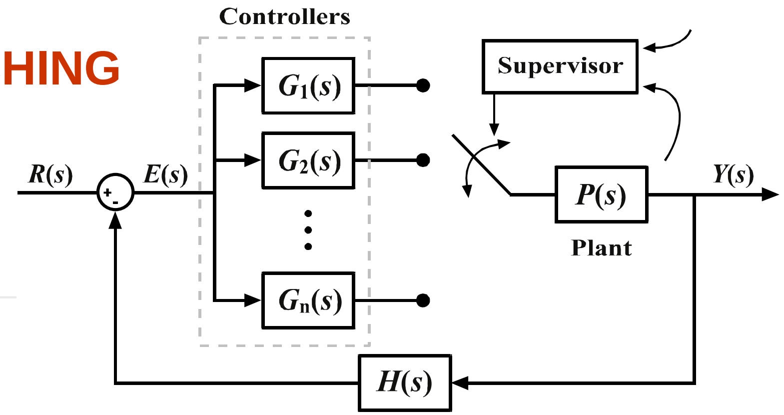

System stability analysis (I)

it has been proved that a system

$$\dot{x}(t) = \mathbf{A}(t)x(t), \quad \mathbf{A}(t) \in \mathcal{A} = \{\mathbf{A}_1, \dots, \mathbf{A}_m\}, \quad \mathbf{A}_i \text{ Hurwitz},$$

with arbitrary switching within the set of matrices **A**

is exponentially **stable**

if there exists a **Common Lyapunov Function** (CLF) for all $\mathbf{A}_i \in \mathcal{A}$

It has also been proved that the existence of a **Common Quadratic Lyapunov Function** (CQLF) for all $\mathbf{A}_i \in \mathcal{A}$ is a sufficient condition for exponential stability

Mario Garcia-Sanz

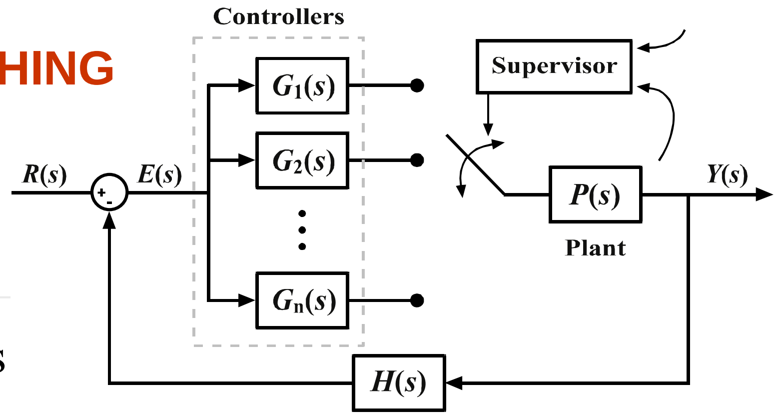

System stability analysis (II)

it has been proved that the **circle criterion** provides

necessary and sufficient conditions

for the **existence of a CQLF** for two systems in companion form

---

In particular the systems $\dot{x}(t) = \mathbf{A}x(t)$ $\quad \dot{x}(t) = (\mathbf{A} - \mathbf{g}\Delta^T)x(t)$

both Hurwitz, with

$$A = \begin{bmatrix} 0 & 1 & 0 & \cdots & 0 & 0 \\ 0 & 0 & 1 & \cdots & 0 & 0 \\ 0 & 0 & 0 & \cdots & 0 & 0 \\ \vdots & \vdots & \vdots & \ddots & \vdots & \vdots \\ 0 & 0 & 0 & \cdots & 0 & 1 \\ -e_0 & -e_1 & -e_2 & \cdots & -e_{n-2} & -e_{n-1} \end{bmatrix}, \quad g = \begin{bmatrix} 0 \\ 0 \\ 0 \\ \vdots \\ 0 \\ 1 \end{bmatrix}, \quad \Delta = \begin{bmatrix} \Delta e_0 \\ \Delta e_1 \\ \Delta e_2 \\ \vdots \\ \Delta e_{n-2} \\ \Delta e_{n-1} \end{bmatrix}$$

have a **CQLF** if and only if

$$\boxed{1 + \mathrm{Re}\{\Delta^T (s\mathbf{I} - \mathbf{A})^{-1}\mathbf{g}\} > 0, \quad s = j\omega, \text{for all frequency } \omega}$$

Mario Garcia-Sanz

System stability analysis (III)

SWITCHING

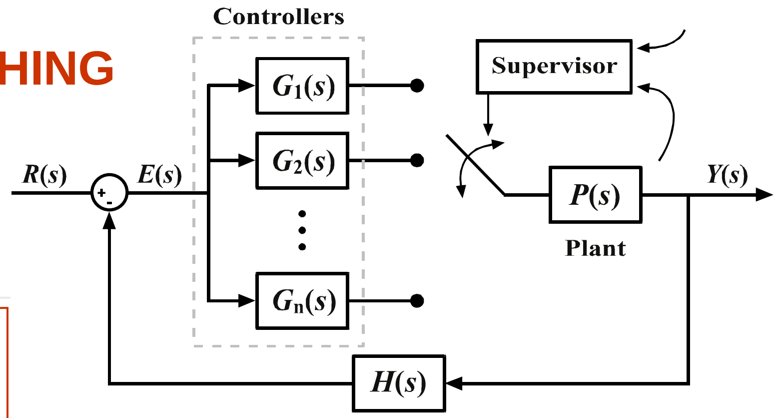

Now we consider stability for arbitrary switching between **two closed-loop systems** with transfer functions

$$T_1(s) = \frac{L_1(s)}{1+L_1(s)} = \frac{N(s)}{D(s)+N(s)}$$

$$T_2(s) = \frac{L_2(s)}{1+L_2(s)} = \frac{N(s)+\Delta N(s)}{D(s)+\Delta D(s)+N(s)+\Delta N(s)},$$

where: $L_1(s) = P(s)G_1(s)$ and $L_2(s) = P(s)G_2(s)$

are proper, have the same number of poles, and the same number of zeros.

$$L_1(s) = \frac{b_{n-1}s^{n-1}+\ldots+b_0}{s^n+a_{n-1}s^{n-1}+\ldots+a_0} = \frac{N(s)}{D(s)}$$

$$L_2(s) = \frac{(b_{n-1}+\Delta b_{n-1})s^{n-1}+\ldots+(b_0+\Delta b_0)}{s^n+(a_{n-1}+\Delta a_{n-1})s^{n-1}+\ldots+(a_0+\Delta a_0)} = \frac{N(s)+\Delta N(s)}{D(s)+\Delta D(s)}.$$

where the characteristic equations are

$$D(s)+N(s) =$$
$$= s^n + e_{n-1}s^{n-1}+\ldots+e_1 s+e_0$$

$$D(s)+\Delta D(s)+N(s)+\Delta N(s) =$$
$$= s^n + (e_{n-1}+\Delta e_{n-1})s^{n-1}+\ldots+(e_0+\Delta e_0),$$

$$e_i = a_i + b_i$$
$$\Delta e_i = \Delta a_i + \Delta b_i.$$

Mario Garcia-Sanz

System stability analysis (IV)

SWITCHING

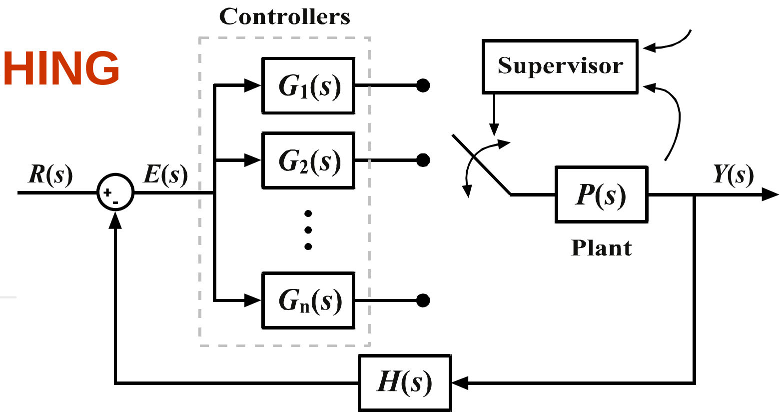

Now, the previous stability condition

$$\boxed{1+\mathrm{Re}\{\boldsymbol{\Delta}^T(s\mathbf{I}-\mathbf{A})^{-1}\mathbf{g}\}>0, \quad s=j\omega, \text{for all frequency } \omega}$$

becomes

$$1+\mathrm{Re}\left\{\frac{\Delta e_{n-1}s^{n-1}+\ldots+\Delta e_1 s+\Delta e_0}{s^n+e_{n-1}s^{n-1}+\ldots+e_1 s+e_0}\right\}>0, \; s=j\omega, \text{ for all frequency } \omega$$

and then

$$\mathrm{Re}\left\{\frac{1+L_2(s)}{1+L_1(s)}\left(\frac{D(s)+\Delta D(s)}{D(s)}\right)\right\}>0, \; s=j\omega, \text{ for all frequency } \omega$$

which, due to symmetry, is

$$\boxed{\left|\arg\{1+L_2(j\omega)\}-\arg\{1+L_1(j\omega)\}+\arg\left\{\frac{D(j\omega)+\Delta D(j\omega)}{D(j\omega)}\right\}\right|<\frac{\pi}{2} \text{ for all } \omega>0}$$

Mario Garcia-Sanz

System stability analysis (V)

SWITCHING

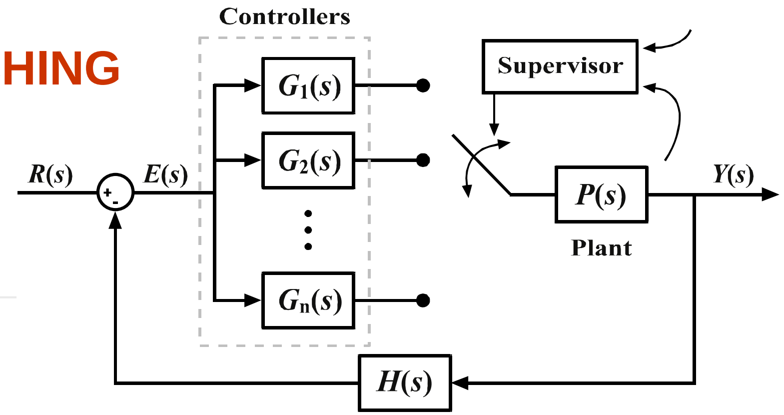

$$\boxed{\left| \arg\{1 + L_2(j\omega)\} - \arg\{1 + L_1(j\omega)\} + \arg\left\{\frac{D(j\omega) + \Delta D(j\omega)}{D(j\omega)}\right\} \right| < \frac{\pi}{2} \text{ for all } \omega > 0}$$

denoting
$$\varphi_{12}(\omega)[\text{deg}] = \left| \arg\{1 + L_2(j\omega)\} - \arg\{1 + L_1(j\omega)\} \right|,$$

$$\alpha(\omega)[\text{deg}] = \left| \arg\left\{\frac{D(j\omega) + \Delta D(j\omega)}{D(j\omega)}\right\} \right|.$$

and applying the triangle inequality

$$\boxed{\varphi_{12}(\omega) < 90 - \alpha(\omega) \text{ deg for all } \omega \geq 0}$$

Mario Garcia-Sanz

System stability analysis (VI)

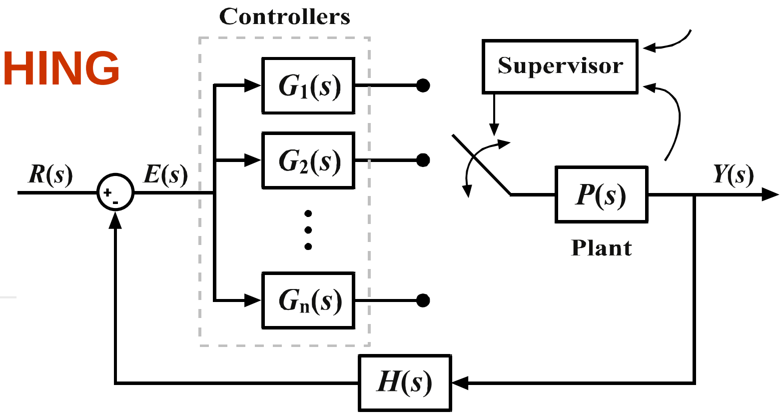

The criterion can be applied graphically in the **Nyquist diagram**

$$\boxed{\varphi_{12}(\omega) < 90 - \alpha(\omega) \text{ deg for all } \omega \geq 0}$$

$$\varphi_{12}(\omega)[\text{deg}] = \left|\arg\{1 + L_2(j\omega)\} - \arg\{1 + L_1(j\omega)\}\right|,$$

$$\alpha(\omega)[\text{deg}] = \left|\arg\left\{\frac{D(j\omega) + \Delta D(j\omega)}{D(j\omega)}\right\}\right|.$$

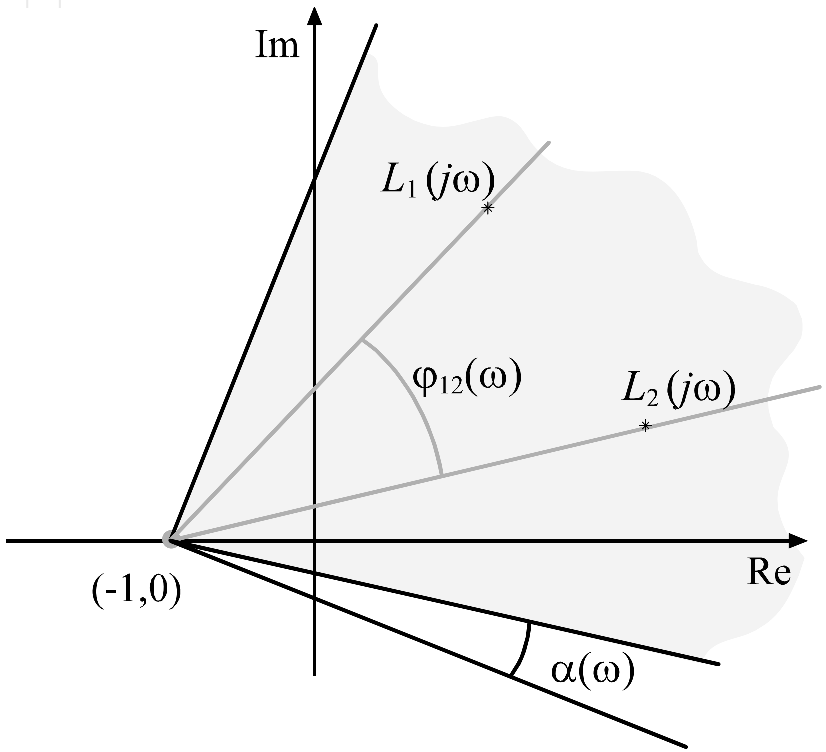

For **stable switching**:

$L_1(j\omega)$ and $L_2(j\omega)$

must be **inside** of an arc of $[90 - \alpha(\omega)]$ deg

around the point (-1,0) at each frequency

Mario Garcia-Sanz

System stability analysis (VII)

SWITCHING

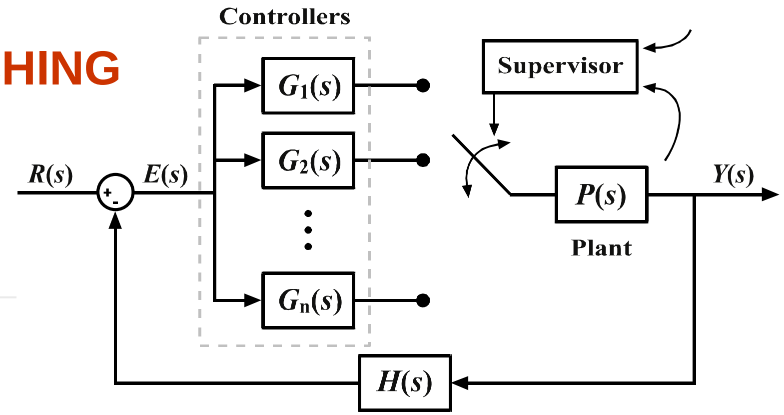

The criterion can be applied graphically in the **Nichols diagram**

$$\boxed{\varphi_{12}(\omega) < 90 - \alpha(\omega) \text{ deg for all } \omega \geq 0}$$

$$\varphi_{12}(\omega)[\text{deg}] = \left|\arg\{1 + L_2(j\omega)\} - \arg\{1 + L_1(j\omega)\}\right|,$$

$$\alpha(\omega)[\text{deg}] = \left|\arg\left\{\frac{D(j\omega) + \Delta D(j\omega)}{D(j\omega)}\right\}\right|.$$

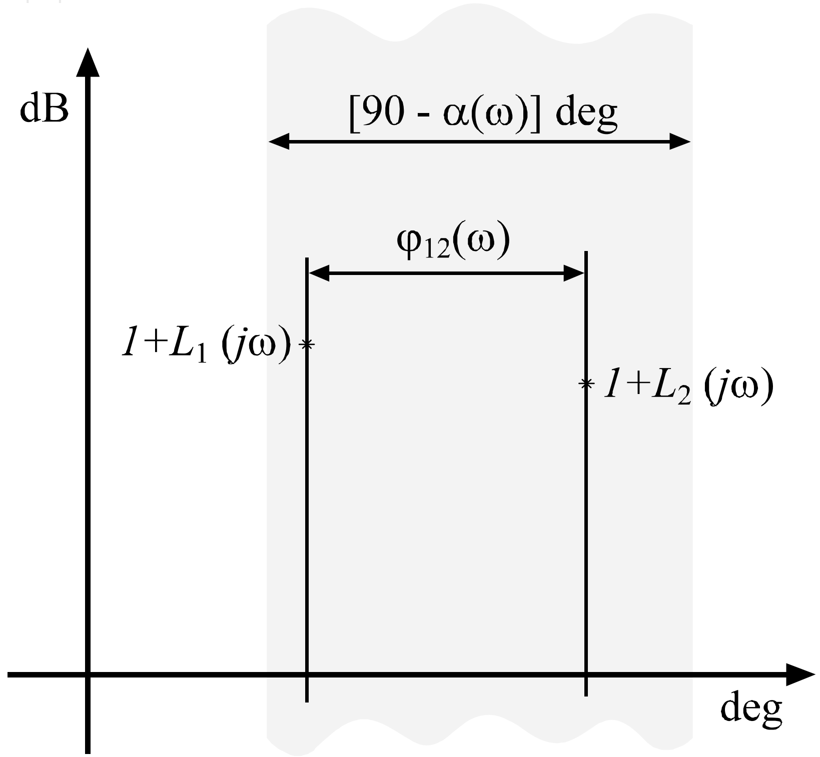

For **stable switching**:

plot $[1 + L_1(j\omega)]$ and $[1 + L_2(j\omega)]$,

the distance $\varphi_{12}(\omega)$ on the horizontal axis at each frequency

must be less than $[90 - \alpha(\omega)]$ deg

Mario Garcia-Sanz

System stability analysis (VIII)

SWITCHING

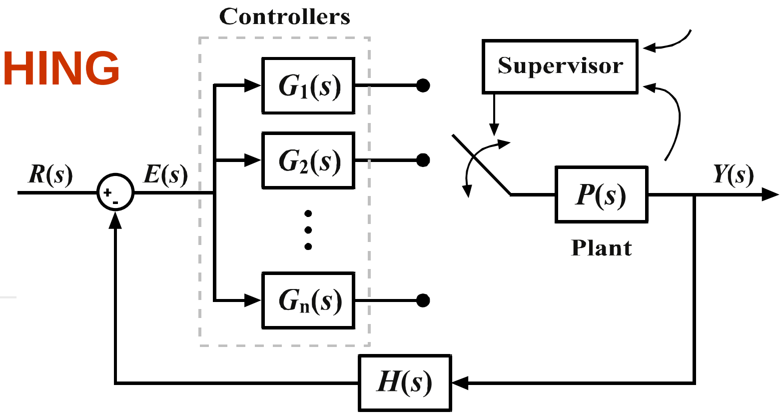

$\alpha(\omega)$ may be considered as a measurement of the **controller poles change**

$$\boxed{\varphi_{12}(\omega) < 90 - \alpha(\omega) \text{ deg for all } \omega \geq 0}$$

$$\varphi_{12}(\omega)[\text{deg}] = \left|\arg\{1 + L_2(j\omega)\} - \arg\{1 + L_1(j\omega)\}\right|,$$

$$\alpha(\omega)[\text{deg}] = \left|\arg\left\{\frac{D(j\omega) + \Delta D(j\omega)}{D(j\omega)}\right\}\right|.$$

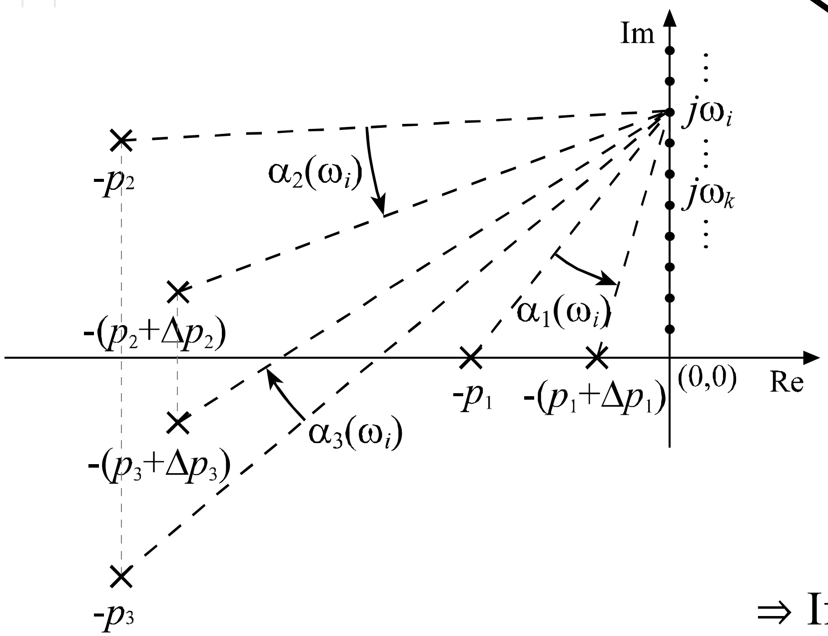

$$\alpha(\omega) = \left|\arg\left\{\frac{D(j\omega) + \Delta D(j\omega)}{D(j\omega)}\right\}\right| = \left|\arg\left\{\frac{\prod_{j=1}^{n}(j\omega + p_j + \Delta p_j)}{\prod_{j=1}^{n}(j\omega + p_j)}\right\}\right| =$$

$$= \left|\sum_{j=1}^{n} \arg\{j\omega + p_j + \Delta p_j\} - \arg\{j\omega + p_j\}\right|$$

$\Rightarrow$ If there aren't moving poles, the angle $\alpha(\omega)$ is null.

Mario Garcia-Sanz

System stability analysis (IX)

SWITCHING

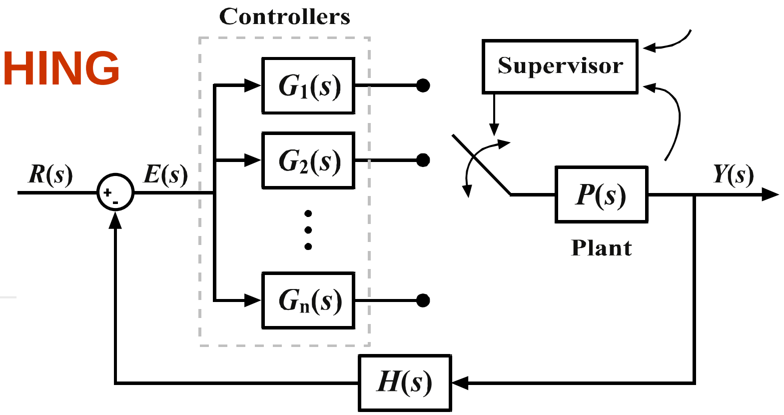

Note 1: Switching among an infinite number of systems (LPV)

Easy if we only move gain and zeros $\Rightarrow \alpha(\omega) = 0$

$$\boxed{\varphi_{12}(\omega) < 90 - \alpha(\omega) \text{ deg for all } \omega \geq 0}$$

$$\varphi_{12}(\omega)[\text{deg}] = \left| \arg\{1 + L_2(j\omega)\} - \arg\{1 + L_1(j\omega)\} \right|,$$

$$\alpha(\omega)[\text{deg}] = \left| \arg\left\{ \frac{D(j\omega) + \Delta D(j\omega)}{D(j\omega)} \right\} \right|.$$

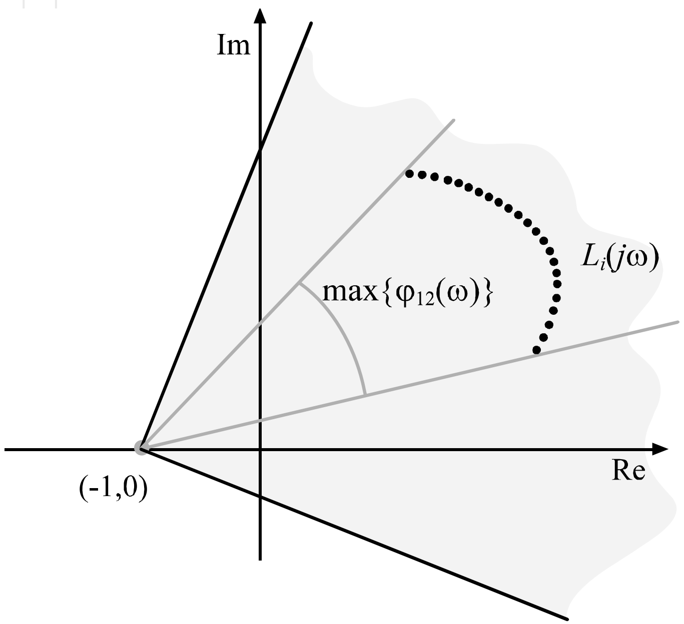

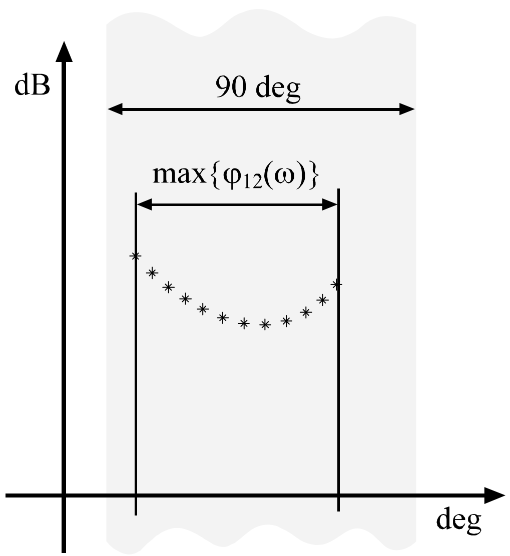

the angle between any two possible systems $L_i(j\omega)$ (or $[1 + L_1(j\omega)]$) is **less than 90 deg**

Mario Garcia-Sanz

System stability analysis (X)

SWITCHING

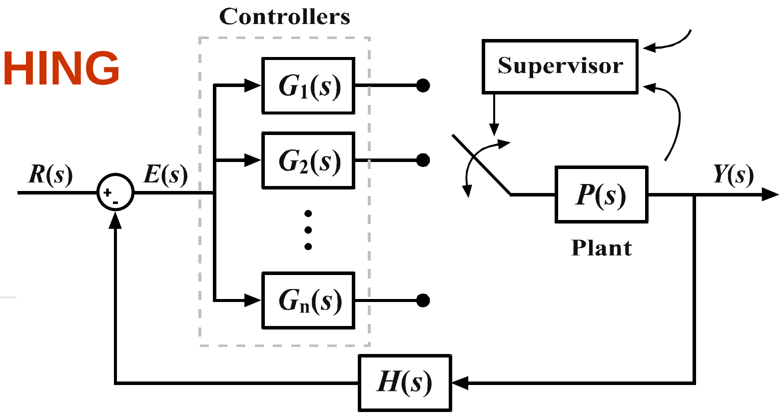

Note 2: To deal with Uncertainty

switching = modifies position and shape of templates of $[1 + L_i(j\omega)]$

$$\boxed{\varphi_{12}(\omega) < 90 - \alpha(\omega) \text{ deg for all } \omega \geq 0}$$

$$\varphi_{12}(\omega)[\text{deg}] = \left|\arg\{1 + L_2(j\omega)\} - \arg\{1 + L_1(j\omega)\}\right|,$$

$$\alpha(\omega)[\text{deg}] = \left|\arg\left\{\frac{D(j\omega) + \Delta D(j\omega)}{D(j\omega)}\right\}\right|.$$

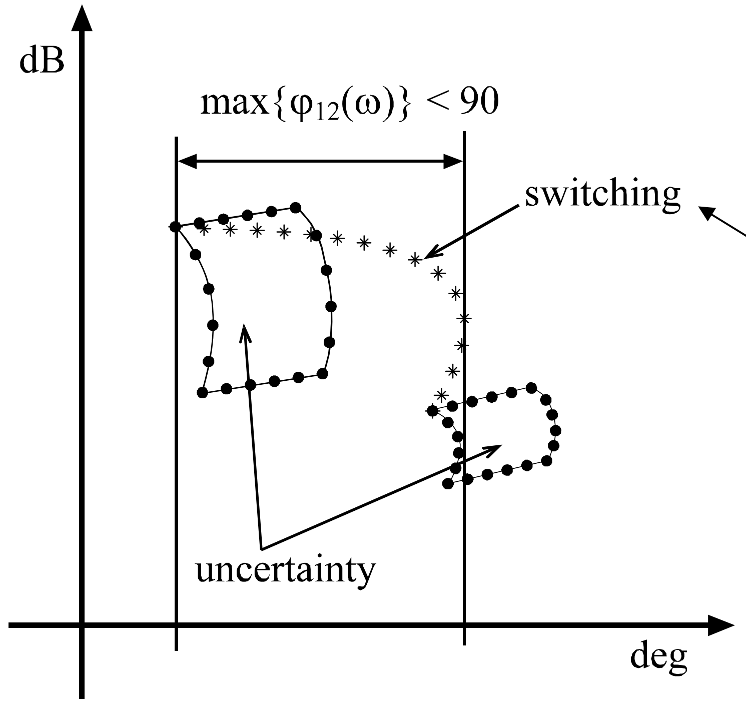

criterion applied to

path from each point of the

departure template to

its corresponding point in the *arrival template*

uncertainty changes the plant slowly in comparison with the system dynamics

Mario Garcia-Sanz

The switching criterion

SWITCHING

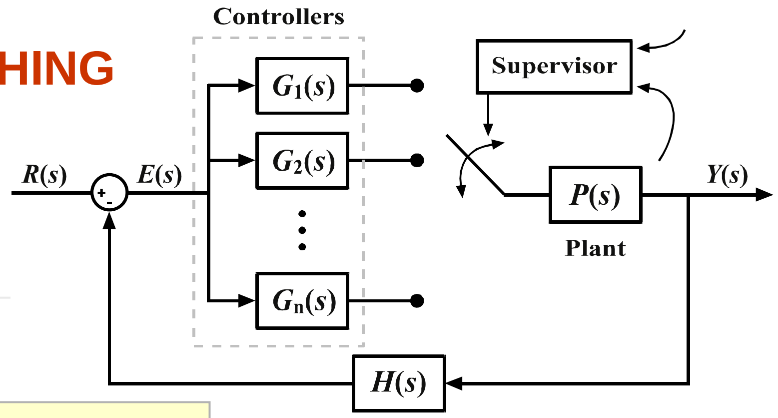

Signal: the error amplitude

Criteria:

i) ***Large error***: large bandwidth (speed), loop gain not very high

ii) ***Small errors***: reduced bandwidth (noise), increased low frequency gain (jitter, tracking error)

LARGE ERROR
↑ STABILITY MARGINS
↑ SPEED,
↓PRECISION

SMALL ERROR
↓ STABILITY MARGINS
↑ LOW FREQUENCY GAIN
(⇒ ↑ PRECISION & DISTURBANCE REJECTION)

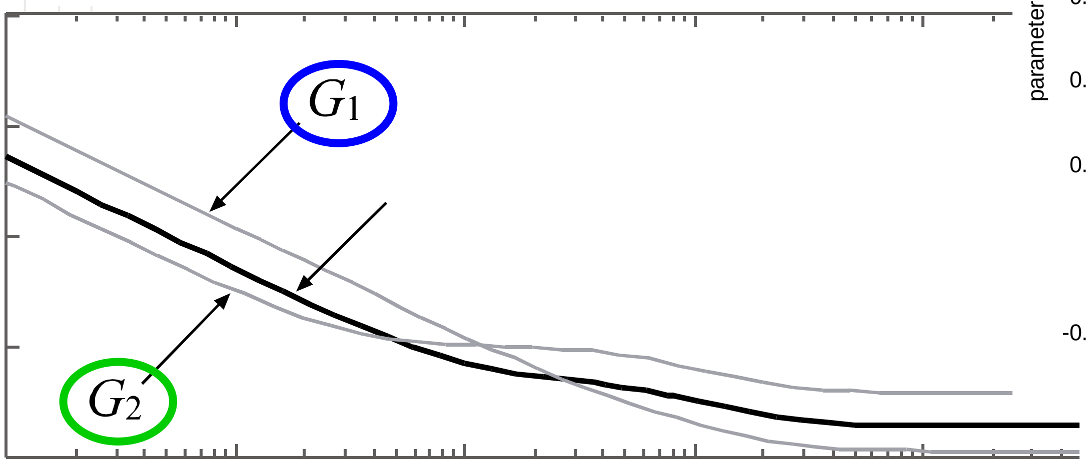

Switching Function:

for example

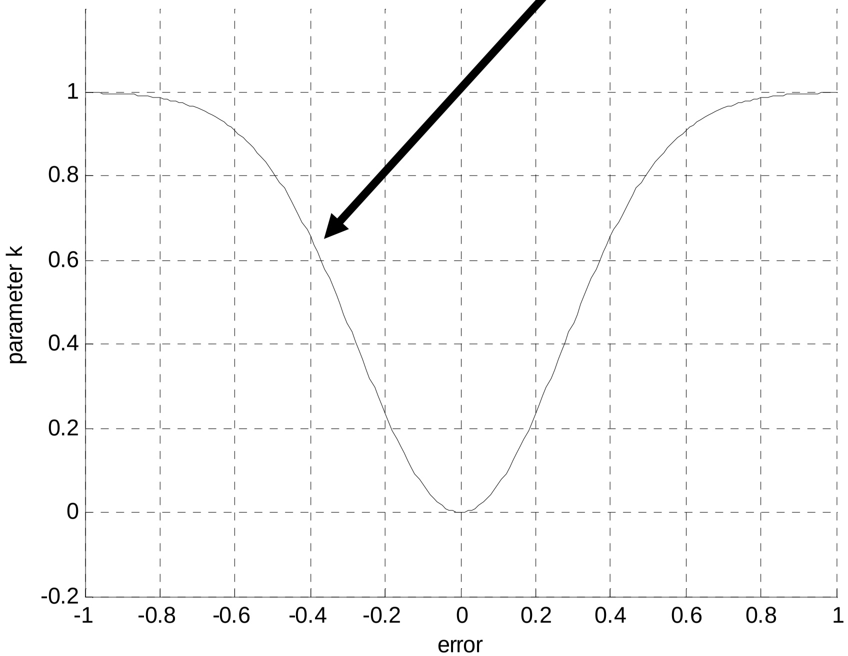

Mario Garcia-Sanz

Controller Design Methodology

SWITCHING

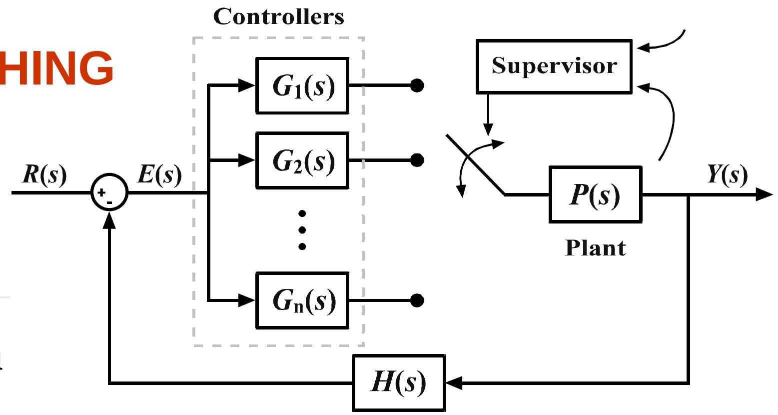

Step 1: **Preliminary QFT linear controller design**
- parametric and/or non-parametric uncertainty,
- stability and performance specifications,
- Templates and QFT-bounds
- design a linear controller by loop-shaping

Step 2: **Design two extreme controllers with the same structure.**
- Gain and zeros vary freely, but poles stand still.
- Their characteristics must be related with the ***error amplitude***:
  i) **Large error**: large bandwidth (speed), loop gain not very high
  ii) **Small errors**: reduced bandwidth (noise), increased low freq.gain (jitter, tracking error)

Step 3: **Check Stability.**
- robust stability of extreme designs guaranteed by QFT.
- stability with switching is assured by new graphical criterion.

Step 4: **Design the Switching function**.
- Simulations of the system governed by each extreme controller.
- Design the function that relates the error amplitude with the controller parameters.

Mario Garcia-Sanz

6.- Example: Switching control for Unmanned Vehicles

Remotely Controlled
Reconnaissance Vehicle

(Dorf)

Plant & parametric uncertainty

$$P(s) = \frac{1}{\left(s^2 + a_1\, s + a_0\right)}$$

where $a_1 \in [1.8, 2.2]$, and $a_0 \in [3.6, 4.4]$

Step 1: **Preliminary linear controller design**

$$G_0(s) = \frac{10\left(s+2\right)}{\left(s+1\right)}$$

(Designed by Dorf)

Mario Garcia-Sanz

$$G_0(s) = \frac{10(s+2)}{(s+1)}$$

Step 2: **Design two extreme controllers with the same structure.**

- Gain and zeros vary freely, but poles stand still.
- Their characteristics must be related with the ***error amplitude***:

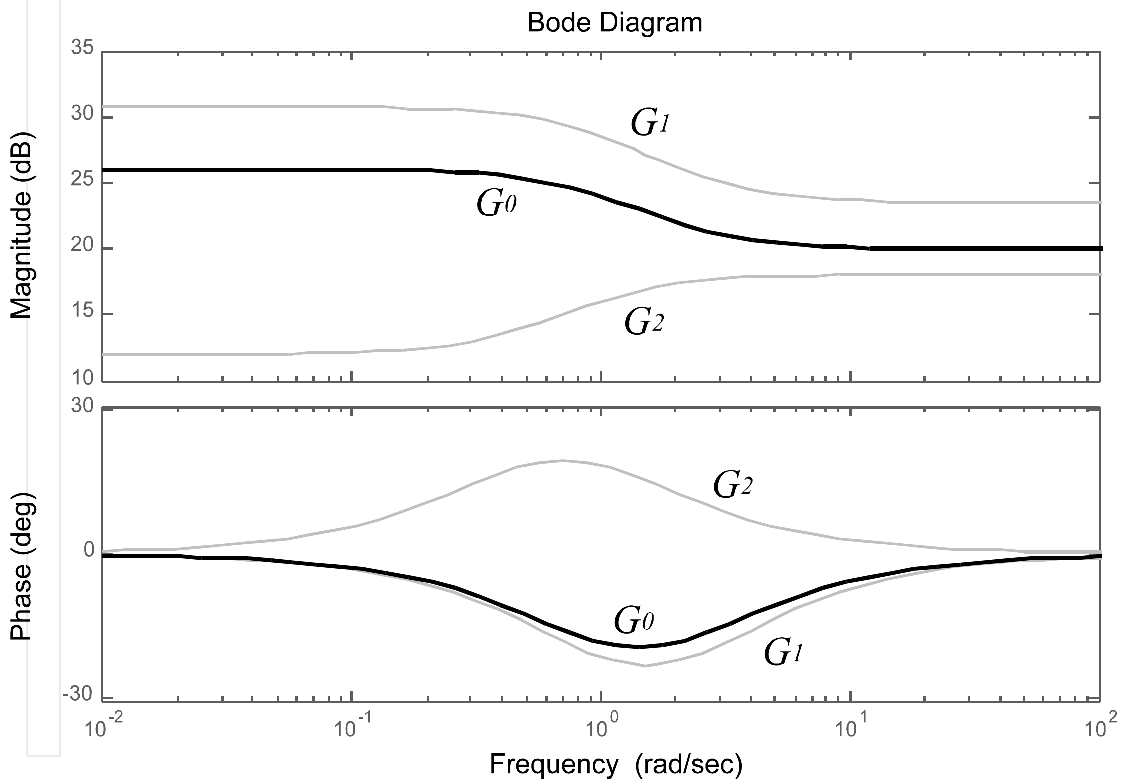

$$G_1(s) = \frac{15(s+2.3)}{(s+1)}$$

$$G_2(s) = \frac{8(s+0.5)}{(s+1)}$$

Mario Garcia-Sanz

$$G_1(s) = \frac{15(s+2.3)}{(s+1)} \qquad G_2(s) = \frac{8(s+0.5)}{(s+1)}$$

Step 3: **Check Stability.**

- robust stability of extreme designs guaranteed by QFT.
- stability with switching is assured by new graphical criterion.

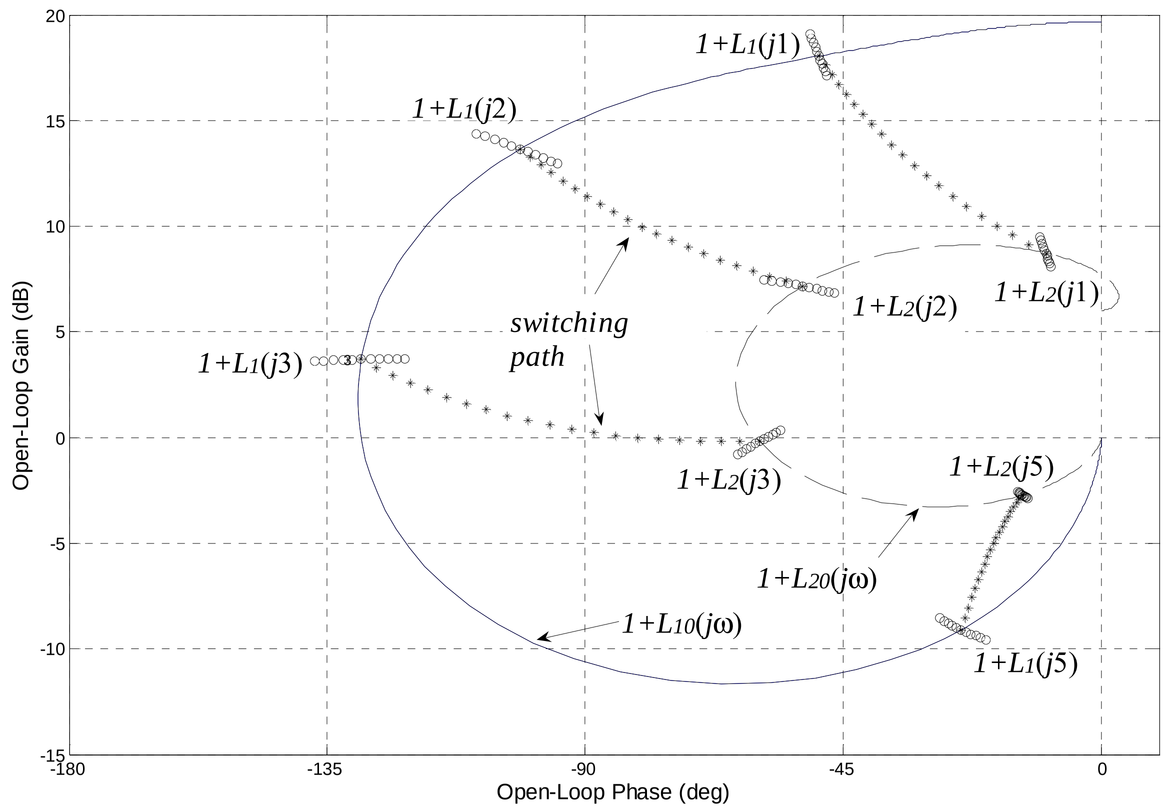

UNCERTAINTY
in the path from each point of the first template to its corresponding point of the second template, the maximum horizontal distance between two points is not higher than 90 deg

Mario Garcia-Sanz

$$G_1(s)=\frac{15(s+2.3)}{(s+1)} \qquad G_2(s)=\frac{8(s+0.5)}{(s+1)}$$

Step 4: **Design the Switching function**.

- Simulations of the system governed by each extreme controller.
- Design the function that relates the error amplitude with the controller parameters.

The switching controller is $$G_{swi}(s)=\frac{(15-7k)(s+2.3-1.8k)}{(s+1)}$$

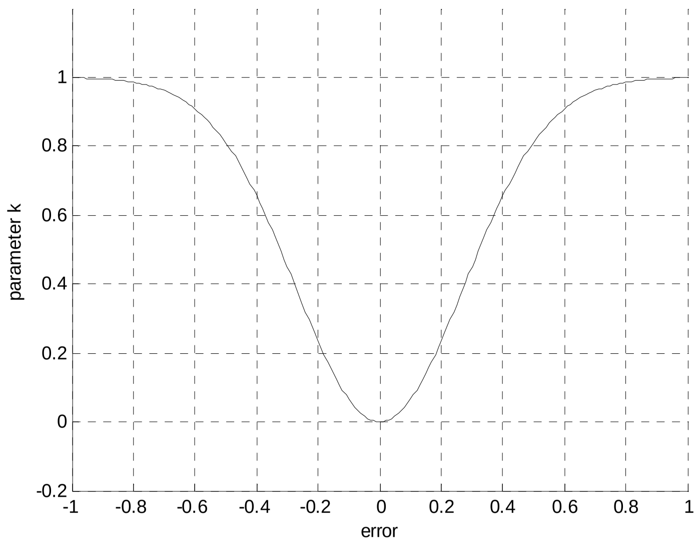

k is given by a function $\mathbb{R} \rightarrow [0, 1]$ of the error signal.

$$k=1-\exp\left(-\frac{e(t)^2}{0.15}\right)$$

smooth function (instead of a relay-type or saturation-type function) to reduce impulse effects

Results

time response to a step input reference tracking (t = 1 sec) and a step disturbance (t = 15 sec)

The switching controller (*Gswi*)
- combines the best characteristics of the extreme controllers (G_1 and G_2),
- improving the response of the original fixed controller (G_0)

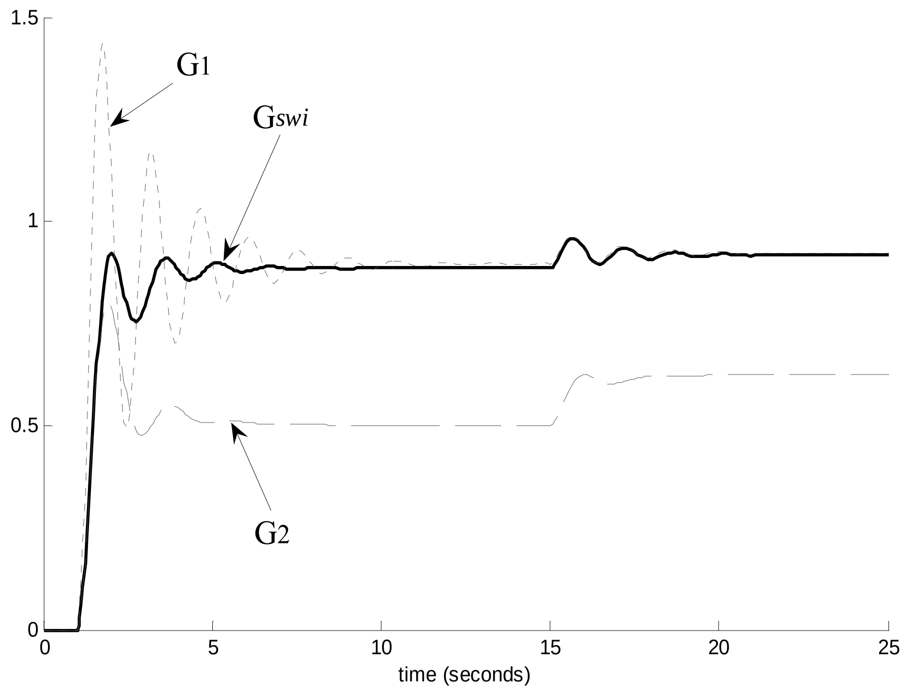

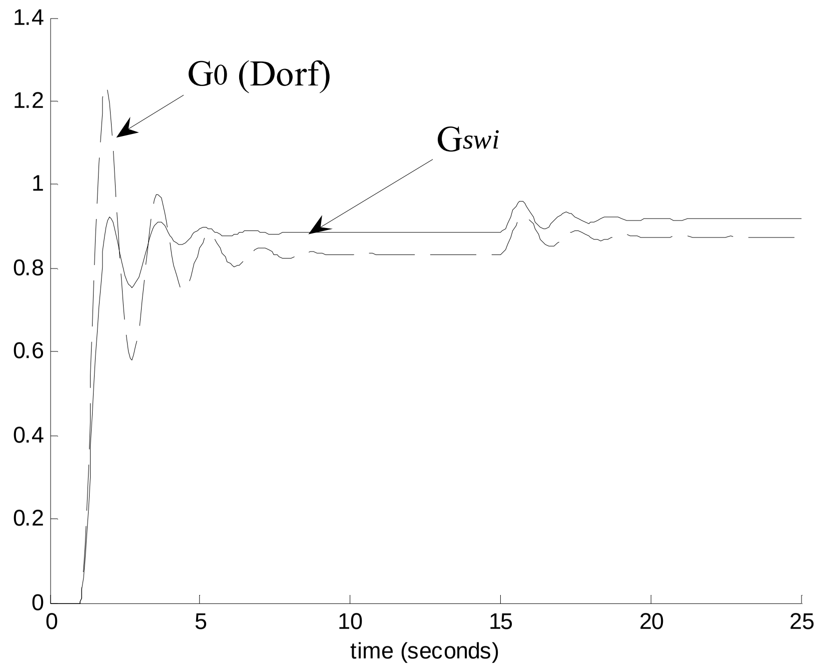

Suitable to be applied to other systems

Wind Turbines control

García-Sanz M., Elso J. (2008). **Beyond the linear limitations by combining switching and QFT: Application to wind turbines pitch control systems**. *Int. J. Robust Nonlinear Control*, Vol. 18, N.12.

UAV control

Spacecraft control

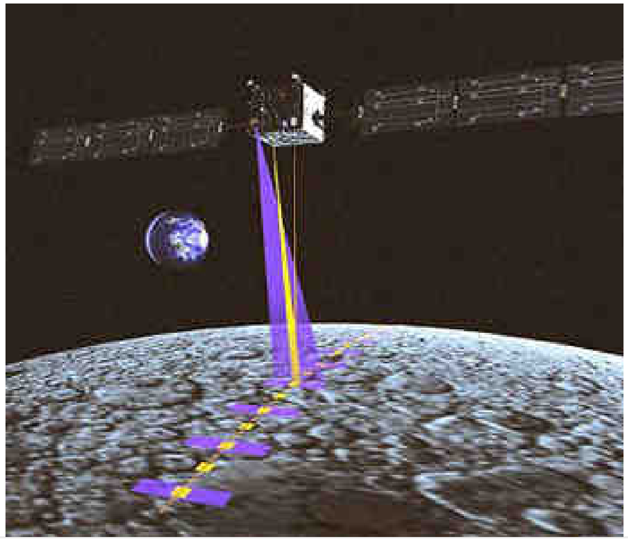


Thanks
Any questions?